RHENIUM(I) COMPLEXES OF TETRAAZATETRAPYRIDOPENTACENE (TATPP): SYNTHESIS, CHARACTERIZATION, REACTIVITY, ANTICANCER POTENTIAL AND LUMINESCENT PROBE TO DETERMINE CELLULAR LOCALIZATION

by

POOJA AHUJA

Presented to the Faculty of the Graduate School of

The University of Texas at Arlington in Partial Fulfillment

of the Requirements

for the Degree of

DOCTOR OF PHILOSOPHY

THE UNIVERSITY OF TEXAS AT ARLINGTON

May 2016

ACKNOWLEDGEMENTS

First and foremost, I would like to express my sincere and deepest gratitude to my advisor Dr. Frederick M. Macdonnell, for his immense support and guidance all throughout my graduate school. From his endless knowledge, outstanding mentoring and supervision to his polite, kind and hospitable behavior, all has educated me with the skills needed to succeed in academia and personal life altogether. His remarkable quality of understanding by 'walking in one's shoe' and his belief in his students is unparalleled. Without his guidance, encouragement, infinite patience and faith in me, I may not have come thus far. I will never forget the important lessons that I have learnt from you and cannot thank you enough for everything you have done for me. I will be grateful forever Dr. Fred !

Secondly, I would like to give my heartfelt special thanks to my committee members Dr. Rasika Dias and Dr. Kayunta Johnsons-Winters for their academic support, feedback and suggestions as well as their personal cheering and motivation at my yearly defenses. Their friendly and supportive approach is simply incomparable. I would also like to extend my deepest gratitude to Dr. Liping Tang in Biomedical Engineering Department at UTA for providing us with the mice for animal toxicity studies. Special thanks to Mr. Alphas Wicker from Biology Department for training me on animal handling and help with animal toxicity experiment.

Thanks to all the previous and current lab members Dr. Issa Faiza, Dr. Shreeyukta Singh, Dr. Joseph Aslan, Dr. David Boston, Dr. Upendra Joshi, Dr. Nagham Alatrash, Dr. Eugenia Narh, Cynthia Griffith, Adam S Dayoub, Angela Dickens, Fakrul Mohammad Islam, Shomita Ferdous, Matthew West, Jimmy Nguyen, Evette A. Odhiambo and Radiyah for their valuable suggestions, constant encouragement and support as well as help in lab in many ways. Special thanks to Adam Dayoub for training me on cell culturing and

cytotoxicity determination methods as well as Nagham Alatrash for guidance with animal biodistribution experiment.

My deepest gratitude is also extended to all the staff members in the Department of Chemistry and Biochemistry, in particular Dr. William Cleaver, Jill Howard, Debbie Cooke, Natalie Croy, Charles Savage, James Garner and Maciej Kukula for their cooperation and help in numerous ways throughout my graduate studies. Special thanks to Dr. Brian Edwards for his willingness to help with any instrument related issue so that research is not delayed or compromised. Thank you very much Brian for that!

To my mom Kamal Ahuja and dad Om Prakash Ahuja for their unconditional love and support all throughout. I cannot forget the hardships that you have been through to make sure that your children receive the best of everything in life and cannot thank you enough for raising me into a human being that I am today. Your teachings in life are precious! And to the two most important people in my life, my dearest husband Manish and my sweet little angel Magan. I have no words to thank you for your patience and understanding throughout this time. This was not possible without your support and encouragement. And Magan you can stop asking “when are you going to be done with your studies Mumma…” coz I am my sweetheart!

April 18, 2016

ABSTRACT

RHENIUM(I) COMPLEXES OF TETRAAZATETRAPYRIDOPENTACENE (TATPP): SYNTHESIS, CHARACTERIZATION, REACTIVITY, ANTICANCER POTENTIAL AND LUMINESCENT PROBE TO DETERMINE CELLULAR LOCALIZATION

Pooja Ahuja, PhD

The University of Texas at Arlington, 2016

Supervising Professor: Frederick M. Macdonnell

The ruthenium polypyridyl complexes $[(phen)_2Ru(\textit{tatpp})Ru(phen)_2]^{4+}$ ($[P]^{4+}$) and $[(phen)_2Ru(\textit{tatpp})]^{2+}$ ($[MP]^{2+}$) are promising anti-tumor agents that arrest H358 NSCLC tumor growth in mouse tumor models and show cytotoxicity in the low micromolar range towards a number of platinum sensitive NSCLC lines (H358, H226, HOP62, H2087). Dose escalation toxicity studies in mice reveal that $[MP]^{2+}$ and $[P]^{4+}$ are tolerated without any short term side effects at levels up to 40 mg drug/kg mouse and >160 mg drug/kg mouse respectively with no obvious side effects, when administered as IP injection. Mechanistic studies reveal that much of the anti-tumor activity is primarily due to the presence of redox active ligand unit *tatpp* that binds to DNA via intercalation and is then reduced to a radical species that cleaves DNA via H-atom abstraction from the deoxyribose unit.

In this work, we examine the hypothesis that the *tatpp* ligand is the key pharmacophore and that coordination to Ru(II) is needed primarily to enhance its solubility and modify its reduction potential, however other transition metals may also satisfy this requirement. In an effort to determine the generality of the tatpp pharmacophore, a number of Re(I) analogues were targeted and tested, where possible, for DNA cleavage activity, cytotoxicity, and animal toxicity. The Re(I)*tatpp* analogues possess lower overall charge and differing coordination environments around *tatpp* which could potentially alter the spectrum of cytotoxic activity against cancer cells and open new potential therapies. In this regards, we prepared a series of homometallic and heterobimetallic Re(I)*tatpp* analogues such as $Re_2(CO)_6$(*tatpp*)Cl_2 [**ReP**], $Re(CO)_3$(*tatpp*)Cl [**MRe**], [$Re_2(CO)_6$ (*tatpp*)$(CH_3CN)_2$]$(PF_6)_2$ **[ReP$_{CH3CN}$]$^{2+}$**,[Ru(phen)$_2$(*tatpp*)Re$(CO)_3(CH_3CN)$]$(PF_6)_3$ **[RuRe$_{CH3CN}$]$^{3+}$**, [Ru(phen)$_2$(*tatpp*)Re$(CO)_3(P(CH_2OH)_3]$$(PF_6)_3$ **[RuRe$_{PR3}$]$^{3+}$** and characterized them by ^{1}H NMR, IR, HRMS, CHN. Unlike Ru(II) complexes [**P**]$^{4+}$and [**MP**]$^{2+}$, Re(I)*tatpp* complex **[ReP$_{CH3CN}$]$^{2+}$** was found to be air sensitive and oxidizes to form a quinone analogue [$Re_2(CO)_6$(*tatpq*)$(CH_3CN)_2$]$(PF_6)_2$ **[ReQ]$^{2+}$** upon visible light irradiation in solution. The compound also can dimerize, whether in solution or solid state, to form a 'dimer of dimers' [$Re_4(CO)_{12}$(*tatpp*)$_2(CH_3CN)_4$]$(PF_6)_4$ **[d-ReP$_{CH3CN}$]$^{4+}$** via an unknown route. The heterobimetallic complex [RuRe$_{CH3CN}$]$^{3+}$ was found to be less reactive than **[ReP$_{CH3CN}$]$^{2+}$** but will also undergo photooxidation to the quinone analogue [Ru(phen)$_2$(*tatpq*)Re$(CO)_3(CH_3CN)$]$(PF_6)_3$ **[RuReQ$_{CH3CN}$]$^{3+}$** after prolonged irradiation of over 72 h under identical conditions (relatively low yield - 33%). Because of solubility reasons, only **[RuRe$_{CH3CN}$]$^{3+}$** and **[RuRe$_{PR3}$]$^{3+}$** were screened for DNA cleavage activity which revealed that these complexes are effective DNA cleaving agents under the same conditions in which Ru(II) complexes [**P**]$^{4+}$ and [**MP**]$^{2+}$ are. Toxicity studies reveal that **[RuRe$_{PR3}$]$^{3+}$** exhibits different spectrum of cytotoxicity against four cancer cell lines and low

animal toxicity (MTD > 160 mg/kg mouse). Biodistribution study reveal gradual body clearance while the mass spectrometry data to support renal clearance is awaited. Representative HPLC studies to show that **[RuRe$_{PR3}$]$^{3+}$** is not only pure but unexpectedly fluorescent are also presented. Confocal microscopy study in H358 cells to determine patterns of uptake and localization is also presented and discussed.

TABLE OF CONTENTS

List of Illustrations

LIST OF TABLES

Chapter 1

RUTHENIUM POLYPYRIDINE COMPLEXES IN CHEMOTHERAPY

1.1 Metal based Anti-cancer drugs

The development of new, safe, and effective drugs for treating cancer is a priority as cancer remains one of the leading causes of death in today's society.[1, 2, 3, 4] Ever since its discovery in 1970s, platinum metal based complex *cis*-$(NH_3)_2PtCl_2$ or cisplatin remains the most successful and widely used chemotherapeutic agent alone or in combination, for the treatment of numerous cancers. [5, 6, 7] and is thus sometimes referred to as 'Gold Standard'. Its mode of action is well studied and understood as due to the adduct formation with DNA bases, however it is also recognized that the platinum agent is non-specific and binds to a host of other cellular targets which could contribute to both its efficacy and observed toxicity. Thus, despite being the most effective anticancer drug in clinic today, chemotherapy with cisplatin is often limited by severe toxic side effects such as nausea, vomiting, neurotoxicity, and nephrotoxicity. [8, 9]

The incidental discovery of cisplatin, nonetheless, provided a new impetus to the field of metal based drugs and soon after numerous studies exploring the anticancer potential of alternative Pt compounds were reported. After tremendous effort in synthesizing and screening alternative platinum-based drugs, only three analogues of cisplatin namely carboplatin, oxaliplatin and nedaplatin (Fig 1.1) have progressed to clinical use and here they are principally used to avoid some of the more serious side effects associated with cisplatin.

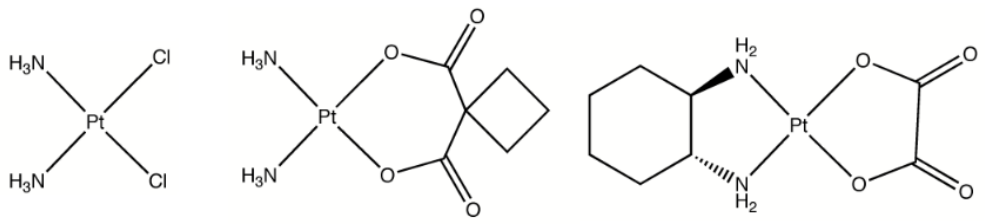

Cisplatin **Carboplatin** **Oxaliplatin**

Figure 1.1 Clinically approved platinum based drugs in use worldwide

Regardless of this, chemotherapy with platinum complexes is accompanied by various side effects,[10] and their activity is often limited in many tumors due to acquired or intrinsic resistance.[11,12] Therefore, there has been an ongoing search for alternative metallo-drugs to extend the spectrum of activity and overcome some of the more severe side-effects seen with platinum therapy.[13, 14] And in this regards, ruthenium based compounds received considerable attention as many of their properties are similar to platinum. Ruthenium complexes, in particular, share similar ligand substitution kinetics as platinum(II) complexes, but unlike platinum, ruthenium favors octahedral coordination geometries, suggesting that their biological recognition, uptake, and selectivity differs from Pt(II) drugs.[23]

In general, transition metal based drugs can be broadly classified into two different categories. One in which like cisplatin, metal is bound to labile ligands, which upon loss in situ allows metal to directly bind to biological entities, usually DNA, and this activity in vivo seems to be responsible for their therapeutic action. NAMI-A [Iimidazolium [trans-imidazoledimethylsulfoxide-tetrachlororuthenate (III)] and KP1109 indazolium [trans-tetrachlorobis(1H-indazole) are two such ruthenium based drugs that have made it to clinical trials (Fig 1.2) and have shown considerable promise against metastatic tumors.[15, 16, 17,18,19.] Like platinum agents, these metallodrugs also show indiscriminate binding to a host of biological molecules that result in substantial premature drug activation and non-specific cellular degradation, which are often manifest in toxic side effects.

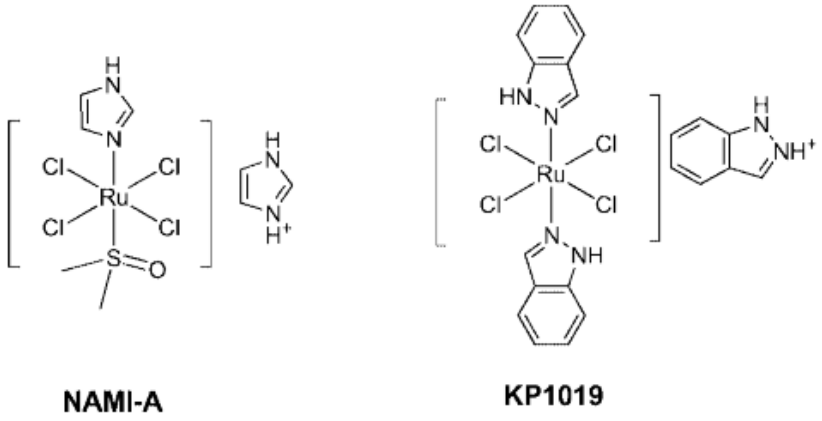

Figure 1.2 Chemical structures of substitutionally labile ruthenium drugs in clinical trials NAMI-A and KP1109

Transition metal polypyridyl complexes, on the other hand, are a class of organometallic compounds in which metal is bound to more inert N-donor polypyridine ligands such as 1,10 phenanthroline (phen) or 2,2' bipyridine (bpy) that renders them coordinatively saturated and substitutionally inert.[12] As a result, they cannot directly form bonds with biological molecules and thus remain intact in vivo.[20] Ruthenium polypyridyl complexes (RPCs) are one such class of ruthenium based drugs with $[Ru(phen)_3]^{2+}$ and $[Ru(bpy)_3]^{2+}$, shown in Fig 1.3, as classical examples of simplest RPCs.

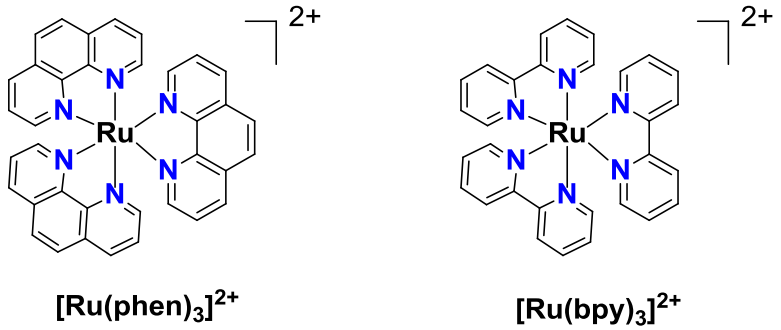

Figure 1.3 Coordinatively saturated and substitutionally inert simplest RPCs

1.2 Ruthenium Polypyridyl Complexes (RPCs) Early Studies

Dwyer and coworkers in 1950s and 60s were the first to investigate the biological activity of $[Ru(phen)_3]^{2+}$ or $Ru(bpy)_3]^{2+}$ and some very important findings of the work that laid the foundation of several studies on RPCs thereafter were as follows:

1. Both complexes were found to not only possess the antimicrobial and antiviral properties, but also arrest the growth of dispersed tumor cells (Landshultz ascites) in cultures and in mice.

2. The tumor cell viability in vitro decreased upon either increasing the lipophilicity of the complex (by substituting one phen ligand in $[Ru(phen)_3]^{2+}$ with 4,7 dimethylphen (4,7 Me_2phen) or 3,4,7,8 tetramethylphen (3,4,7,8 Me_4phen) or lowering the charge overall.[20, 21, 22, 23]

3. In vivo stability and toxicity studies using radiolabeled $[^{106}Ru(phen)_3]^{2+}$ revealed that majority of the complex (97-99%), could be recovered in urine over a period of 24 h following intraperitoneal injection (IP) and hence the biological activity was due to the intact complex overall and not due to any individual components.[24]

Despite the stability and bioactivity in vivo, development of $[Ru(phen)_3]^{2+}$ and related early RPCs as potential chemotherapeutics remained questionable due to neurotoxicity as observed in mouse studies (IP injection), which was often lethal as doses as low as 6 mg/kg mouse. Classic neurotoxin symptoms of labored breathing, tremors, seizures and paralysis which were attributed to inhibition of the enzyme acetylcholinesterase (AChE), an important enzyme necessary for proper functioning of central nervous system. Since RPCs are extremely stable in vivo and do not dissociate,[24] the enzyme interaction was perceived to be due to the electrostatics between positively charged cation unit as a whole with negative site on enzyme. Koch and Dwyer in a pioneering work on a series of substituted analogues of $[Ru(phen)_3]^{2+}$ such as $[Ru(5\text{-nitro-phen})_3]^{2+}$, $[Ru(5\text{-chloro-phen})_3]^{2+}$ and $[Ru(5\text{-methyl-phen})_3]^{2+}$ found that enzyme inhibitory action to have some dependence on the magnitude of the positive charge on metal ion. The inhibitory activity increases in the order $[Ru(5\text{-nitro-phen})_3]^{2+} < [Ru(5\text{-chloro-phen})_3]^{2+}$

< $[Ru(5\text{-methyl-phen})_3]^{2+}$ which was presumed to be due to the decrease in electrophilicity of substituted phens in the order of 5-nitro-phen > 5-chloro-phen > 5-methyl-phen, thereby decreasing the positive charge on the metal ion.[25] Since then there have been numerous studies reporting on the DNA binding, [26,27] cytotoxicity,[26, 27, 28], animal toxicity,[21, 22] antimicrobial,[29, 30] antiviral,[29, 31] and anti-tumor[20] activity of RPC's in vitro and in vivo.

Studies, in particular by Barton and coworkers, have shown that RPCs in general target DNA electrostatically, due to the presence of +2 cation, and thread into DNA helix via intercalation of the planar, aromatic polypyridine ligand. [32, 33, 34, 35]. Further it has been shown that the DNA binding increases upon attachment of a second metal center (due to higher charge)[36, 37] or increasing the length of the polypyridine ligand (due to increase in surface area resulting in better intercalation and stacking between DNA base pairs (Fig 1.4.).[36, 37, 38, 39] For example, $[Ru(phen)_3]^{2+}$ has a modest binding constant of ~ 10^3 M^{-1} owing to electrostatics and partial intercalation of polypyridine ligand [40], however, binding constants as high as ~10^{12} M^{-1} can be attained when ligands of extended planarity and aromaticity are used such as in dimetallic $[Ru(phen)_2(bidppz)Ru(phen)_2]^{2+}$ complex.[39, 41] Since majority of anticancer drugs act via disrupting most important cellular process of rapid DNA replication in cancer cells thereby inducing apoptosis, RPCs high binding affinity for DNA was considered as one important feature in their candidacy for drug development.

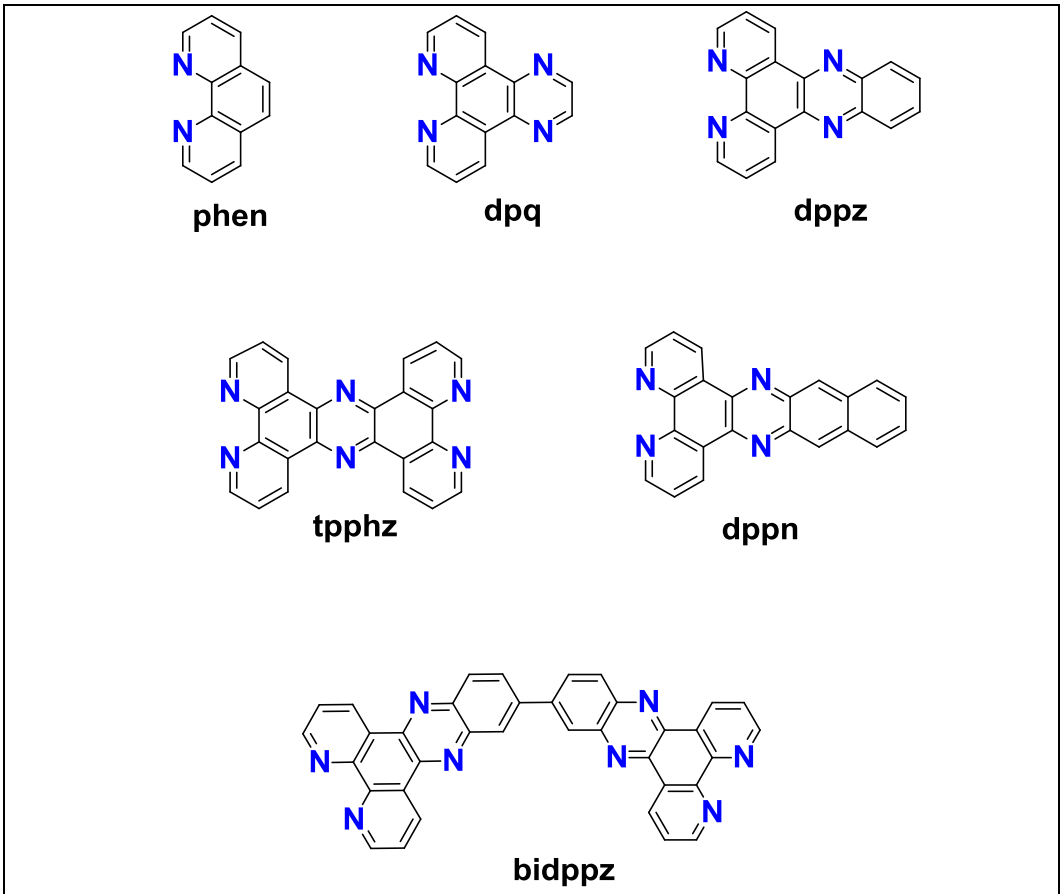

Figure 1.4 Intercalating polypyridine ligands

In vitro cytotoxicity studies of $[Ru(phen)_3]^{2+}$, $[Ru(phen)_2(dppz)]^{2+}$, $[Ru(phen)_2(tpphz)]^{2+}$ and $[Ru(phen)_2(tpphz)Ru(phen)_2)]^{4+}$against a number of common cancer cell lines such as lung carcinoma (H358), colon carcinoma (HCC226), and breast carcinoma (MCF7) reveal that these RPCs are modestly cytotoxic (IC_{50} > 50 μM)[42], while $[Ru(phen)_2(bidppz)Ru(phen)_2]^{2+}$ also effective against certain platinum resistant tumor cells. In another comparative cytotoxicity study, Schatzschneider and coworkers tested five RPCs, $[Ru(bpy)_3]^{2+}$, $[Ru(phen)_3]^{2+}$, $[Ru(phen)_2(dpq)]^{2+}$, $[Ru(phen)_2(dppz)]^{2+}$ and related complex $[Ru(phen)_2(dppn)]^{2+}$ against human colon HT-29 and human breast MCF7 cancer cell lines and found that the later exhibited high cytotoxicity of 6.4 and 3.3 μM which is comparable to cisplatin (7.0 and 2.0 μM) against both cells lines respectively.[43] Although the DNA binding and cytotoxic properties of RPCs were encouraging, but the lack of selectivity for cancer vs normal cells and high animal toxicity were two important consideration that needed to be addressed. High animal toxicity is apparent by low Maximum Tolerable Dose (MTD), which is the maximum amount of drug tolerated by animal without showing signs of sickness or morbidity, and thus, low MTDs < 6 mg/kg mouse for $[Ru(phen)_3]^{2+}$, $[Ru(phen)_2(dppz)]^{2+}$, $[Ru(phen)_2(tpphz)]^{2+}$, $[Ru(phen)_2(tpphz)Ru(phen)_2)]^{4+}$ imply high animal toxicity.[42]

While DNA binding may be a good indicator of a drug's potential as developmental chemotherapeutic, high cytotoxicity, low in vivo toxicity and selective killing of cancer cells are as much desirable attributes. Dwyer and coworkers in their pioneer work later argued that the animal toxicity was associated with the rate of perfusion through tissue and absorption into the blood stream. If this happens too rapidly, the peak blood concentration of the drug exceeds some threshold and results in acute neurotoxicity. However, if the

compound is slower at getting into the bloodstream, renal clearance and absorption rate act to prevent a peak blood concentration above the neurotoxic threshold and the drug is well tolerated without any observable side effects.[22, 25] Thus it seems plausible that the therapeutic attributes of such drugs are realizable so long as the absorption rate into blood is properly controlled.

Altering the complex lipophilicity was seen as one way of increasing the drug uptake and retention by lipophilic tissue, which was thought to slow its perfusion into the blood stream.[44, 45] This can be attained either by using lipophilic ancillary ligands such as 4,7-diphenyl-1,10-phenanthroline (DIP) or appending the intercalating ligand with lipophilic substituents. Glazer and coworkers used flow cytometry and confocal microscopy to show rapid uptake of lipophilic $[Ru(DIP)_3]^{2+}$ (Figure 1.5) by human nonsmall lung carcinoma (A549) cells in comparison to parent complex $[Ru(phen)_3)]^{2+}$, while Barton and coworkers reported on greater uptake of $[Ru(DIP)_2(dppz)]^{2+}$ complex in Hela Cells as compared to less lipophilic $[Ru(phen)_2(dppz)]^{2+}$.[46, 47] However, it was found that such modification did not decrease the animal toxicity, at least in the present case. It has also been shown that small structural changes can affect the targeting of specific cellular components and which in turn can alter the observed bioactivity.[48, 49] For example, Lincoln et al reported that $[Ru(phen)_2(dppz)]^{2+}$ derivatives $[Ru(phen)_2(dppzCH_2OC_2H_5)]^{2+}$ (D_2), $[Ru(phen)_2(dppzCH_2OC_4H_9)]^{2+}$ (D_4) and $[Ru(phen)_2(dppzCH_2OC_6H_{13})]^{2+}$ (D_6) as shown in Figure 1.5 obtained by appending dppz ligand with alkyl ether chains of varying lengths have different cellular targets. The least lipophilic complex, D_2, localized primarily in the nucleus while the most lipophilic complex, D_6 outside nucleus. Complex D_4 was evenly distributed inside the nucleus and cytoplasm as determined by in vitro luminescence experiments.[48]

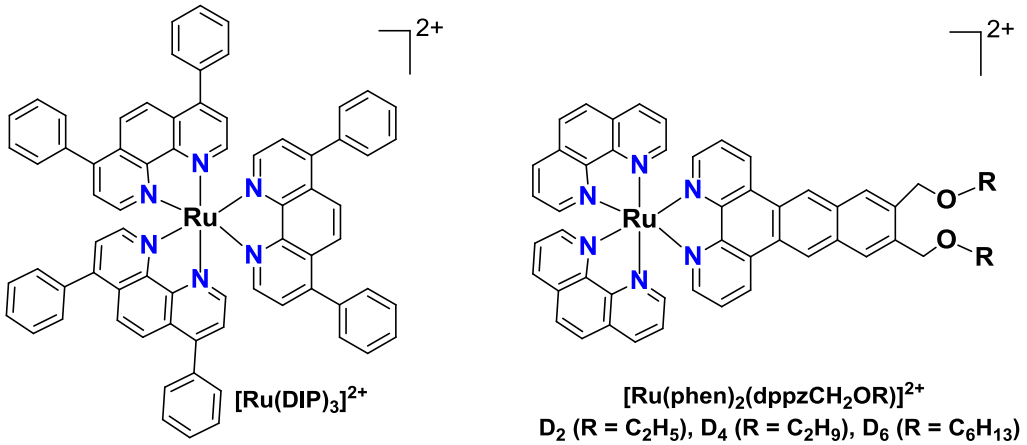

Figure 1.5 RPCs lipophilic modifications

Given the high binding affinity, nuclear DNA was generally assumed to be the prime cellular target of RPCs which Dwyer and later Barton used the inherent luminescence of $[Ru(phen)_3]^{2+}$, $[Ru(phen)_2(dppz)]^{2+}$ and established localization in mitochondria via confocal microscopy while $[Ru(phen)_2(tpphz)]^{2+}$ and $[Ru(phen)_2(tpphz)]^{4+}$ localized to some extent in nucleus and in mitochondria mostly.[50] Still, despite the strong DNA binding, none of these or related RPCs damage DNA unless photo-activated to give excited state complexes. The excited state then mediates the DNA damage, either via direct oxidation or generation of reactive oxygen species (ROS), such as hydroxyl radical or peroxides.[51, 52] Such a process has implications in photodynamic therapy (PDT) that selectively targets the irradiation of the cancerous cells in the affected area while essentially leaving the healthy cells unaffected.[53] This approach, however, has its own limitations such as for a drug to be an effective PDT agent, it must be able to reach its

intended target unmodified and be substantially less toxic in dark.[54] The major limitation of PDT is that such treatment is not systemic and the location of the tumor must be known in order to irradiate and thus activate the drug at the proper location. This strategy is valuable for the targeting of inoperable tumors but does not address the issue of micro-metastases which may be present and need be eliminated by an agents capable of circulating throughout the body and killing these lesions before they grow and spread further.

The MacDonnell group on the other hand, has reported on a unique and catalytic DNA cleavage mechanism of two RPCs $[(phen)_2Ru(tatpp)]^{2+}$ ($[\mathbf{MP}]^{2+}$) and $[phen)_2Ru(tatpp)Ru(phen)_2]^{4+}$ ($[\mathbf{P}]^{4+}$), shown in Figure 1.6, and their potential not as PDT agents but instead as systemic chemotherapeutics.

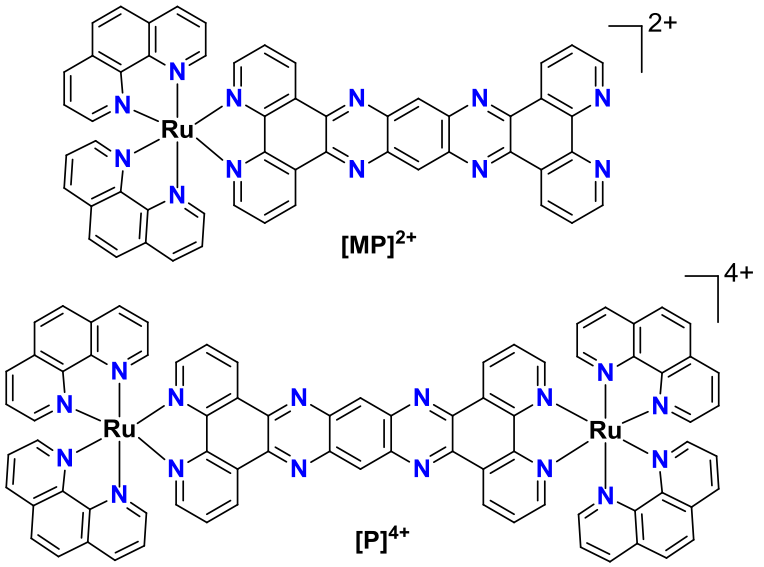

Figure 1.6 Ru(II) tatpp complexes $[\mathbf{P}]^{4+}$ and $[M\mathbf{P}]^{2+}$

These RPCs are DNA metallointercalators which are chemically activated by a reaction with cellular reducing agents, such as γ-L-Glutamyl-L-cysteinylglycine (GSH), to form a corresponding radical species $[(phen)_2Ru(tatpp^{\cdot-})]^{+}$ and $[phen)_2Ru(tatpp^{\cdot-})Ru(phen)_2]^{3+}$ cleaves DNA by H-atom abstraction from the deoxyribose moieties.[55] In the absence of this redox-active ligand tatpp, no DNA cleavage in this manner is observed by any RPC with or without GSH, and thus tatpp, we believe is the key pharmacophore.[55, 56]

The redox-activity due to the presence of tatpp appears to be associated with the ease at which this ligand moiety is reduced by common cellular reductant such as GSH. This is shown in the plot of first reduction potential (Figure 1.7) of $[\mathbf{MP}]^{2+}$ and $[\mathbf{P}]^{4+}$ in comparison to four other RPCs (vs. NHE at pH 7.0). The redox couple of GSH to corresponding disulfide, GSSH, is indicated at -0.3 V and since only $[\mathbf{MP}]^{2+}$ and $[\mathbf{P}]^{4+}$ fall to the right of this couple, meaning only they would be reduced by GSH.[57, 58, 59] The large planar structure of tatpp places these two RPCs in the potential range in which common cellular reducing agents, such as GSH, are competent for their reduction.

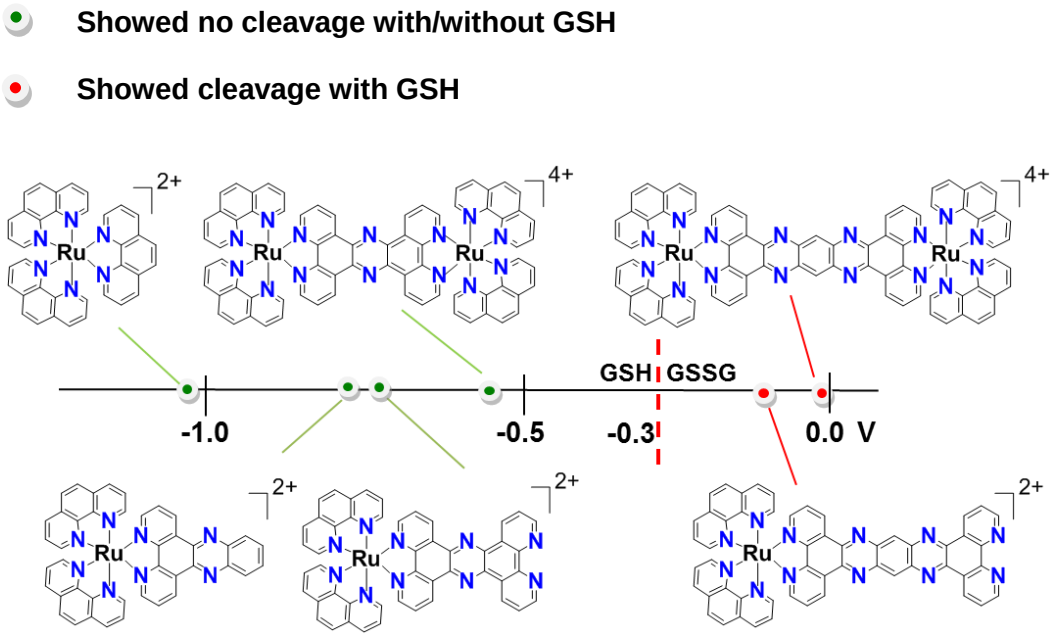

Figure 1.7 Plot of RPCs first reduction potential (vs. NHE)

The unique DNA cleavage mechanism by which [**MP**]$^{2+}$ and [**P**]$^{4+}$ are believed to induce apoptosis is shown in Figure 1.8. GSH drives the reduction of **P** to the radical species **P**$^{\bullet-}$ and finally to the doubly-reduced species **H$_2$P**. O_2 drives the oxidation of the reduced species back to **P**. The formation of **P**$^{\bullet-}$ and **H$_2$P** is thus contingent upon [GSH]/[O_2] ratio. In the complete absence of O_2, **H$_2$P** is formed quantitatively. We have demonstrated that the radical **P**$^{\bullet-}$ is the active species for DNA cleavage and acts by abstraction of an H-atom from the deoxyribose unit, leading to strand scission. Importantly, the radical **P**$^{\bullet-}$ is unstable, unless the complex is intercalated into DNA which alters the pK_a of the protonated radical. In the absence of intercalation, the radical protonates at pH 7.2 and disproportionates to give **P** and **H$_2$P** exclusively.[58] This means that the reactive radical is

only formed when complex is bound to its intended target. Moreover, when $\mathbf{P}^{\bullet-}$ is formed in presence of DNA, it is surprisingly non-reactive for a radical species and can be observed to persist for hours at room temperature by EPR spectroscopy. Eventually, the radical quenches by H-atom abstraction from both C1 and C5 positions of the neighboring deoxyribose unit. Upon H-atom abstraction, the radical $\mathbf{P}^{\bullet-}$ is not consumed but instead converted to the doubly reduced species $\mathbf{H_2P}$, which under these steady state conditions, is reoxidized in situ to form **P (**or $\mathbf{P}^{\bullet-}$) by intracellular O_2 and is therefore competent for another cycle of DNA cleavage, i.e. catalytic.[60]

This redox activity unique to the presence of tatpp somehow results in substantial increase in cytotoxicity and selectivity for malignant cells, low animal toxicity (Figure 1.9) and demonstrable tumor regression in mouse tumor models.[61]

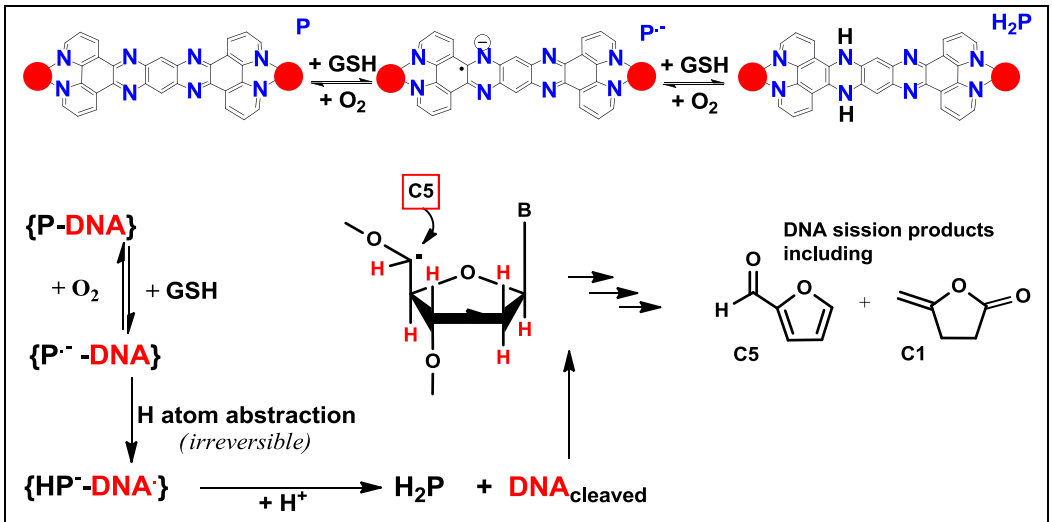

Figure 1.8 DNA Cleavage mechanism $[\mathbf{P}]^{4+}$ and $[\mathbf{MP}]^{2+}$ adapted from manuscript to be submitted.[60] Red circles indicate $[Ru(phen)_3]^{2+}$

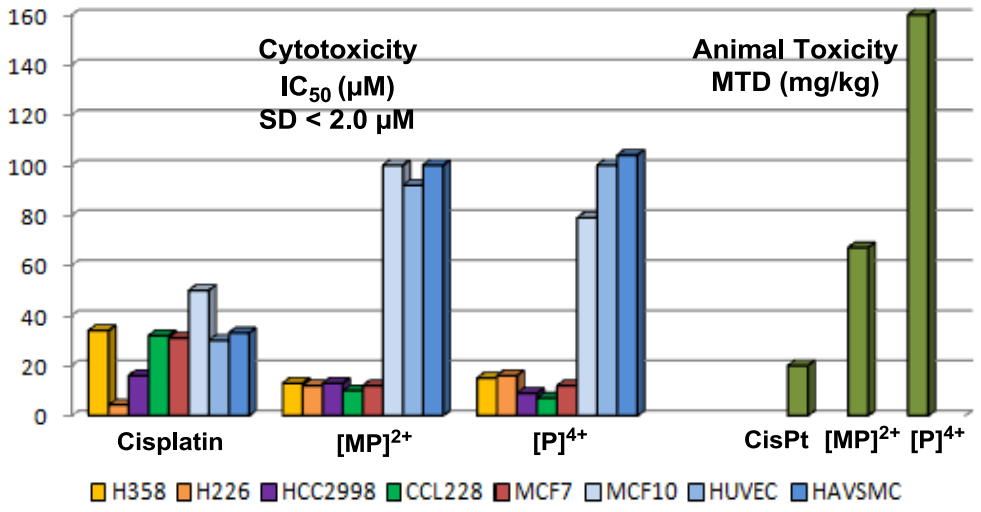

Figure 1.9 Cytotoxicity in malignant and non-malignant cells lines: $IC_{50's}$ of $[\mathbf{MP}]^{2+}$,$[\mathbf{P}]^{4+}$ and cisplatin against various malignant and non-malignant cell lines as follows: Lung Carcinomas (H358, H226), colon carcinoma (HCC2998, CCL228), breast carcinoma (MCF7), normal human Umbilical Vein Endothelial cells (HUVEC) and normal Human Aorta Vascular Smooth Muscle Cells (HASMC). Far right in green is the animal toxicity, MTD in mg drug per kg mouse of the three agents.

We postulate that the enhanced cytotoxicity of $[\mathbf{MP}]^{2+}$ and $[\mathbf{P}]^{4+}$ over other RPCs is that they not only have some activity as mitochondrial poisons (as all RPCs do) but also function as DNA cleaving agents upon reduction in vivo. We believe that this added functionality is responsible for the consistently low micromolar cytotoxicity of $[\mathbf{MP}]^{2+}$ and $[\mathbf{P}]^{4+}$ against malignant cell lines and the selectivity we see in that non-malignant cell lines such as normal human breast epithelial cells (MCF 10), Human Umbilical Vein Endothelial cells (HUVEC), Human Aorta Vascular Smooth Muscle Cells (HASMC) generally have IC_{50s} on the order of 80-120 µM. $[\mathbf{MP}]^{2+}$ and $[\mathbf{P}]^{4+}$ have also demonstrated tumor regression activity against non-small lung cell cancer (H358) tumors in nude mice. [55]

Inspired by the pioneering work of Dwyer and Barton, Alatrash and MacDonnell performed a structure-activity study, accessing the lipophilicity of terminal phen ligands on the animal acute toxicity as well as cytotoxicity of derivatives of [**MP**]$^{2+}$ and [**P**]$^{4+}$. Either 3,4,7,8-tetramethylphen (Me_4phen) or 4,7-diphenylphen (DIP) replaced the terminal phenanthroline's with the presumption that the increased complex lipophilicity would result in enhanced cytotoxicity, due to greater uptake, and lessened acute animal toxicity due to slower diffusion into the blood. While the new lipophilic analogues demonstrated comparable DNA cleavage activity and lessened animal toxicity, however, the cytotoxicity was varied, with some analogues showing increased cytotoxicity in some malignant lines, but the overall results were mixed indicating the cytotoxicity is a more complex issue. At the conclusion of the study, [**MP**]$^{2+}$ and [**P**]$^{4+}$ still demonstrated the best average cytotoxicity in the malignant lines screened and thus remained the most promising drug candidates. [42]

In present study, we examined the role of the metal $Ru(phen)_2$ fragment in the drug performance. While tatpp is insoluble alone, coordination of one or two $Ru(phen)_2$ moieties to yield [**MP**]$^{2+}$ and [**P**]$^{4+}$ makes the ligand water soluble and alters the reduction potential to, presumably, more positive values. That being said, the role of the $Ru(phen)_2$ fragment may be secondary to the drugs activity and replaceable with other metal fragments. In this thesis work, we explore the effect of replacing the $Ru(phen)_2$ fragment with an isoelectronic Re(I) ion core to prepare monometallic and dimetallic Re(I)tatpp complexes that are either neutral, +1 or +2 in charge. This can be attained by using $Re(CO)_3L$ core as depicted in Figure 1.9 where, N^N = bidentate polypyridyl ligand and L = substitutable axial ligand which could be anionic or neutral in which case n=0 or 1 respectively.

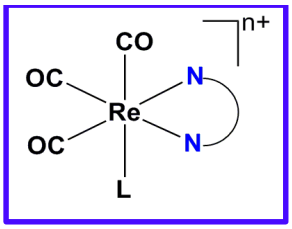

Figure 1.10 General structure of Re(I)tricarbonyl polypyridine complexes

1.3 Re(I) tricarbonyl polypyridine complexes

The motivation behind using Re(I) tricarbonyl core was multifold:

1) Re(I) polypyridine complexes of the type $Re(CO)_3(N^N)L$ are isoelectronic with Ru(II) and display similar kinetic inertness and photophysical properties common to other d^6 Ru(II), Ir(III) polypyridine systems.

2) L represents a substitutable axial ligand, (usually a pyridine derivative) that can be varied systematically to generate a series of complexes with lower charge and varying lipophilicities.

3) Synthetic flexibility

Additionally, there is growing body of literature on their potential as cellular imaging agents as well as anticancer agents due to high DNA binding, cytotoxicity and selectivity towards malignant cell lines. [62, 63] Further, in a study by Wong and coworkers they have shown that the two complexes $[Ru(^tBu_2bpy)(2\text{-appt})](PF_6)_2$ [**1**.$(PF_6)_2$] and $[Re(CO)_3(2\text{-appt})Cl]$ (**2**), containing 2-appt as the common polypyridine ligand (where 2-appt = [2-amino-4-phenylamino-6-(2-pyridyl)-1,3,5-triazine]) but differing by the presence of metal fragment core as shown in Figure 1.11 show almost similar DNA binding affinities and

bioactivity, K_b = 8.9 x 10^4 M^{-1} (1), 3.6 x 10^4 M^{-1} (2), given that complex 2 is neutral.[64] Thus we predict that the incorporation of $Re(CO)_3L$ core would not compromise the competent bioactivity that we see with [**MP**]$^{2+}$ and [**P**]$^{4+}$ but the presence of an additional coordination site, L, would rather provide biologic handles to modify aqueous solubility, lipophilicity, cellular uptake and localization as desired.

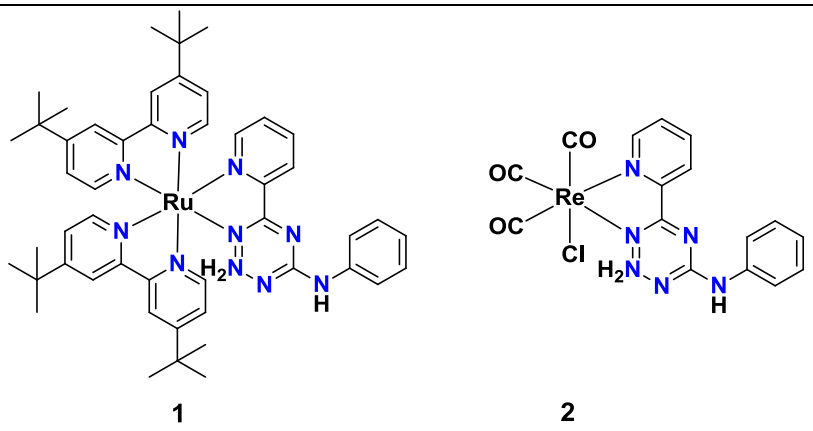

Figure 1.11 Chemical structure of complex [Ru(^{t}Bu$_2$bpy)(2-appt)](PF$_6$)$_2$ [**1**.(PF$_6$)$_2$] and [Re(CO)$_3$(2-appt)Cl] (**2**)

Various other studies have indeed used similar approaches: For example, in a collaborative work between Cheng and Lo research groups, they were able to increase the aqueous solubility of $[Re(CO)_3(N^N)L]^+$ complexes, where (N^N = phen, Me_4phen or DIP) by replacing L with polyethylene glycol (PEG).[65] Cellular uptake and localization studies by Coogan and coworkers, showed that axial ligand could be chosen so as to direct complex localization into selective cellular regions.[66] For example, chloromethylpyridine group is known to target mitochondria[67] and using laser scanning confocal microscopy they were

able to show that the $[Re(CO)_3(dppz)(3\text{-chloromethylpyridine})]^+$ complex localizes almost exclusively in mitochondria of HeLa cells.[66] While there are numerous studies reporting on the DNA binding of Re(I) polypyridine complexes, by comparison to RPCs however, there are relatively few reports on the cytotoxicity of Re(I) complexes,[66, 68, 69] and reports on their animal toxicity are only beginning to appear now.[68, 70]

1.4 Scope of Dissertation:

The goal of present work is to prepare a series of monometallic and bimetallic Re(I)tatpp analogues and study the effect of replacing the $Ru(phen)_2$ metal fragment core in $[\mathbf{MP}]^{2+}$ and $[\mathbf{P}]^{4+}$ with $Re(CO)_3L$ core on the bioactivity of tatpp ligand. Given the high DNA binding and cytotoxic properties of Re(I) polypyridyl complexes with high selectivity towards cancer cell lines and low toxicity to normal cells, we postulate that this derivatization would alter the selectivity of novel analogues in a therapeutically beneficial way without sacrificing the DNA cleavage ability unique to the presence of tatpp ligand. Additionally, we believe that the added functionality of an open coordination site, L, in $Re(CO)_3L$ core would allow us to prepare a series of closely related Re(I)tatpp analogues that are either neutral or cationic, labile or substitutionally inert, hydrophobic or hydrophilic and determine how this variation affects the bioactivity overall. Such structure activity relationships play a crucial role in establishing the ground rules for the design and development of future therapeutics.

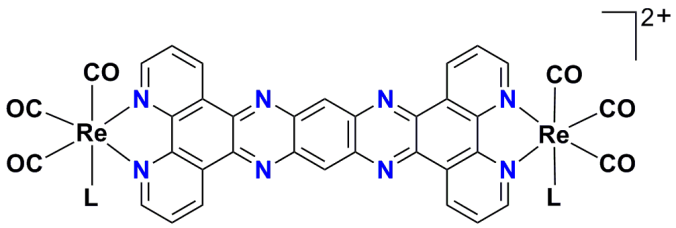

$[Re(CO)_3L(tatpp)Re(CO)_3L]^{2+}$ ($[ReP_L]^{2+}$)

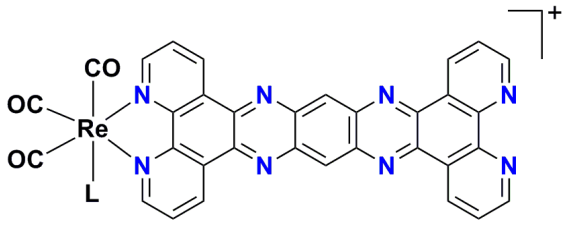

$[Re(CO)_3(tatpp)L]^{+}$ ($[MRe_L]^{+}$)

Figure 1.12 Target monometallic and bimetallic Re(I) tatpp complexes, where L = pyridine derivative such as 4-methylpyridine or 4-hydroxypyridine

The shorthand notation of **$[MRe]^{+}$** is used to signify monometallic Re(I)tatpp complex and **$[ReP]^{2+}$** for bimetallic complex. This notation is purposely chosen to keep it in line with the analogy used in naming complexes $[\mathbf{MP}]^{2+}$ and $[\mathbf{P}]^{4+}$ earlier. If the axial ligand is chloride, in which case the complexes would be neutral, the subscript ($^{+}$ or $^{+2}$) is dropped and only **[MRe]** or **[ReP]** notation is used. If axial position is taken up by a neutral ligand such as CH_3CN, 4-methylpyridine or 4-hydroxypyridine, subscripts CH_3CN, 4-CH_3Py or 4-

OHPy are used to indicate the nature of the ligand at that position, for example, **[ReP$_{CH3CN}$]$^{2+}$** notation would denote [(CH$_3$CN)Re(CO)$_3$(tatpp)Re(CO)$_3$(CH$_3$CN)]$^{2+}$ complex.

In Chapter 1, pertinent literature and recent advances in the use of metal based pharmaceuticals in cancer treatment are discussed. In particular, the importance of RPCs and Re(CO)$_3$L polypyridyl complexes to this area and their relevance to the basis of this project is outlined.

Chapter 2 describes the synthesis and characterization of a series of Re(I) tricarbonyl polypyridyl complexes such as [Re(CO)$_3$Cl(tatpp)] (**[MRe]),** [Re(CO)$_3$Cl(tatpp) Re(CO)$_3$Cl] (**[ReP]),** [Re(CO)$_3$(CH$_3$CN)(tatpp)Re(CO)$_3$(CH$_3$CN)]$^{2+}$ (**[ReP$_{CH3CN}$]$^{2+}$**), Re(CO)$_3$(dadppz)Cl, [Re(CO)$_3$(4-OPyH)(phen-5,6-dione)][PF$_6$] (**[Redione$_{4\text{-}OPyH}$]**), [Re(CO)$_3$(phendione)(CH$_3$CN)][PF$_6$] (**[Redione$_{CH3CN}$]$^{+}$**), [Re(CO)$_3$(phendione)(4-methylpyridine)][ClO$_4$] (**[Redione$_{4\text{-}CH3Py}$]$^{+}$**), with phendione or tatpp as the bisimine ligand and varying axial ligands via ^{1}H NMR, ESI-HRMS, IR, CHN and in some cases by X-Ray crystallography. The rhenium complexes often had poor solubility overall, even in organic solvents, making their study difficult. They also were far more susceptible to air oxidation, photooxidation, and dimerization indicating that the tatpp ligand was 'activated' relative to the ruthenium analogues. The oxidation product of **[ReP$_{CH3CN}$]$^{2+}$** is a quinone species [(CH$_3$CN)Re(CO)$_3$(tatpq)Re(CO)$_3$(CH$_3$CN)]$^{2+}$ (**[ReQ$_{CH3CN}$]$^{2+}$**) and dimerization product is the 'dimer of dimers' [Re$_4$(CO)$_{12}$(*tatpp*)$_2$(CH$_3$CN)$_4$](PF$_6$)$_4$ (**[d-ReP$_{CH3CN}$]$^{4+}$**). Relevant ^{1}H NMR, ESI-HRMS, IR, CHN data to support such reactivity is also presented.

In Chapter 3 we explore the utility of two heterobimetallic Ru(II)-Re(I) tatpp complexes [(phen)$_2$Ru(tatpp)Re(CO)$_3$(CH$_3$CN)]$^{3+}$ (**[RuRe$_{CH3CN}$]$^{3+}$**) and [(phen)$_2$Ru(tatpp)Re(CO)$_3$(P(CH$_2$OH)$_3$)]$^{3+}$ (**[RuRe$_{PR3}$]$^{3+}$**) which display intermediate properties relative to the all ruthenium and all rhenium complexes. In this respect, they

have more favorable solubility in aqueous solution than the rhenium complexes and lessened sensitivity to air oxidation or photooxidation. While lessened, **[RuRe$_{CH3CN}$]$^{3+}$** will undergo photooxidation to respective quinone analogue **[RuReQ$_{CH3CN}$]$^{3+}$** after prolonged irradiation in air while the related compound [**MP**]$^{2+}$ shows no such reactivity even after 72 h of irradiation under identical conditions. Screening of both complexes, **[RuRe$_{CH3CN}$]$^{3+}$** and **[RuRe$_{PR3}$]$^{3+}$** for DNA cleavage and **[RuRe$_{PR3}$]$^{3+}$** complex for cytotoxicity towards common malignant cell lines is also presented and discussed. As expected, both analogues cleave DNA under reducing conditions with **[RuRe$_{CH3CN}$]$^{3+}$** inducing the most. Acute animal toxicity as determined by MTD reveal that **[RuRe$_{PR3}$]$^{3+}$** is safe at levels up to >160 mg drug/kg mouse and with no obvious side effects, when administered via IP injection. While [**MP**]$^{2+}$ is relatively toxic (MTD < 40 mg/kg), it appears that the attachment of a second metal center has an advantage of lowering the acute animal toxicity independent of metal fragment core used, at least in the present case. Biodistribution profile as apparent by visual analysis of various organs 24 h post injection revealed that the drug accumulates in the heart, kidney, lungs and intraperitoneal tissues initially but no build up was observed in mice sacrificed 12 days after the last dose administered suggesting body clearance gradually.

Chapter 4 focusses on representative HPLC studies to establish the purity and unexpected fluorescence of heterobimetallic **[RuRe$_{CH3CN}$]$^{3+}$** and **[RuRe$_{PR3}$]$^{3+}$** complexes. Cellular colocalization study using confocal microscopy to demonstrate the accumulation of **[RuRe$_{PR3}$]$^{3+}$** in the nucleus of H358 lung carcinoma cells is also presented.

Chapter 2

SYNTHESIS, CHARECTERIZATION AND REACTIVITY OF RE(I) POLYPYRIDINE COMPLEXES

2.1 Introduction

The success of platinum-based chemotherapeutics[71] has led to the search for new drugs based on other metal complexes. In particular, ruthenium complexes have enjoyed extensive attention due to similar substitution kinetics as seen in Pt(II) complexes yet possessing an octahedral coordination sphere which alters its biological specificity and toxicity.[72, 73] Two Ru(III) complexes, imidazolium [trans-imidazoledimethylsulfoxide-tetrachlororuthenate (III)] (NAMI-A) and indazolium [trans-tetrachlorobis(1H-indazole) ruthenate(III)] (KP1019) have advanced to Stage 1 clinical trials and appear to be well-tolerated and potentially efficacious in some instances. Interestingly, unlike cisplatin, neither KP1019 nor NAMI-A appear to act on DNA, revealing that these ruthenium complexes differ in mechanism considerably from that of platinum.[74, 75]

RPCs became a widely studied class of anticancer drugs in recent years due to their strong interactions with DNA. Owing to their inert nature and lack of labile leaving groups, RPCs differ from the well-established platinum-based drugs such as cisplatin and the recent ruthenium-based drug IT-139[6] which function via the loss of labile chloride ligands, in that the nature of their interaction with biomolecules is purely physical.

Regarding their potential as drugs, Dwyer and coworkers in 1950's and Becarri in 1960s were the first to report on the antiproliferative activity of simplest RPC $[Ru(phen)_3]^{2+}$ in vitro, but it was the acute animal toxicity in vivo leading to death shortly after IP injection that posed a big challenge.[76] Later it was shown that the animal toxicity could be modified

by increasing the lipophilicity of the complexes. Toxicity studies using monovalent mixed ligand complex (MML), such as $[Ru(phen)_2(acac)]^+$ (shown in Fig. 2.1, where acac = acetylacetonato ligand) revealed that this complex was significantly less toxic and led to a more gradual and unidentified type of death at high doses. Following these early findings, a detailed in vitro study on DIL and MML complexes in which polypyridine ligand was varied from 1,10-phenanthroline to its methyl substituted analogues shown in Figure 2.1, was undertaken. The results of the study indicated dramatic increase in the cytocidal potency for MML complexes and was speculated to be due to the lower overall charge of the complexes. The increase in bioactivity showed a strong correlation with lipophilicity in that $[Ru(3,4,7,8\text{-tetramethylphen})_2(acac)]^+$ and $[Ru(3,5,6,8\text{-tetramethylphen})_2(acac)]^+$ showed greater inhibition of P388 leukemia cells. [77]

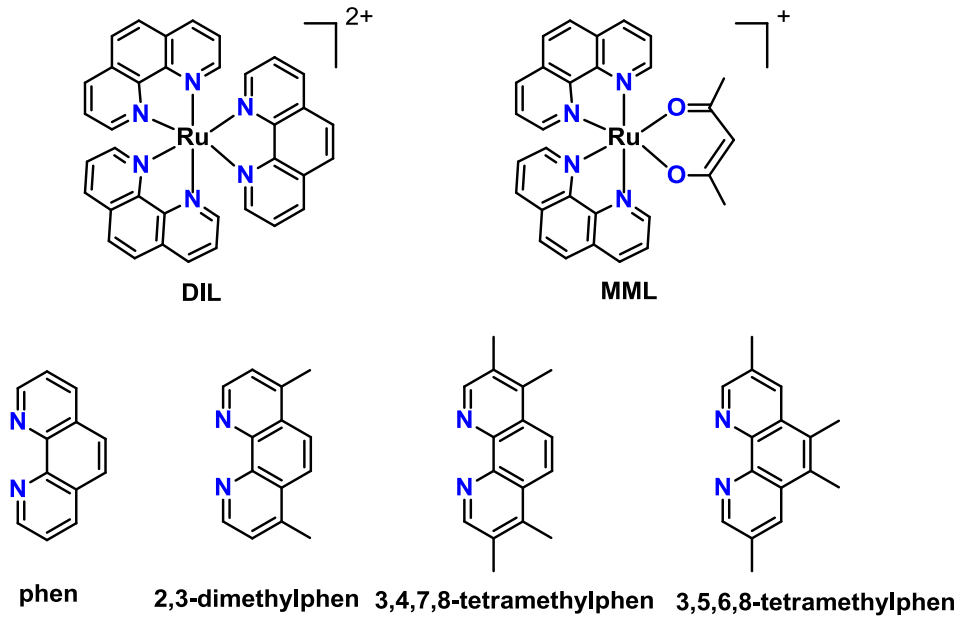

Figure 2.1 DIL $[Ru(N^N)_3]^{2+}$ and MML $[Ru(N^N)_2(acac)]^{+}$ analogues

More recently, our research group has shown that RPCs $[\mathbf{MP}]^{2+}$ and $[\mathbf{P}]^{4+}$ (Fig 1.6) are promising anticancer drugs with DNA cleavage activity, high cytotoxicity and selectivity, low animal toxicity and demonstrable tumor regression in mouse tumor models. Much of the anti-tumor activity is presumed to be primarily due to the presence of redox active ligand unit tatpp that binds to DNA via intercalation and is then reduced to a species that cleaves DNA.[55, 61] Since increased lipophilicity and lower overall charge of RPCs has been anticipated to be correlated with increased cytocidal potency and lower animal toxicity, we became interested in exploring the substitution of the Ru(II) ion in $[P]^{4+}$and $[MP]^{2+}$ with isoelectronic Re(I) ion to make Re(I) tatpp complexes with lower overall charge, as shown in Figure 2.2.

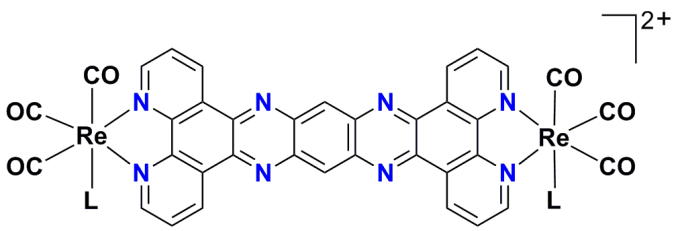

$[Re(CO)_3L(tatpp)Re(CO)_3L]^{2+}$ ($[ReP_L]^{2+}$)

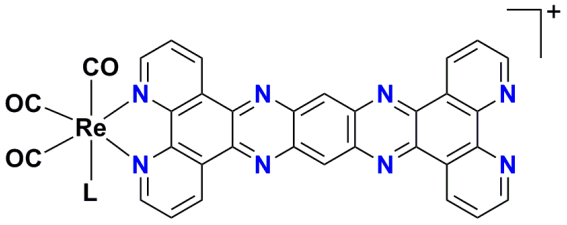

$[Re(CO)_3(tatpp)L]^{+}$ ($[MRe_L]^{+}$)

Figure 2.2 Target monometallic and bimetallic Re(I) tatpp complexes, where L = pyridine derivative such as 4-methylpyridine or 4-hydroxypyridine

We postulate that these novel Re(I)tatpp complexes will hopefully retain the useful antitumor activity due to the presence of tatpp while potentially exhibiting a different spectrum of cytotoxicity and animal toxicity. Such a study would also allow us to study the effect of changing the metal fragment core on the bioactivity of the essential pharmacophore, tatpp.

In this chapter, we report on the synthesis and characterization of monometallic and bimetallic Re(I) tatpp analogues of $[\mathbf{MP}]^{2+}$ and $[\mathbf{P}]^{4+}$, as well as various Re(I) phendione

analogues. We also report on the unusual and unexpected reactivity of complex $[Re(CO)_3(CH_3CN)(tatpp)(CH_3CN)(CO)_3Re][PF_6]_2$ - **$[ReP_{CH3CN}]^{2+}$**.

2.2 Experimental

2.2.1 General Methods

Compounds $Re(CO)_5Cl$, $AgPF_6$, $AgClO_4$, 1,10-phenanthroline (phen), 4-hydroxypyridine, 4-methylpyridine, 1,2,4,5-benzenetetraamine tetrahydrochloride, hydrated ruthenium(III) chloride were purchased from either Sigma Aldrich or Alfa Aesar and used as such. All solvents were reagent grade and used as received unless otherwise indicated. All ligands, 4,5-dinitro-N^1,N^2-ditosyl-o-phenylenediamine[78], 4,5-dinitro-*o*-phenylenediamine[78], 11,12-diaminodipyridophenazinedadppz (dadppz)[78], 1,10-phendione (phendione)[79], 9,11,20,22-tetraazatetrapyridopentacence (tatpp)[80] were synthesized as per literature methods. Complexes $[Ru(phen)_2(phendione)][Cl]_2$ and $Re(CO)_3(phendione)Cl$ were prepared following literature procedures.[38, 81] Unless otherwise indicated, all synthesis were conducted under N_2 and in dark environment.

2.2.2 Physical Measurements

^1H and ^{13}C NMRs were recorded on JEOL Eclipse 500 MHz spectrophotometer. Chemical shifts are reported in ppm and referenced to $(Me)_4Si$ as standard. FTIR spectra were recorded on Bruker Vector 22 FT-IR spectrometer as KBR pellets. ESI-HRMS were recorded on a Shimadzu LCMS IT-TOF at the Schimadzu Center for Advanced Analytical Chemistry (SCAAC) at UTA. UV-Vis spectra were obtained on a Hewlett-Packard HP8453A spectrophotometer in MeCN. ^1H NMR and IR annotations used: s = singlet, d = doublet, t = triplet, m = multiplet, br = broad

2.2.3 Synthesis of complexes

2.2.3.1 $Re(CO)_3$(dadppz)Cl

The synthesis of this complex was carried out by a slight modification of the literature method.[82] A suspension of $Re(CO)_5Cl$ (0.14 g, 0.038 mmol) and dadppz (0.10 g, 0.032 mmol) was stirred at reflux in EtOH (100 mL) for 18 h and subsequently cooled to room temperature. The deep red brown solution was filtered off and the supernatant concentrated to a minimum volume (~5 mL) under reduced pressure. Product was isolated by dropwise addition of Et_2O, collected by filtration, washed with 30 mL of $CHCl_3$ and air dried (0.17 g, 86% yield). ^{1}H NMR (500 MHz, dmso-d_6, δ) 9.70 (2H, d, J = 8.3 Hz), 9.38 (2H, d, J = 4.9 Hz), 8.14 (2H, dd, J_1 = 8.0 Hz, J_2 = 5.2 Hz), 7.20 (1H, s), 6.62 (4H, s). IR (υ_{CO}, KBR pellet, cm-1): 2022 (s), 1883 (br).

2.2.3.2 $Re(CO)_3Cl$(tatpp)$Re(CO)_3Cl$ - **[ReP]**

Method A: A suspension of 0.16 g (0.26 mmol) of Re(dadppz)$(CO)_3Cl$ and 0.21 g (0.41 mmol) of $Re(CO)_3$(phendione)Cl in 100 mL of EtOH and 10 mL of acetic acid was heated at reflux for 18 h. The precipitate formed was collected by suction filtration, washed with 100 mL ethanol followed by 20 mL acetone. The residue obtained was recrystallized in $CHCl_3$ and air dried to afford the pure product as dark red brown solid (0.22 g, 77 % yield).

Method B: A suspension of 0.33 g (0.92 mmol) of $Re(CO)_5Cl$ and 0.15 g (0.31 mmol) of tatpp was stirred at reflux in 200 mL of dry toluene for 6 d. The dark red brown precipitate formed was collected by suction filtration, washed with 100 mL ethanol and recrystallized in $CHCl_3$ to afford the pure product as dark red brown solid (0.18 g, 54 % yield). ^{1}H NMR (500 MHz, $CDCl_3$, δ) 9.95 (4H, d, *J* = 8.6 Hz), 9.70 (2H, s), 9.52 (4H, d, *J* = 5.2 Hz), 8.10 (4H, dd, J_1 = 8.0 Hz, J_2 = 5.2 Hz). HRMS-ESI $[M]^+$ calc. 1097.9528, observed. 1097.9212.

IR (U_{CO}, KBR pellet, cm^{-1}): 2013 (s), 1872 (br). Anal. Calcd for $C_{36}H_{14}Cl_2N_8O_6Re_2.0.7CHCl_3$: C, 37.31; H, 1.25; N, 9.48; Found: C, 37.63; H, 0.83; N, 9.00.

2.2.3.3 $[Re(CO)_3(CH_3CN)(tatpp)(CH_3CN)(CO)_3Re][PF_6]_2$ - **$[ReP_{CH3CN}]^{2+}$**

A mixture of 0.10 g (0.09 mmol) of $[Re(CO)_3Cl(tatpp)Re(CO)_3Cl]$ and 0.23 g (0.91 mmol) of $AgPF_6$ was heated at reflux in 200 mL of dry CH_3CN for 24 h in dark. After cooling, the solution was filtered to remove AgCl and filtrate concentrated to ~5 mL by rotary evaporation. The crude product was then obtained by dropwise addition of Et_2O, collected by suction filtration, washed with ethanol (30 mL) followed by 1:10 CH_3OH:CH_2Cl_2 (50 mL) and air dried to yield the product as deep red solid (0.05 g, 40 % yield). ^1H NMR (500 MHz, CD_3CN, δ) 10.01 (4H, d, J = 8.3 Hz), 9.74 (2H, s), 9.52 (4H, d, J = 5.2 Hz), 8.27 (4H, dd, J_1 = 8.3 Hz, J_2 = 5.2 Hz), 2.17 (6H, s). HRMS-ESI $[M-2PF^6]^{2+}$ calc. 555.0383, observed. 555.0289. IR (U_{CO}, KBR pellet, cm^{-1}): 2036 (s), 1914 (br). Anal. Calcd for $C_{40}H_{20}F_{12}N_{10}O_6P_2Re_2.5CH_2Cl_2$: C, 29.64; H, 1.66; N, 7.68. Found: C, 29.50; H, 1.29; N, 8.18.

2.2.3.4 $[Re(CO)_3(CH_3CN)(tatpq)(CH_3CN)(CO)_3Re][PF_6]_2$ - **$[ReQ_{CH3CN}]^{2+}$**

A solution of 0.02 g (0.36 mmol) of $[Re(CO)_3(CH_3CN)(tatpp)(CH_3CN)(CO)_3Re][PF_6]_2$ in 40 mL MeCN was irradiated with LED light (470 $\pm$ 15 nm) for 24 h in presence of air. The orange red solution was filtered and the supernatant concentrated to approximately 5 mL volume under reduced pressure. To this, Et_2O was added dropwise to obtain a red precipitate which was collected by filtration, washed with 100 mL EtOH, 5 mL THF and air dried to afford the product as deep red solid (0.016 g, 82 % yield). ^1H NMR (500 MHz, CD_3CN, δ) 9.98 (4H, d, J = 8.3 Hz), 9.61 (4H, d, J = 5.2 Hz), 8.33 (4H, dd, J_1 = 8.1 Hz, J_2 = 5.2 Hz). Methyl protons for CH_3CN were seen at (500 MHz, CD_3COCD_3, δ) 2.19 (3H, s).

HRMS-ESI $[M-2PF_6]^{2+}$ calc. 570.0254, observed. 570.0212, IR (U_{CO}, KBR pellet, cm^{-1}): 2041 (s), 1938 (br), 1710 (s). Anal. Calcd for $C_{40}H_{18}F_{12}N_{10}O_8P_2Re_2.\ 4H_2O$: C, 32.01; H, 1.75; N, 9.33. Found: C, 32.44; H, 1.92; N, 8.63.

2.2.3.5 $Re(CO)_3$(tatpp)Cl - **[MRe]**

A solution of complex $Re(CO)_5Cl$ (60 mg, 0.01 mmol) and phendione (20 mg, 0.11 mmol) was heated at reflux in 100 mL of EtOH and 10 mL of CH_3COOH overnight. The precipitate formed was collected by suction filtration, washed with 200 mL EtOH, followed by 20 mL acetone and air dried to obtain the pure product as a red brown solid. (0.067 g, 85 % yield). Anal. Calcd for $C_{33}H_{14}ClN_8O_3Re.0.5H_2O$.: C, 49.47; H, 1.89; N; 13.99. Found: C, 49.28; H, 1.78; N, 14.15. HRMS-ESI ($[M]^-$) calc. 792.0440, observed: 792.0483.

2.2.3.6 $[Re(CO)_3(4\text{-}OPyH)(phendione)][PF_6]$ – **$[Redione_{4\text{-}OPyH}]^+$**

A solution of $Re(CO)_3$(phendione)Cl (0.10 g, 0.20 mmol), $AgPF_6$ (0.07 g, 0.30 mmol) and 4-hydroxypyridine (0.03 g, 0.30 mmol) was refluxed in 30 mL DCM for 12 h. The precipitated AgCl was removed by filtration and supernatant concentrated to ~5 mL volume under reduced pressure. To this, Et_2O was added dropwise to precipitate the crude product which was collected by suction filtration, washed with 100 mL H_2O, 5 mL EtOH and air-dried to yield the pure product as deep yellow solid. X-Ray quality crystals were obtained by slow vapor diffusion of Et_2O in CH_3CN solution (0.21 g, 74% yield). ^1H NMR (500 MHz, CD_3CN, δ) 9.22 (2H, d, J = 5.4 Hz), 8.75 (2H, d, J = 8.0 Hz), 7.86 (4H, m), 6.60 (2H, d, J = 7.5 Hz). HRMS-ESI ($[M-PF_6]^+$) calc. 576.0247, observed. 576.0174. IR (U_{CO}, KBR pellet, cm^{-1}): 2029 (s), 1930 (s), 1896 (s), 1703 (s). Anal. Calcd for $C_{20}H_{11}F_6N_3O_6PRe$: C, 33.34; H, 1.54; N, 5.83. Found: C, 33.41; H, 1.32; N, 6.16.

2.2.3.7 $[Re(CO)_3(phendione)(CH_3CN)][PF_6]$ – **$[Redione_{CH3CN}]^+$**

A solution of $Re(CO)_3(phendione)Cl$ (0.20 g, 0.40 mmol) and $AgPF_6$ (0.15 g, 0.60 mmol) in CH_3CN (30 ml) was refluxed for 12 h in dark. The precipitated AgCl was removed by filtration and solution reduced to ~5 mL by rotary evaporation. To this, Et_2O was added dropwise to yield an orange solid which was collected by vacuum filtration, washed with 50 mL $CHCl_3$, 30 mL Et_2O and air dried to yield the pure product as red solid. X-Ray quality crystals were obtained by layering hexane over CH_3CN solution X-Ray quality crystals were obtained by layering hexane over CH_3CN solution (0.0.241 g, 93 % yield). ^1H NMR (500 MHz, CD_2Cl_2, δ): 9.18 (2H, d, J = 5.4 Hz), 8.83 (2H, d, J = 8.0 Hz), 7.91 (2H, dd, J_1 = 8.0 Hz, J_2 = 5.2 Hz), 2.23 (3H, s)**.** HRMS-ESI ($[M\text{-}PF_6]^+$) calc. 522.0142, observed. 522.0078. IR (U_{CO}, KBR pellet, cm^{-1}): 2033 (s), 1908 (br), 1896 (s), 1704 (s). Anal. Calcd for $C_{17}H_9F_6N_3O_5PRe.CHCl_3$: C, 27.51; H, 1.28; N, 5.35. Found: C, 28.21; H, 1.70; N, 5.43.

2.2.3.8 $[Re(CO)_3(phendione)(4\text{-methylpyridine})][ClO_4]$ – **$[Redione_{4\text{-}CH3Py}]^+$**

A mixture of of $Re(CO)_3(phendione)Cl$ (0.12 g, 0.23 mmol), $AgClO_4$ (0.34 g, 1.63 mmol) and 4-methlypyridine (0.15g, 1.63 mmol) in 20 mL toluene was heated at reflux overnight. To this, 20 mL of hexane was added and precipitate containing the product and AgCl was collected by filtration, redissolved in ~5 mL CH_3COCH_3 and filtered to remove the insoluble AgCl. Dropwise addition of Et_2O to the supernatant resulted in a precipitate which was collected by suction filtration, washed with 200 mL of Et_2O and 50 mL hexane. X-Ray quality crystals were obtained by slow evaporation of the product in CH_3COCH_3 solution. ^1H NMR (500 MHz, $(CD_3)_2CO$, δ): 9.71 (2H, d, J = 5.45 Hz), 8.89 (2H, d, J = 8.03 Hz), 8.48 ($2H_{py}$, d, J = 6.9 Hz), 8.23 (2H, dd, J_1 = 8.03 Hz, J_2 = 5.73 Hz), 7.31 ($2H_{py}$, d, J = 6.3 Hz), 2.32 ($3H_{py}$, s). HRMS-ESI ($[M\text{-}PF_6]^+$) calc. 575.0491, observed. 575.0327

2.2.3.9 $[Re(CO)_3(tatpp)X]^+$ **- $[MRe_x]^+$**

$[Re(CO)_3(4\text{-}OPyH)(phendione)][PF_6]$ (0.05 g, 0.08 mmol) and dadppz were dissolved in 100 mL of EtOH and 10 mL of CH_3COOH and stirred at reflux overnight. The resulting suspension was filtered hot via suction filtration and residue washed with 100 mL EtOH, followed by 50 mL hexane and air dried to afford $[Re(CO)_3(tatpp)X]^+$ as red brown solid ^1H NMR (500 MHz, $CDCl_3$:CH_3COOH (90:10), δ): 10.12 (2H, d, J = 8.0 Hz), 9.99 (2H, d, J = 8.35 Hz), 9.73 (2H, s), 9.60 (2H, d, J = 5.15 Hz), 9.42 (2H, d, J = 5.15 Hz), 8.31 (2H, d, J_1 = 8.03 Hz, J_2 = 5.73 Hz), 8.14 (2H, d, J_1 = 8.6 Hz, J_2 = 5.15 Hz). IR (υ_{CO}, KBR pellet, cm^{-1}): 2018 (s), 1881 (br).

2.2.4 Photolysis

Photochemical reactions were performed in a standard 5 mm NMR tube which was irradiated in a custom built photoreactor that has been described previously.[83] In short, it consists of one hundred and twenty, 5 mm LED's with an emission wavelength of 470 $\pm$ 15 nm, arranged in a circle about a 25 mm diameter cavity. In a typical NMR scale experiment, a solution of 1.0 mg of complex in 1.0 mL of CD_3CN is placed in a 5 mm diameter NMR tube and the sealed tube placed in a photoreactor at ambient temperature. The reaction progress was monitored by removing the sample and obtaining a ^1H NMR spectrum approximately every 15 min.

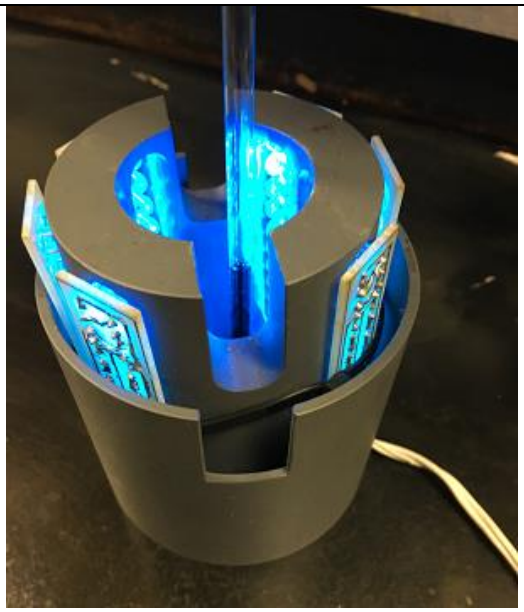

Figure 2.3 Demonstration of NMR scale photooxidation process in photoreactor

2.3 Results and Discussion

2.3.1 Synthesis of dinuclear Re(I) polypyridyl complexes

The synthesis of neutral Re(I) polypyridine complexes of the type $Re(CO)_3Cl(N^N)$ where N^N = polypyridine ligand such as phen or bpy, is very well documented in literature[81, 84, 85] In general, they are prepared by two different methods :

1. Either via complexation of the free polypyridine ligand with equimolar amount or slight excess of $Re(CO)_5Cl$ in a suitable solvent, generally toluene, as utilized by Bates et al[86] for the preparation of $Re(CO)_3Cl(dppz)$ complex (where dppz = dipyridophenazine). Another study by Waterland et al used similar approach but dry methanol as a solvent to prepare $Re(CO)_3(dppz)Cl$ complex. [87]

2. Or via Schiff's base condensation reaction of $Re(CO)_3$(phendione)Cl complex, itself prepared as described by Bates et al[86], with derivatized ortho-phenylenediamine or ortho-diamine ligand of choice as utilized by Stoeffler et al[88] for the synthesis of $Re(CO)_3$(dppz)Cl complex.

The binuclear Re(I) tatpp complex [**ReP**] was obtained in modest yields by both the methods discussed above. The synthetic strategy to both methods is depicted in Figure 2.4. Due to the poor solubility of the tatpp ligand, the ligand displacement Method A is only moderately successful with a 54% yield. The longer route, Method B, of building up the complex from the phendione complex, gives a 77% yield, but the extra steps make Method A generally preferable. Complex [**ReP**] is only sparingly soluble in most common solvents, but soluble enough in chloroform to record its NMR spectrum. Complex $Re(CO)_3$(dadppz)Cl was prepared by a slight modification of literature method in that the free dadppz was allowed to react with a slight excess of $Re(CO)_5Cl$ in refluxing ethanol (in comparison to toluene) for 48 h, which resulted in better yield .

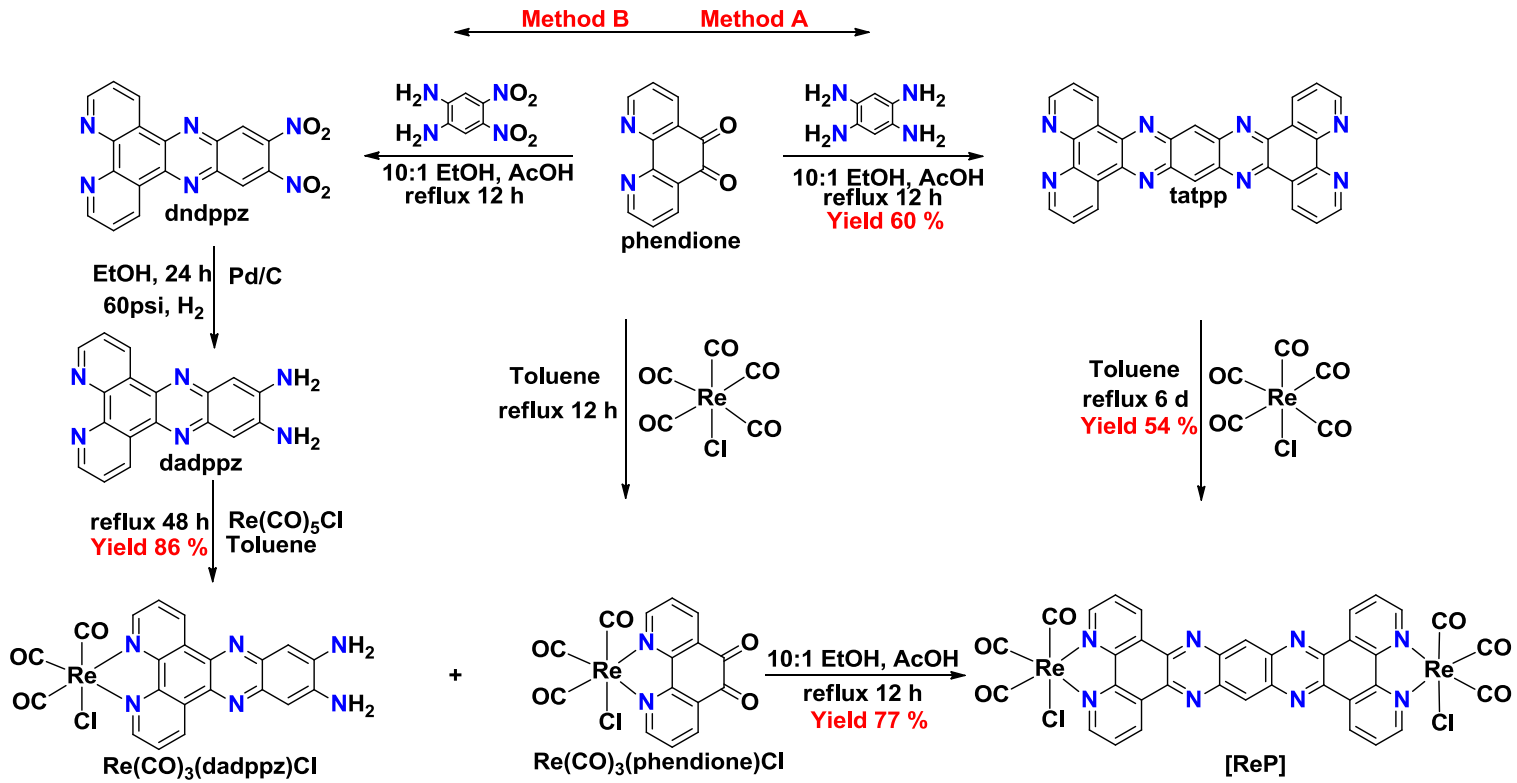

Figure 2.4 Reaction pathways for synthesis of complex [ReP]

$Re(CO)_3Cl(N^N)$ complexes may then undergo ligand exchange reaction by refluxing with an excess of axial ligand of choice (for example, pyridine) in presence of silver salt such as $AgPF_6$ or $AgBF_4$ in DMF as employed by Stoeffler et al[88] to prepare $[Re(CO)_3(4\text{-methylpyridine})(dppz)]^+$ complex. However, recent work by Coogan and coworkers has indicated that the activation of the neutral $Re(CO)_3Cl(N^N)$ complexes as acetonitrile derivatives $[Re(CO)_3(CH_3CN)(N^N)]^+$ via halide abstraction by silver salt may be desirable to facilitate the coordination of pendant pyridine.[67, 89] In our case, attempts to generate acetonitrile coordinated reactive intermediate $[\mathbf{ReP_{CH3CN}}]^{2+}$ by reacting [**ReP**] with $AgPF_6$ in refluxing MeCN gave unusual results, in that, both the binuclear complex $[\mathbf{ReP_{CH3CN}}]^{2+}$ and its tetranuclear dimer $[d\text{-}\mathbf{ReP_{CH3CN}}]^{4+}$ are obtained, upon ether precipitation. This complex mixture was freely soluble in MeCN as PF_6^- salt and underwent photooxidation to form the quinone analogue $[\mathbf{ReQ_{CH3CN}}]^{2+}$ upon visible light irradiation under aerobic conditions. Alternatively, a pure sample of $[\mathbf{ReP_{CH3CN}}]^{2+}$ as obtained by washing the complex residue of $[\mathbf{ReP_{CH3CN}}]^{2+}$ and dimer $[d\text{-}\mathbf{ReP_{CH3CN}}]^{4+}$ with 1:10 CH_3OH:CH_2Cl_2 also formed the photoproduct $[\mathbf{ReQ_{CH3CN}}]^{2+}$ under identical conditions of irradiation. This unusual reactivity is summarized in Figure 2.5.

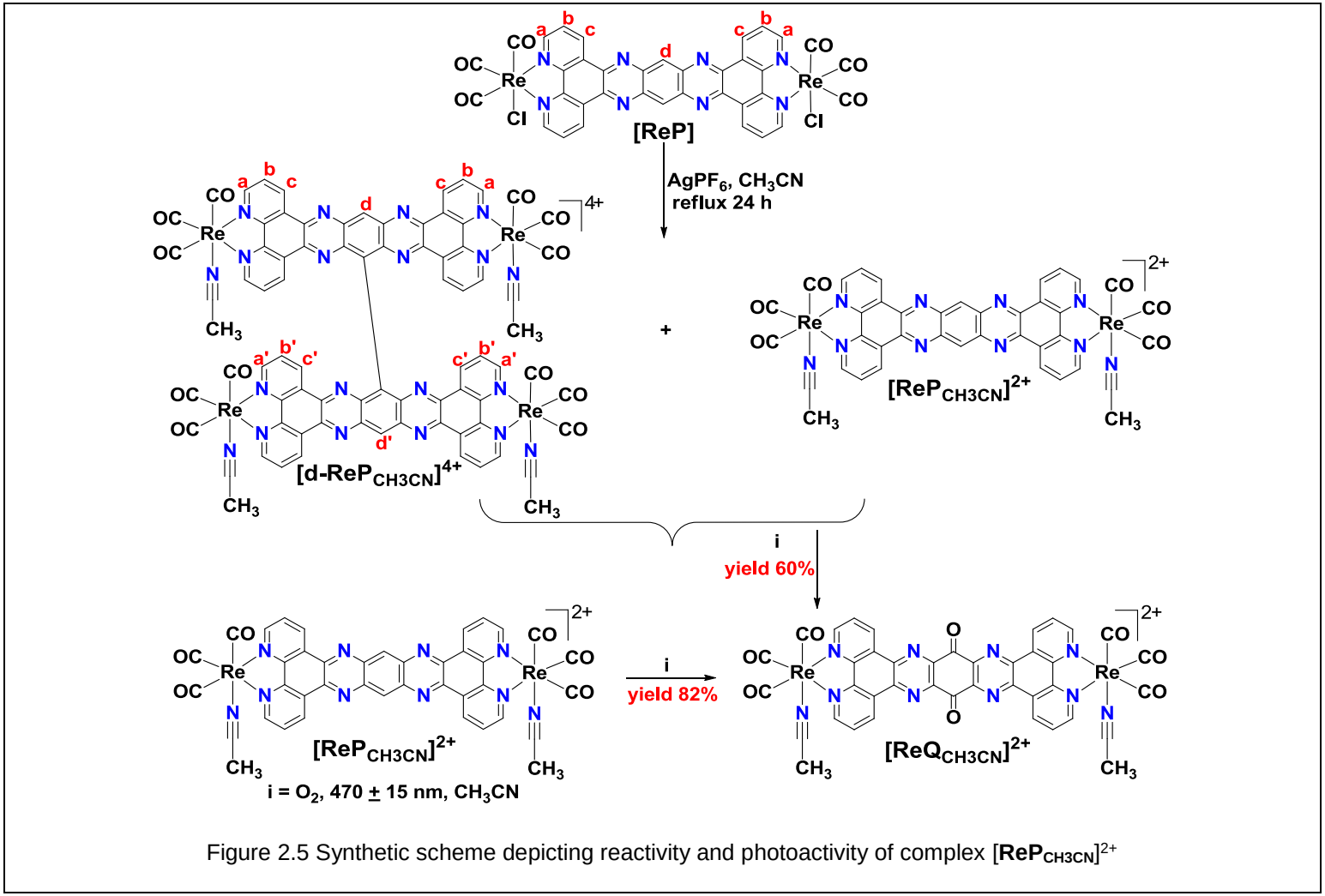

Figure 2.5 Synthetic scheme depicting reactivity and photoactivity of complex $[\mathbf{ReP}_{CH3CN}]^{2+}$

2.3.2 Synthesis of mononuclear Re(I) polypyridyl complexes

The mononuclear neutral Re(I) tatpp complex [**MRe**] was obtained in 85% yield by a Schiff base condensation reaction analogous to the preparation of [**ReP**] except that $Re(CO)_3Cl(phendione)$[90] was reacted with the free dadppz ligand in this case. While the insolubility of [**MRe**] in most common solvents allowed easy separation from unreacted starting materials, limited solubility in $CDCl_3$ permits to record ^1H NMR. The pyridine coordinated cationic complex $[\mathbf{MRe_{4\text{-}OHPy}}]^+$ may be prepared either by derivatizing $Re(CO)_3$(phendione)Cl complex with axial ligand of choice, such as 4-OHPy (4-hydroxypyridine), via halide abstraction reaction prior to condensation with dadppz (Figure 2.6, Method C) or derivatizing [**MRe**] with 4-OHPy after dadppz complexation (Fig 2.6, Method D), in a manner analogous to that utilized by Stoeffler et al[88] for the synthesis of $[Re(CO)_3$(4-methylpyridine)(dppz)$]^+$

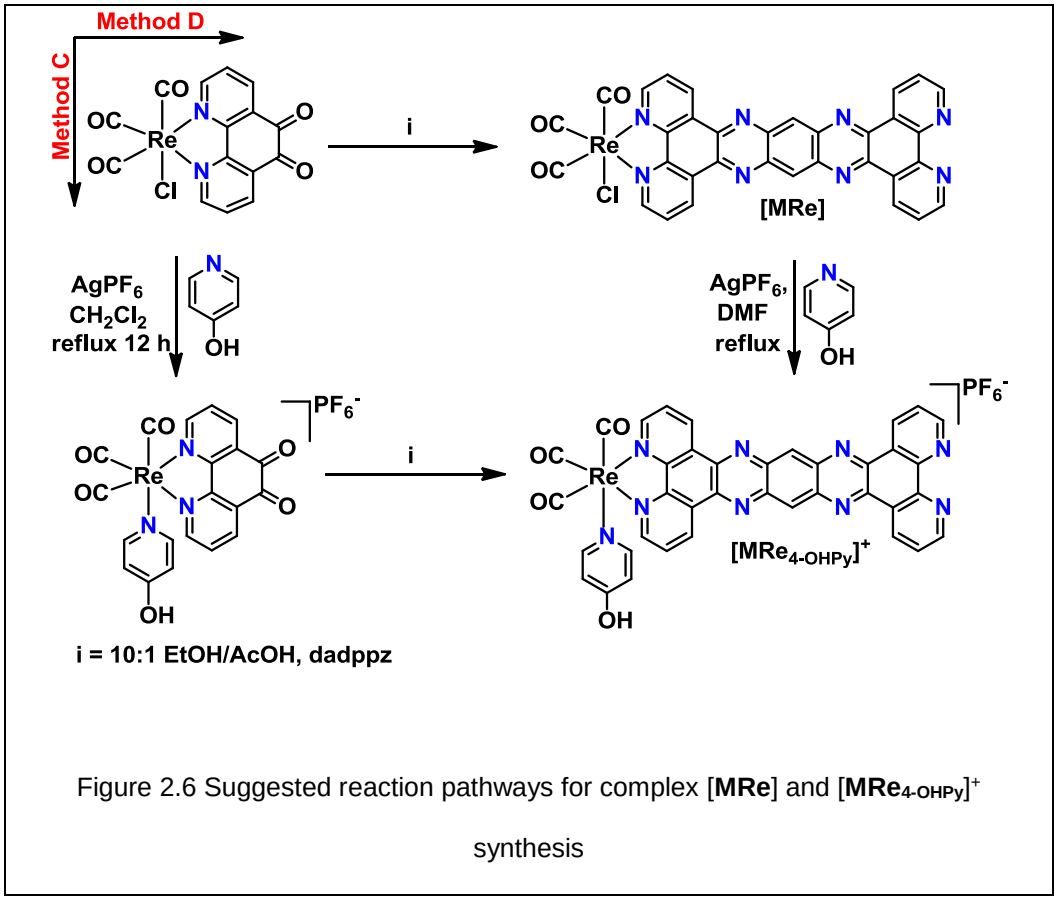

Figure 2.6 Suggested reaction pathways for complex [**MRe**] and [**MRe**$_{4\text{-OHPy}}$]$^{+}$ synthesis

In the present case, initial attempts to synthesize 4-OHPy coordinated mononuclear complex [**MRe**$_{4\text{-OHPy}}$]$^{+}$ via former method (C) as depicted in Figure 2.6 gave unusual results in that the resonances belonging to the coordinated pyridine ligand were absent in ^{1}H NMR, with only set of peaks belonging to the central tatpp ligand, each integrating for 2 protons, present in the aromatic region. This kind of observation would be entirely unexpected as pyridine coordination once obtained for [Re(CO)$_3$(N^N)L]$^{+}$ analogues should not exchange under normal conditions, given the fact that Re(CO)$_3$(N^N)Cl complexes require further activation by silver salts to aid pendant pyridine coordination indicating their low reactivity.

The X-ray crystal structure as obtained for $[Re(CO)_3(phendione)(4\text{-}OHPy)]PF_6$ complex later, revealed that pyridine coordination is not achieved via N site of pyridine and an *O*-coordinated complex $[\mathbf{Redione}_{\mathbf{4\text{-}OPyH}}]^+$ was formed in the process instead (Fig. 2.7), in which case, the axial ligand may be expected to be labile and may have been substituted (by a solvent molecule probably) during the condensation process instead. The complete schematic is represented in Fig 2.8, though synthesis via Method D was not attempted.

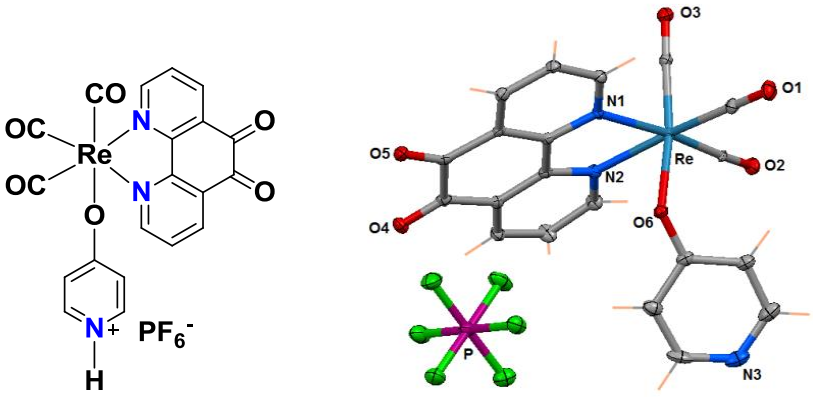

Figure 2.7 The solid state structure of $[\mathbf{Redione}_{\mathbf{4\text{-}OPyH}}]^+$ as determined by X-Ray crystallography. Refer to Appendix A for detailed crystallographic data

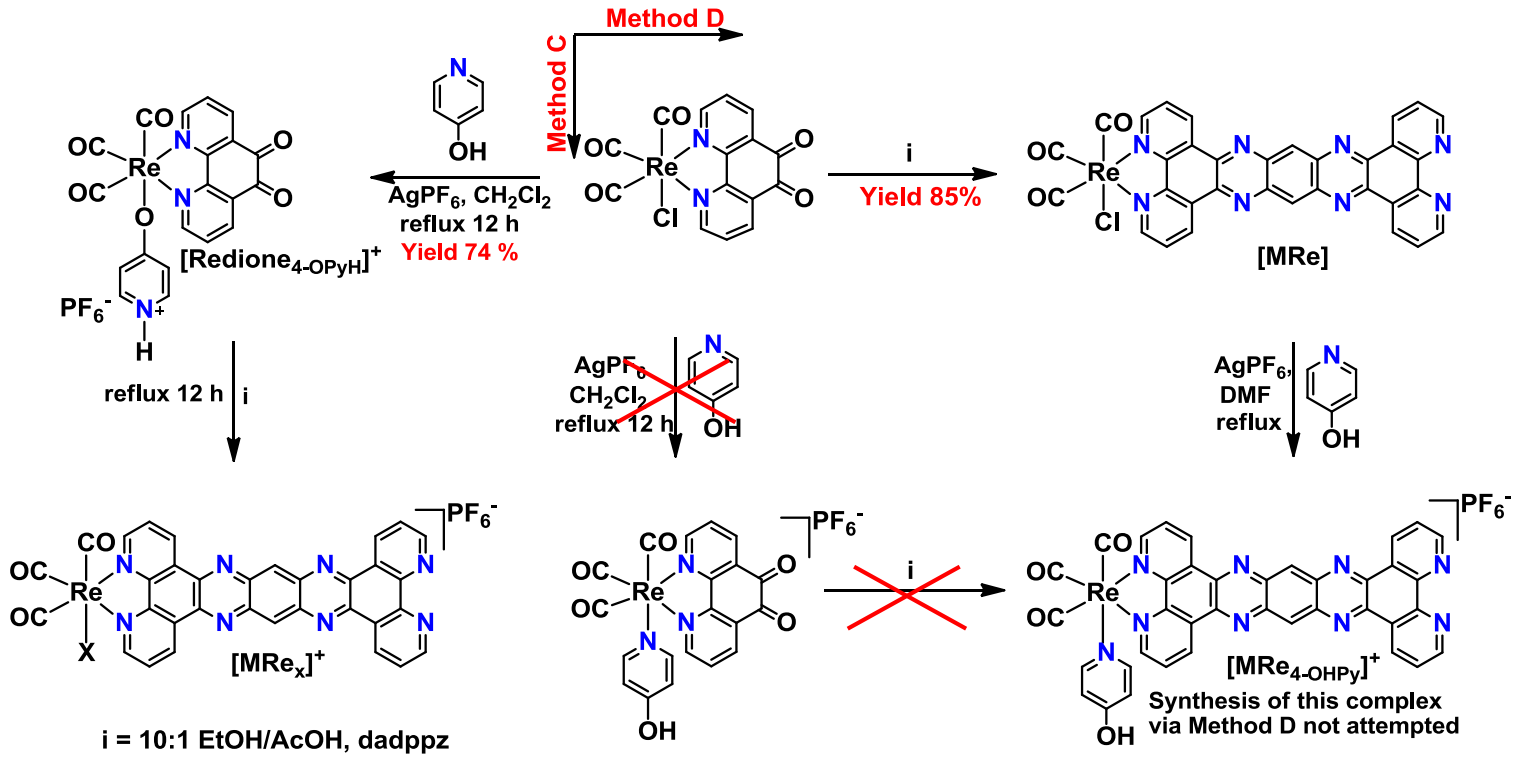

Figure 2.8 Reaction pathways for complex [**MRe**], [**[Redione$_{4\text{-OPyH}}$]$^{+}$** and [**MRe$_{x}$**]$^{+}$

No attempts were made to characterize the Re(I) tatpp complex $[\mathbf{MRe_x}]^+$ obtained or identify the axial ligand in this case. Complex $[Re(CO)_3(phendione)(4\text{-}CH_3Py)]ClO_4$, $[\mathbf{Redione_{4\text{-}CH3Py}}]^+$, was prepared instead, where 4-CH_3Py = 4-methylpyridine, by refluxing $Re(CO)_3$(phendione)Cl in presence of $AgClO_4$ and 7 fold excess of 4-CH_3Py in toluene. Schiff's base condensation reaction of $[\mathbf{Redione_{4\text{-}CH3Py}}]^+$ with dadppz resulted in the desired product $[\mathbf{MRe_{4\text{-}CH3Py}}]ClO_4$ with some impurities, but due to the poor solubility of the complex in any solvent, no attempts were made to obtain it in pure form.

X-Ray quality crystals of complex $[\mathbf{Redione_{4\text{-}CH3Py}}]^+$ were obtained by slow evaporation of the concentrated solution in $(CH_3)_2CO$. Complex $[\mathbf{Redione_{CH3CN}}]^+$ was prepared as a reactive intermediate as outlined in the experimental section and crystals suitable for X-Ray diffraction were obtained by layering hexane over CH_3CN solution (Fig 2.9).

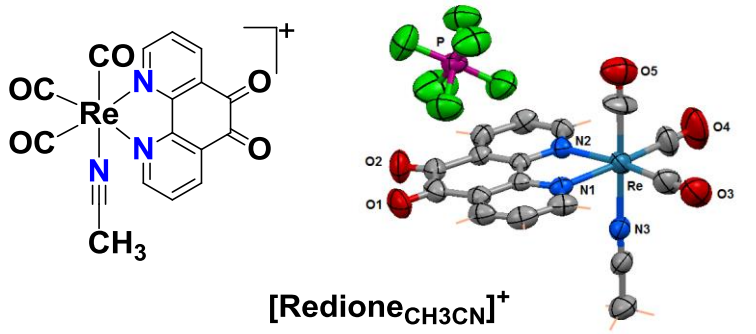

[Redione$_{CH3CN}$]$^+$

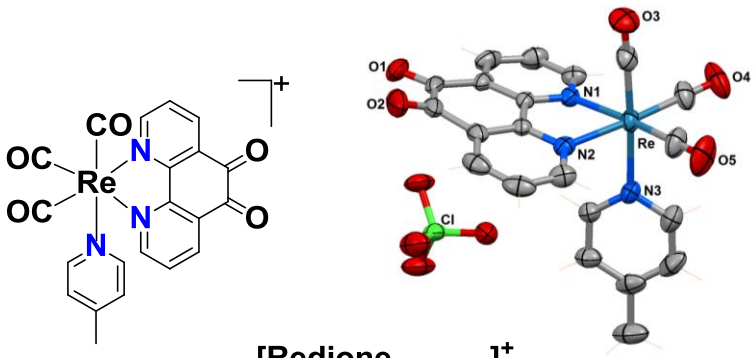

[Redione$_{4\text{-}CH3Py}$]$^+$

Figure 2.9 The solid state structure of [**Redione$_{CH3CN}$**]$^+$ and [**Redione$_{4\text{-}CH3Py}$**]$^+$ as determined by X-Ray crystallography. Refer to Appendix A for detailed crystallographic data

2.3.3 Characterization of complexes

The formation of the tatpp bridge in [**ReP**] via Method B is evident in the simplicity of the ^{1}H NMR, and notable downfield shift of the H_d and H_c protons to 9.70 and 9.95 ppm respectively upon pyrazine ring formation (Fig 2.10). Such an extent of deshielding of H_d and H_c protons of tatpp has been reported previously for complex $[P]^{4+}$ due to their proximity to neighboring pyrazine nitrogen atoms.[80] The signals for [**ReP**] were assigned based on the peak integrals and coupling constants, as well as by the comparison of the ^{1}H NMR of free tatpp ligand. [**ReP**] is only sparingly soluble in most common solvents, but soluble enough in chloroform to record its NMR spectrum. In principle, this product exists as two regioisomers in which the chloride ligands are arranged in a cis and trans position relative to the central tatpp plane, however the large distance between stereocenters, estimated at 17°A, results in a single set of NMR peaks, indicating the spectra of the cis and trans isomers are identical. There is a mirror plane symmetry element containing a pseudo two-fold axes intersecting in the central benzene ring of the molecule and a mirror plane along the Re-Re axis, thus approximating C_{2v} symmetry. This leads to a very simple NMR spectrum consisting of two doublets and a doublet of doublets at 9.52, 8.10, and 9.95 ppm, respectively for the H_a, H_b, and H_c positions on the tatpp ligand. The free tatpp ligand is insoluble but can be dissolved in chloroform upon addition of CF_3COOH (TFA) to a suspension of tatpp in $CDCl_3$. With its D_{2h} symmetry, the only difference in the ^{1}H NMR spectrum is the chemical shifts which are observed at 8.33, 8.36, and 10.20 ppm, respectively. The differences in chemical shifts due to metal coordination in [**ReP**] as opposed to free tatpp or axial ligand displacement in $[\mathbf{ReP_{CH3CN}}]^{2+}$ cannot be truly compared and contrasted since the spectra collected are in different solvents which is chosen based on the solubility of the complexes. (Fig 2.10 and 2.11).

The effect of metal coordination, however, is evident in the ^{1}H NMR of $Re(CO)_3$(dadppz)Cl by the displacement of splitting pattern to higher chemical shift values by 0.25-0.35 ppm in comparison to the free dadppz ligand due to reduced charge density (Figure 2.10). Similar effect is observed for phendione complexes [**Redione$_{4\text{-OPyH}}$**], [**Redione$_{CH3CN}$**]$^{+}$ and [**Redione$_{4\text{-CH3Py}}$**]$^{+}$ upon metal coordination.

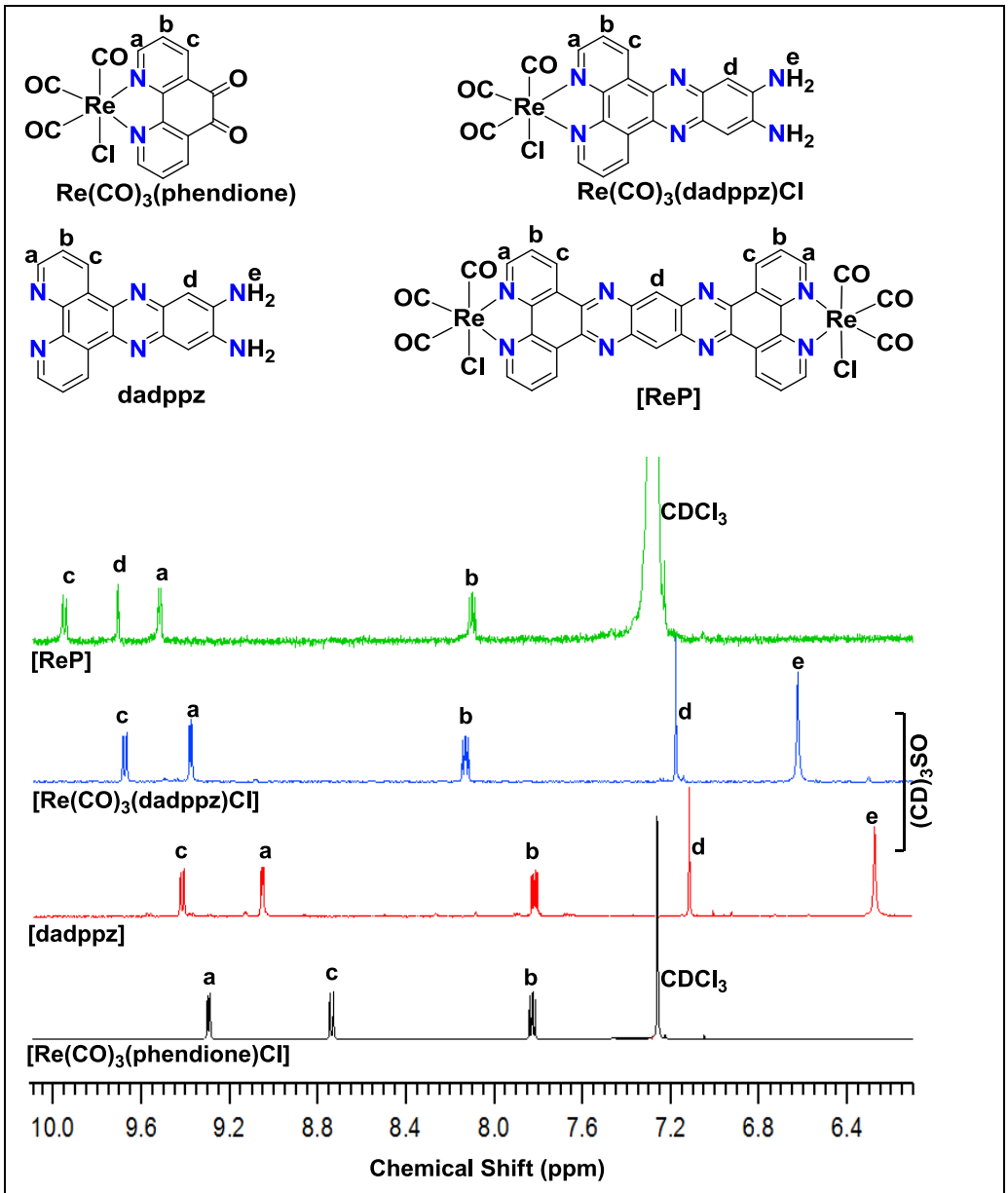

Figure 2.10 ^{1}H NMR spectra aromatic region, **Re(CO)$_3$(dadppz)Cl** and [**ReP**]

For complex [**ReP$_{CH3CN}$**]$^{2+}$ (Fig 2.11), we noticed that the tatpp peaks appear significantly downfield (ca 0.3-1.4 ppm) relative to the tatpp protons in complex [**P**]$^{4+}$ when spectra collected in CD_3CN for both complexes is compared. For example, H_a, H_b and Hc in [**ReP$_{CH3CN}$**]$^{2+}$ appear at 9.52, 8.27 and 10.01 ppm in comparison to 8.15, 7.82, 9.70 ppm respectively in [**P**]$^{4+}$, while no noticeable difference in the position of H_d protons in both the complexes is observed. Such an effect on H_a, H_b and Hc is probably due to enhanced Re to CO π backdonation in [**ReP$_{CH3CN}$**]$^{2+}$ which would ultimately increase the positive charge on the metal center and decrease the electron density on the phen protons of tatpp, particularly H_a, which is also the most displaced in [**ReP$_{CH3CN}$**]$^{2+}$ as per the chemical shift data.

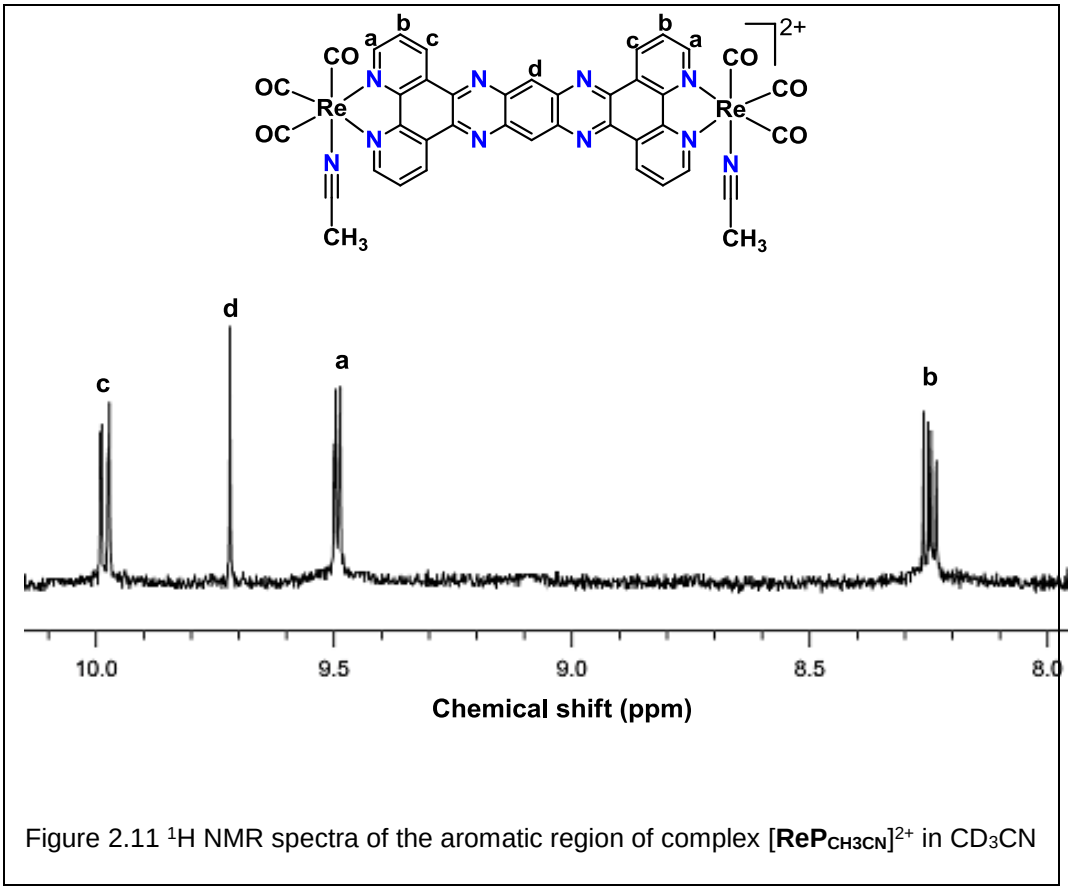

Figure 2.11 ^{1}H NMR spectra of the aromatic region of complex [**ReP$_{CH3CN}$**]$^{2+}$ in CD_3CN

When comparing the $[Re(CO)_3(phendione)]^+$ complexes [**Redione$_{4\text{-OPyH}}$**] and [**Redione$_{CH3CN}$**]$^+$ with analogous $[Ru(phen)_2(phendione)]^{2+}$ complex in CD_3CN, similar displacement for H_a, H_b and H_c protons is observed. In general, proton H_a appear more downfield, for example at 9.21 and 9.25 ppm in [**Redione$_{4\text{-OPyH}}$**] and [**Redione$_{CH3CN}$**]$^+$ respectively (Fig 2.13 and 2.12) in comparison to 8.47 ppm in complex $[Ru(phen)_2(phendione)]^{2+}$, which is about 0.7 ppm shift to higher value. Table. 1 summarizes the ^{1}H NMR chemical shift values for all the complexes discussed in this chapter.

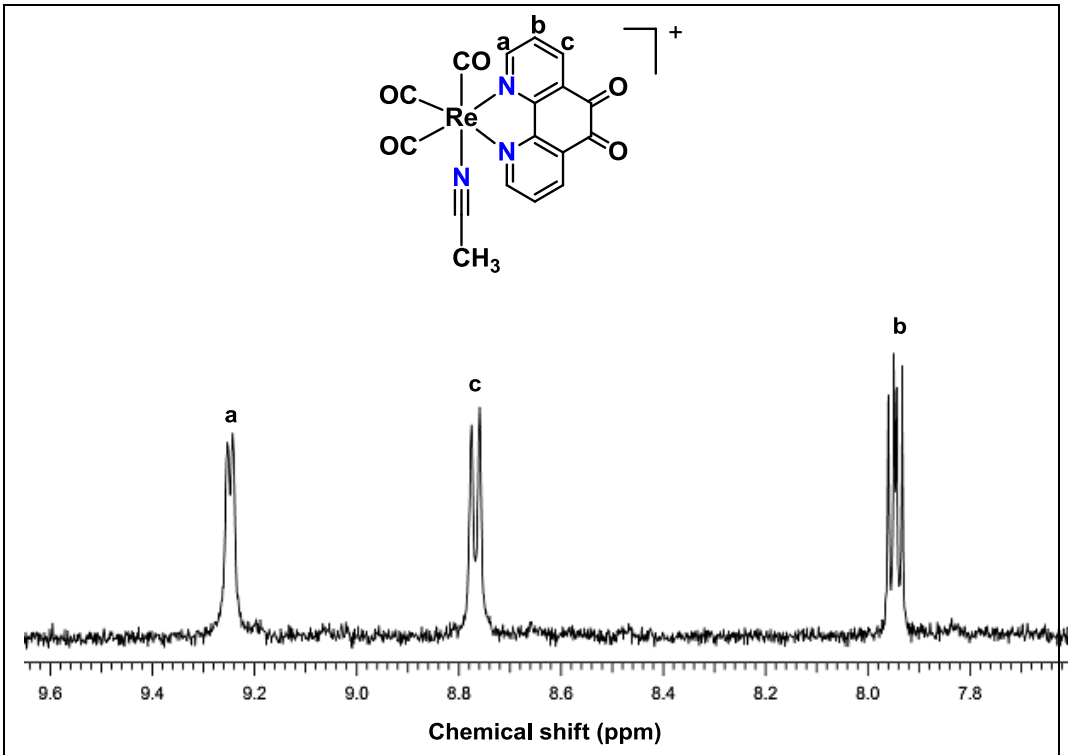

Figure 2.12 ^{1}H NMR spectra aromatic region of complex [**Redione$_{CH3CN}$**]$^+$ in CD_3CN

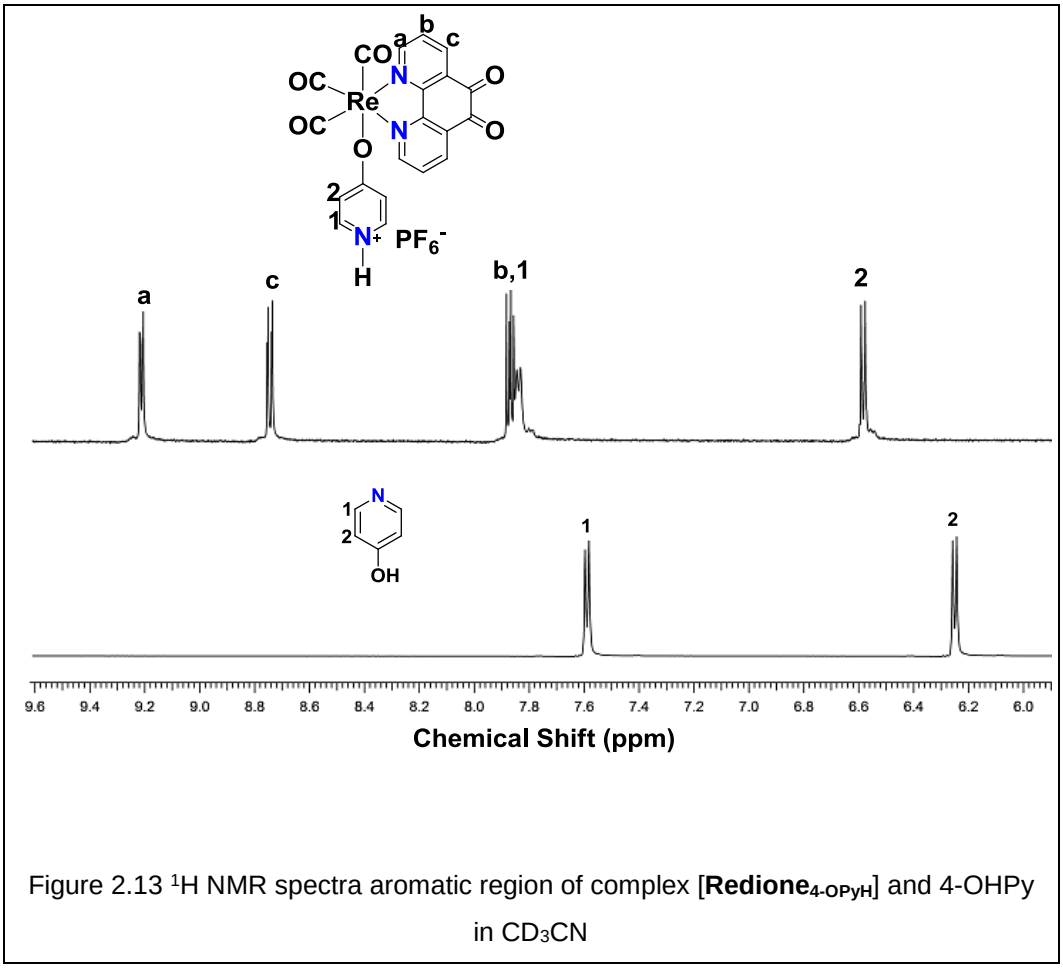

Figure 2.13 ^{1}H NMR spectra aromatic region of complex [**Redione$_{4\text{-OPyH}}$**] and 4-OHPy in CD_3CN

The formation of tatpp in [**MRe$_x$**]$^{+}$ upon condensation is also evident by the ^{1}H NMR splitting pattern. Like the binuclear complex, the compound is only sparingly soluble in most solvents, however the ^{1}H NMR could be obtained in a mixture of $CDCl_3$ and TFA (90:10). This compound exists as a single stereoisomer with C_{2V} symmetry, which results in two coupled sets: H_a, H_b, H_c,, and $H_{a'}$, $H_{b'}$ and $H_{c'}$ protons in the range of 10.12 – 8.14 ppm as expected of a monometallated tatpp complex (Fig 2.14). The peak assignments were made on the basis of the fact that metal coordination would deshield H_a, H_b and H_c protons

more than $H_{a'}$, $H_{b'}$ and $H_{c'}$ as well as by comparison to the chemical shifts observed for these protons in complex [**ReP**].

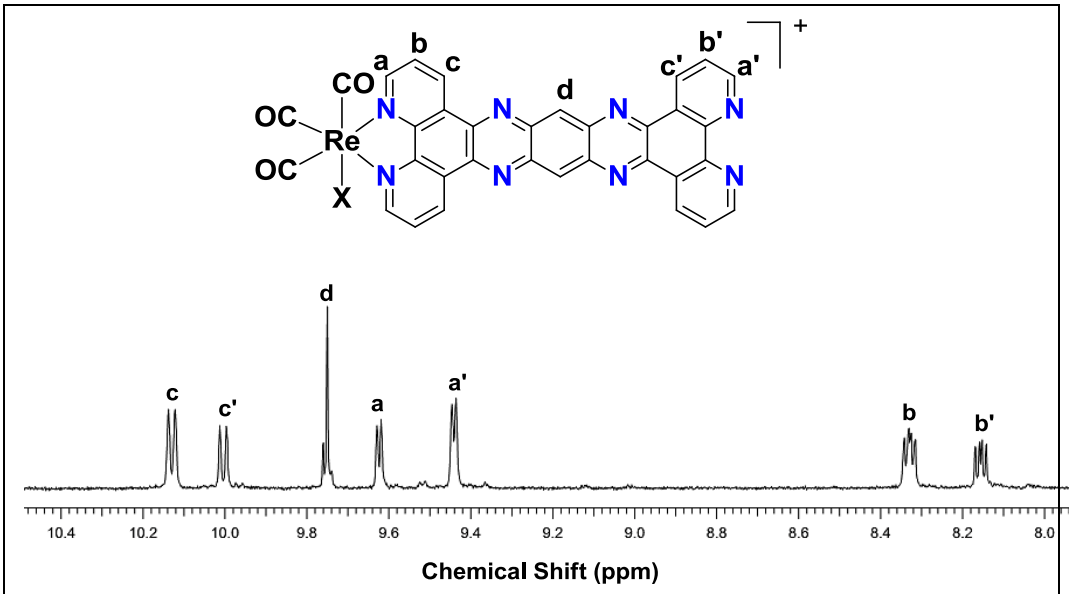

Figure 2.14 ^{1}H NMR spectra of the aromatic region of complex [**MRe**]$^{+}$ in $CDCl_3$:TFA (90:10)

Table 1 Summary of ^{1}H NMR spectroscopic data

Compound	Chemical Shifts (ppm)							
	H_a	H_b	H_c	H_d	$H_{a'}$	$H_{b'}$	$H_{c'}$	$H_{d'}$
^{A}**tatpp**	8.33	8.36	10.20	9.79				
^{C}**tatpp**	9.27	8.33	9.96	9.59				
^{B}**[ReP]**	9.52	8.1	9.95	9.7				
^{D}[**ReP$_{CH3CN}$**]$^{2+}$	9.52	8.27	10.01	9.74				
^{D}**[d- ReP$_{CH3CN}$]$^{4+}$**	9.47	8.30	10.11	10.22	9.11	7.50	8.50	10.22
^{D}**[ReQ$_{CH3CN}$]$^{2+}$**	9.61	8.33	9.98					
^{A}[**MRe**]$^{+}$	9.6	8.31	10.12	9.73	9.42	8.14	9.99	
^{D}**[Redione$_{4\text{-}OPyH}$]**	8.75	7.87	9.21					
^{D}**[Redione$_{CH3CN}$]$^{+}$**	8.78	7.95	9.25					
^{E}**[Redione$_{CH3CN}$]$^{+}$**	8.83	7.92	9.18					
^{D}**[Redione$_{4\text{-}CH3Py}$]$^{+}$**	8.89	8.23	9.71					

^{A}CDCl$_3$ + TFA, ^{B}CDCl$_3$, ^{C}CD$_3$CN + Zn(BF)$_4$, ^{D}CD$_3$CN, ^{E}CD$_2$Cl$_2$, ^{F}(CD$_3$)$_2$CO

IR spectroscopy is a very diagnostic and useful tool in regards to the characterization of Re(I) tricarbonyl polypyridine complexes as the appearance of sharp CO stretching bands in the IR spectrum signify the formation of Re complexes. As for all the complexes discussed above, the IR spectrum is characterized by two or three intense bands in the range of 1870-2050 cm^{-1}, characteristic of a facial CO orientation. For complexes exhibiting two bands, the broad lower energy band is a combination of two CO stretching bands.[91] The expected trend is seen in the stretching frequency of the carbonyl groups, with cationic species [**ReP$_{CH3CN}$**]$^{2+}$ absorbing at higher wavenumbers in comparison to corresponding neutral complex [**ReP**] or [**MRe**]. This is seen as a consequence of reduced Re to CO π backdonation due to decreased electron density at the metal center upon substitution of an anionic, σ donating chloride ligand with a neutral CH_3CN ligand. The phendione complexes [**Redione$_{4\text{-}OPyH}$**] and [**Redione$_{CH3CN}$**]$^{+}$ are characterized by an

additional band for ketonic CO stretch at 1703 and 1704 cm^{-1} respectively**.** Additionally, a sharp band at ~840 cm^{-1} for υ(P-F) shows the presence of PF_6^- counterion in cationic complexes.

The ESI-HRMS spectra of the complexes show characteristic parent ion peaks as for neutral tatpp complexes [**ReP**] and [**MRe**] at m/z 1097.95 for $[M^+]$ and 792.05 for $[M^-]$ respectively and cationic $[\mathbf{ReP_{CH3CN}}]^{2+}$ at m/z 555.03 for $[M\text{-}2PF6]^{2+}$**.** The phendione complexes [$\mathbf{Redione_{4\text{-}OPyH}}$], $[\mathbf{Redione_{CH3CN}}]^+$, $\mathbf{[Redione_{4\text{-}CH3Py}]^+}$ showed parent ion peaks for $[M\text{-}PF6]^+$ at m/z 576.02, 522.01 and 575.0327 respectively.

2.3.4 Reactivity and Photoactivity of complex $[\mathbf{ReP_{CH3CN}}]^{2+}$

2.3.4.1 Photooxidation

The observed reactivity and oxygen sensitivity of complex $[\mathbf{ReP_{CH3CN}}]^{2+}$ was discovered by chance when the halide abstraction reaction of [**ReP**] to yield $[\mathbf{ReP_{CH3CN}}]^{2+}$ gave ambiguous results. We noticed that the synthesis was not reproducible, yielding the product $[\mathbf{ReP_{CH3CN}}]^{2+}$ along with a side product in varying ratios each time under the same experimental conditions. Figure 2.15 shows the overlay of the ^1H NMR of the residue obtained after the reaction work up from two different synthesis under similar reaction conditions.

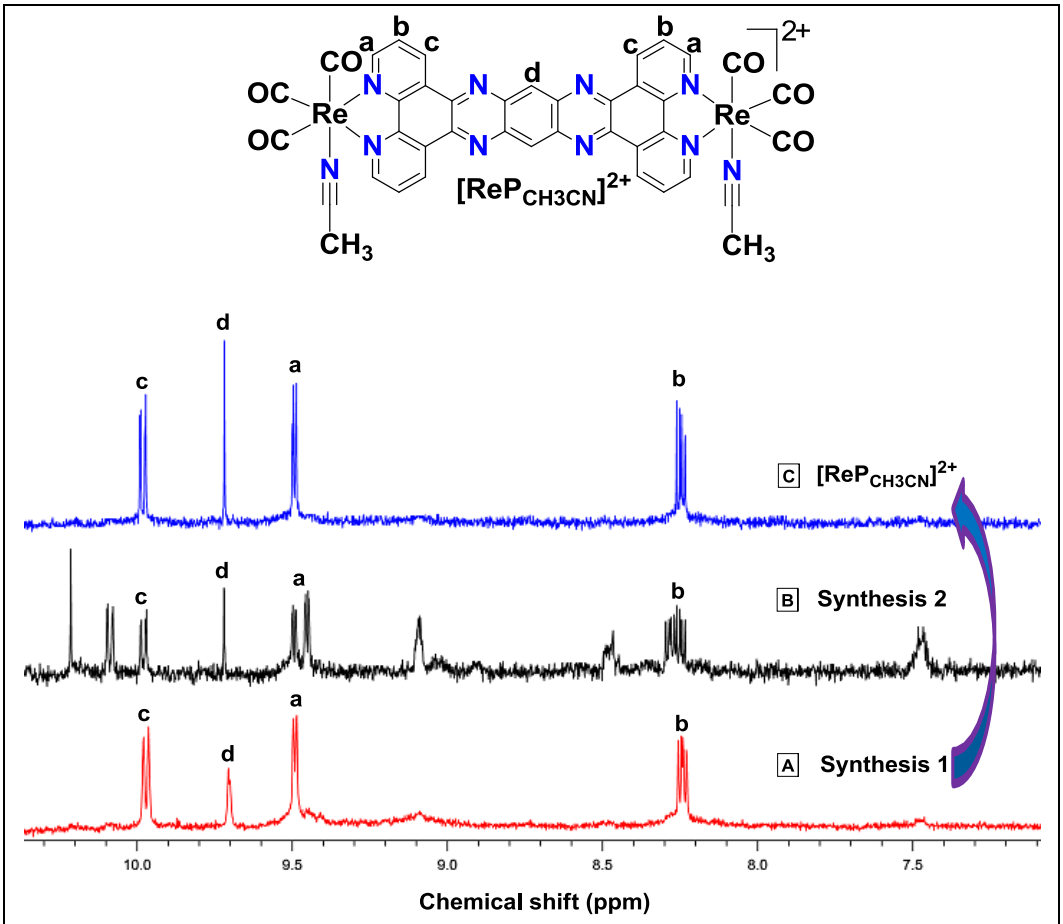

Figure 2.15 ^{1}H NMR of the residue obtained after the reaction work up of complex [**ReP$_{CH3CN}$**]$^{2+}$ from two different synthesis (A and B) under similar reaction conditions and pure [**ReP$_{CH3CN}$**]$^{2+}$ obtained after purification (C)

While relatively clean conversion of [**ReP**] to [**ReP$_{CH3CN}$**]$^{2+}$ from synthesis 1 (Figure 2.15 A) permitted isolation of the pure product by washing the residue with 1:10 MeOH:DCM and identify the product peaks, but the presence of the side product every time complicated the spectra and compromised the yield of the product [**ReP$_{CH3CN}$**]$^{2+}$. The ESI-HRMS data of the complex mixture ([**ReP$_{CH3CN}$**]$^{2+}$ + side product) from both the

synthesis, 1 and 2, indicated no left over starting material [**ReP**] or mono halide substituted product $[Re(CO)_3(CH_3CN)(tatpp)(Cl)(CO)_3Re][PF_6]$, while there was evidence of product, $[\mathbf{ReP_{CH3CN}}]^{2+}$, formation each time. In addition to this, formation of the side product was also observed in a clean sample of $[\mathbf{ReP_{CH3CN}}]^{2+}$ upon storage as a residue or as a solution in MeCN, which suggested beyond doubt that the side product is actually a product of $[\mathbf{ReP_{CH3CN}}]^{2+}$ reacting with something to form it.

Such unusual observation prompted us to investigate into the photoactivity and probe possible involvement of any light induced reactivity of $[\mathbf{ReP_{CH3CN}}]^{2+}$ to produce the side product. To evaluate this, an NMR scale experiment was conducted in which a sample of pure $[\mathbf{ReP_{CH3CN}}]^{2+}$ (1.0 mg in 1.0 mL CD_3CN) was irradiated with visible light (470 $\pm$ 15 nm) and reaction monitored by ^1H NMR spectroscopy. The data obtained indicated photoinduced oxidation of $[\mathbf{ReP_{CH3CN}}]^{2+}$ to its quinone analogue $[\mathbf{ReQ_{CH3CN}}]^{2+}$ in just 30 min of irradiation under aerobic conditions. The NMR splitting pattern of $[\mathbf{ReQ_{CH3CN}}]^{2+}$ is very similar to $[\mathbf{ReP_{CH3CN}}]^{2+}$ except a small downfield shift of the H_a and H_b protons by less than 0.1 ppm is observed, but the most diagnostic criteria is the absence of the sharp singlet of H_d proton in $[\mathbf{ReQ_{CH3CN}}]^{2+}$ due to the oxidation at that position (Fig 2.16. Another important characteristic of quinone formation in $[\mathbf{ReQ_{CH3CN}}]^{2+}$ is the appearance of carbonyl absorption at 1711 cm^{-1} in FTIR spectrum which is absent in $[\mathbf{ReP_{CH3CN}}]^{2+}$. The formation of $[\mathbf{ReQ_{CH3CN}}]^{2+}$ is further confirmed by ESI-HRMS by the increase in mass of $[M\text{-}2PF_6]^{2+}$ peak to m/z 570 as opposed to 555 in $[\mathbf{ReP_{CH3CN}}]^{2+}$. It is noteworthy that no such photooxidation was observed in the absence of light or air.

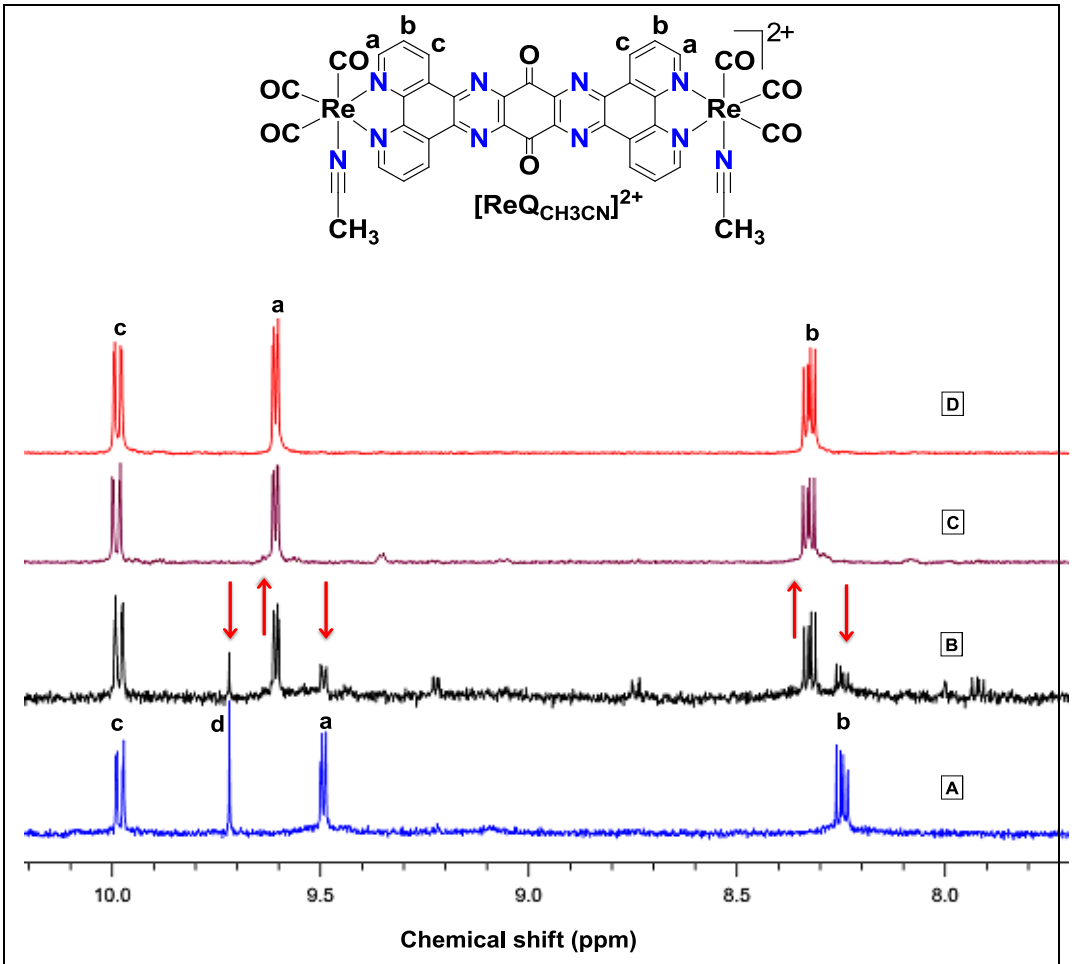

Figure 2.16 Demonstration of ^{1}H NMR scale photooxidation of $[\mathbf{ReP}_{CH3CN}]^{2+}$ in CD_3CN (A) 0 min irradiation, (B) 15 min irradiation, (C) 30 min irradiation, (D) photoproduct $[\mathbf{ReQ}_{CH3CN}]^{2+}$ after purification

While photooxidation to quinone under aerobic conditions is not unusual and has been reported for $[Ru(tbbpy)_2(dppn)]^{2+}$ complex (Fig 2.17), where dppn= benzodipyridophenazine, this was a very unusual observation for tatpp based compound since none of the Ru-tatpp compounds $[\mathbf{MP}]^{2+}$, $[\mathbf{P}]^{4+}$ or related tbbpy complex

$[Ru(tbbpy)_2(tatpp)Ru(tbbpy)_2]^{2+}$ undergo oxidation via photochemical route even after prolonged irradiation of over 72 h under identical conditions.[80, 92] However, it can be driven by a very strong oxidant such as ammonium peroxydisulfate.[80]

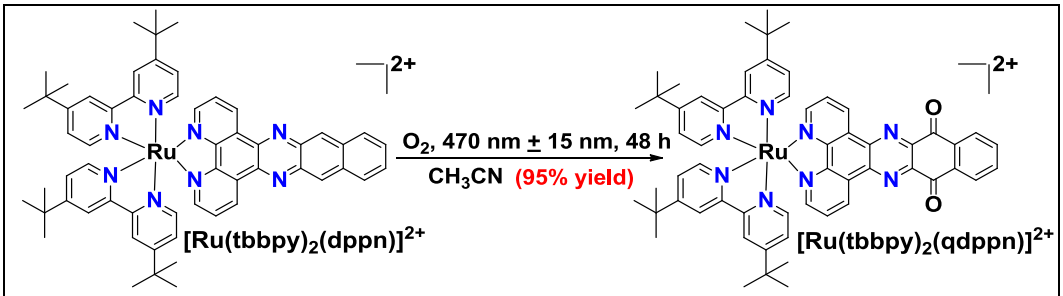

Figure 2.17 Photooxidation of $[Ru(tbbpy)_2(dppn)]^{2+}$ complex

The fact that the oxidation of $[\mathbf{ReP}_{CH3CN}]^{2+}$ to $[\mathbf{ReQ}_{CH3CN}]^{2+}$ is only observed in the presence of light and air, suggests that oxidation process may proceed via singlet oxygen formation. While Ru(II) and Re(I) polypyridine complexes are known in literature for their ability to sensitize oxygen[93, 94, 95] which due to its high reactivity, can bring about chemical transformations such as photooxidation reactions [95] or photocleavage of DNA[51] which has important implications in photodynamic therapy for treating cancer[96], but to the best of our knowledge, this is the first example of a tatpp based complex or a Re(I) polypyridine complex to undergo such kind of transformation process where product is isolated in high purity and good yield.

2.3.4.2 Dimerization

Despite the established photooxidation of [**ReP$_{CH3CN}$**]$^{2+}$ to quinone analogue, its proton NMR spectrum was inconsistent with the proton peaks for the side product that is formed as a byproduct of [**ReP$_{CH3CN}$**]$^{2+}$ reactivity (Fig 2.18). In addition, under the same conditions of irradiation, a 1:1 mixture of [**ReP$_{CH3CN}$**]$^{2+}$ **:** side product from synthesis 2 also yielded the quinone analogue [**ReQ$_{CH3CN}$**]$^{2+}$ almost entirely (Fig 2.18). This observation suggested beyond doubt that whatever this side product is, may contain the same ligand moiety tatpp. Thus we investigated into the possibility of dimerization since the dimerization of tatpp ligand has been reported previously as a very small byproduct (0.07% yield) of tatpp synthesis and is supported by the crystal structure.[83]

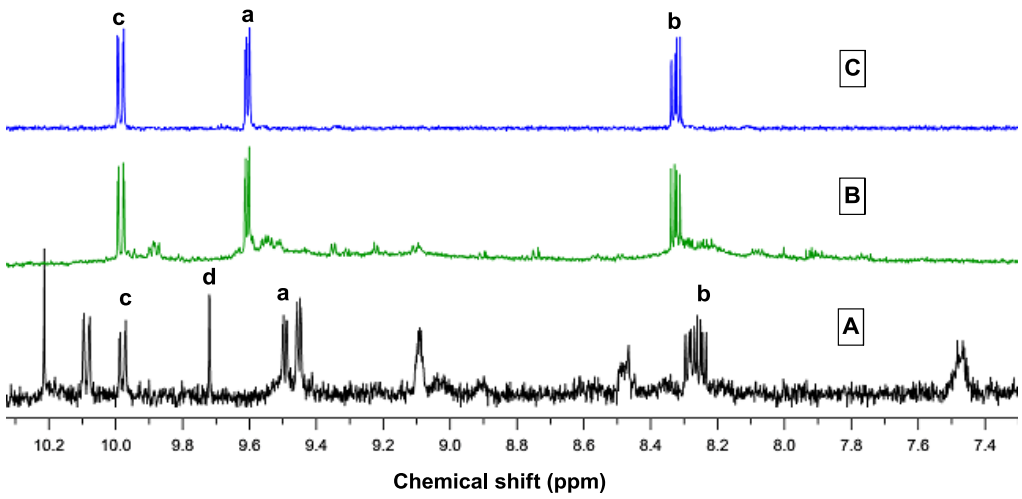

Figure 2.18 Demonstration of ^{1}H NMR scale photooxidation of 1:1 mixture of [**ReP$_{CH3CN}$**]$^{2+}$**:** side product (from synthesis 2) in CD_3CN (A) 0 min irradiation, (B) 30 min irradiation, (C) photoproduct [**ReQ$_{CH3CN}$**]$^{2+}$ after purification (as mentioned previously)

Fig 2.19 shows an overlay of the ^{1}H NMR of the Zn(dtatpp) adduct (where dtatpp = dimerized tatpp ligand), and a 1:1 mixture of [**ReP$_{CH3CN}$**]$^{2+}$ with side product in CD_3CN. The good agreement between the splitting pattern and integration of the side product with dtatpp spectrum indicate the presence of tetranuclear dimer [d-**ReP$_{CH3CN}$**]$^{4+}$. This is further supported by ESI-HRMS which show peaks corresponding to [M-4PF_6]$^{4+}$ at *m/z* 554 and [M-3PF_6]$^{3+}$ at *m/z* 788 for [d-**ReP$_{CH3CN}$**]$^{4+}$ in addition to [M-2PF_6]$^{2+}$ at *m/z* 555 for [**ReP$_{CH3CN}$**]$^{2+}$.

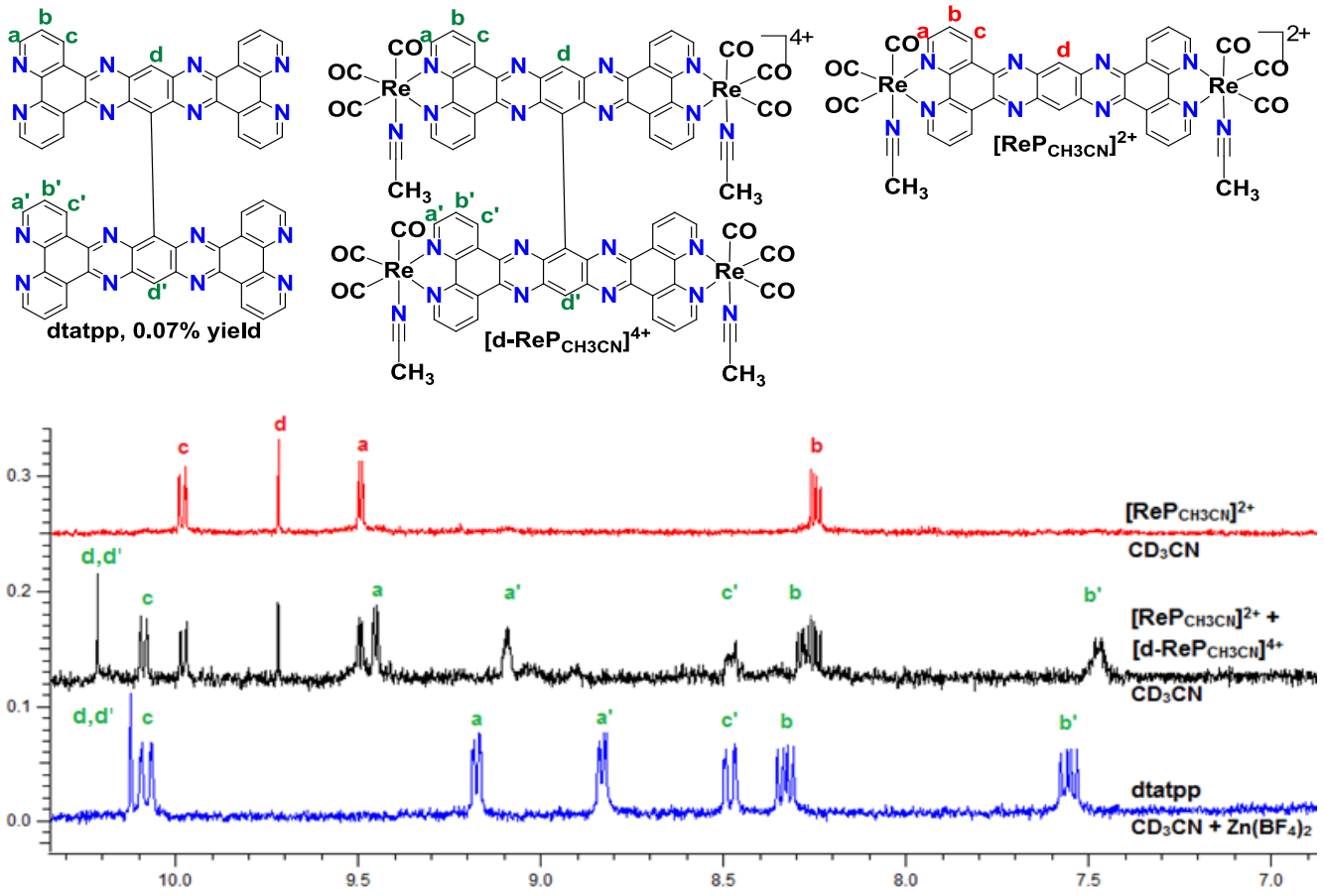

Figure 2.19 ^{1}H NMR spectra of dtatpp (bottom), complex mixture of [**ReP$_{CH3CN}$**]$^{2+}$ with side product (middle) and pure [**ReP$_{CH3CN}$**]$^{2+}$ in CD_3CN.

Attempts to isolate and recover [d-**ReP**$_{CH3CN}$]$^{4+}$ from the complex mixture via column chromatography using different solvent mixtures as eluant on silica gel did not prove very fruitful, in that the resultant yield and purity was low. Fig 2.20 shows the ^{1}H NMR of the isolated [d-**ReP**$_{CH3CN}$]$^{4+}$ after column purification using 80:20:5 DCM:MeOH:MeCN as eluant and this is the best that we have been able to isolate it so far. Further purification was not attempted due to low yield (>5 %) irrespective of the purification method attempted. Additionally probing the mechanism of photooxidation process or isolating the dimer was not the focus of this study. [d-**ReP**$_{CH3CN}$]$^{4+}$ is a byproduct of [**ReP**$_{CH3CN}$]$^{2+}$ synthesis and yield of the reaction is considerably compromised due to this side reaction. If these complexes were to be pursued any further, an ideal approach would be to design a strategy for pushing the reaction to where it selectively yields [**ReP**$_{CH3CN}$]$^{2+}$ or [d-**ReP**$_{CH3CN}$]$^{4+}$.

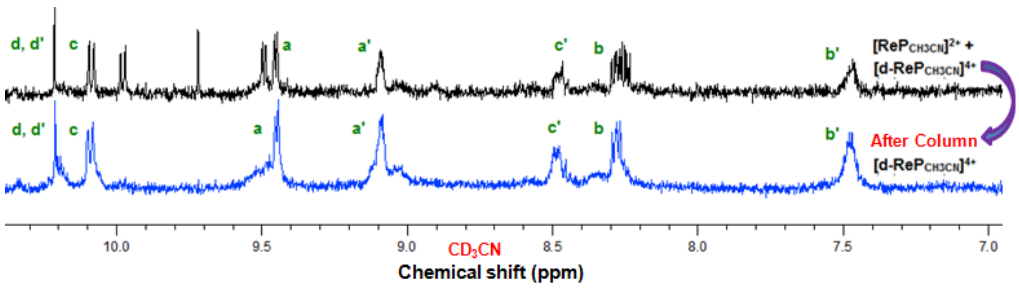

Figure 2.20 ^{1}H NMR spectra [d-**ReP**$_{CH3CN}$]$^{4+}$ in CD_3CN after column purification (bottom)

At this point, we are unclear as to what may be driving this dimerization process which, in principle, would proceed via radical formation mechanism. The lack of

electrostatic repulsion between two interacting molecular units (as in dicationic complexes versus tetracationic) or lesser steric bulk around the ligand has been shown to result in such dimerization processes.[57, 97] In our case, both factors seem to be contributing in that complex [**ReP$_{CH3CN}$**]$^{2+}$ is dicationic, as well as terminal CO groups present less steric hindrance compared to bulky phen groups in complex [**P**]$^{4+}$ that prevent its dimerization.[57]

2.4 Conclusion

A range of Re(I) polypyridine complexes have been prepared and characterized by ^{1}H NMR, IR, HRMS and CHN. Potential reactivity, photoactivity and oxygen sensitivity of Re(I)tatpp complex [**ReP$_{CH3CN}$**]$^{2+}$ is explored to show both: rapid photooxidation to its quinone analogue [**ReQ$_{CH3CN}$**]$^{2+}$ upon visibe light irradiation under aerobic conditions and dimerization to yield the tetrametallic dimer [d-**ReP$_{CH3CN}$**]$^{4+}$. While facile formation of [**ReQ$_{CH3CN}$**]$^{2+}$ in good yield and high purity may be useful synthetically, further studies are needed to understand the mechanism of such a transformation. The neutral complexes [**ReP**] and [**MRe**] are found to be poorly soluble in common organic solvents then their cationic counterparts. The solubility and reactivity issues of Re(I)tatpp complexes reported herein will limit their utility as therapeutics and thus none were pursued any further for biological studies. Only the DNA cleavage for the complex [ReP$_{CH3CN}$]$^{2+}$and [ReP] was assessed, but they appeared to precipitate out due to poor solubility and thus the results are inconclusive and included in the appendix for archival purposes. A new direction was followed instead which is discussed in the next chapter.

Chapter 3

SYNTHESIS, CHARACTERIZATION AND ANTICANCER ACTIVITY OF HETEROBIMETALLIC RU(II)-RE(I)TATPP COMPLEXES : A HYBRID APPROACH

3.1 Introduction

We recently reported that ruthenium complexes, [**P**]$^{4+}$ and [M**P**]$^{2+}$ exhibit low acute animal toxicity, low micromolar cytotoxicity against a number of malignant cell lines, good selectivity for malignant over normal cells, and most significantly, 83% tumor regression in non-small cell lung carcinoma (H358) human tumor xenografts in mice and double survival time.[61] In vitro studies show that [**P**]$^{4+}$ and [M**P**]$^{2+}$ induce DNA damage in a manner inversely proportional to the pO_2, suggesting a mechanism which does not involve reactive oxygen species.[98] These two tatpp-based complexes are unique among all RPCs known to date in that they do not require external activation by light or other stimuli to induce DNA damage. Instead, the DNA cleavage activity is associated with the ease at which the tatpp moiety is reduced in situ to form DNA-bound reactive radical intermediates. The first reduction for [**P**]$^{4+}$ and [M**P**]$^{2+}$ occur at potentials positive of -0.25 V (vs. NHE at pH 7.0)[58, 59] which is well within the reducing potential of common cellular reductants, such as glutathione (GSH). Assuming DNA cleavage is the mechanism by which [**P**]$^{4+}$ and [M**P**]$^{2+}$ induce apoptosis, their activity in the absence of external stimuli would potentially make them useful for the treatment of systemic disease in which the location of the micro-metastases is not always known.

The large extended planar structure of tatpp is presumed to be responsible for the low observed reduction potential and places [**P**]$^{4+}$ and [M**P**]$^{2+}$ in the range in which common cellular reducing agents are competent for their reduction to reactive radical species, while RPCs that lack tatpp are reduced at much positive potentials and therefore do not cleave

DNA in this manner. Additionally we have shown that the tatpp based reactive radical is only formed when [**P**]$^{4+}$ is intercalated in DNA[61, 98] suggesting that the complex reaches its intended target unchanged and thus may not be involved in unwanted side reactions, that ultimately seem to be responsible for low toxicity of [**P**]$^{4+}$ in comparison to other RPCs. This is further supported by animal toxicity data that reveal [**P**]$^{4+}$ is well tolerated by mice (MTD >160 mg/kg) as compared to related small RPCs[42].

In this study, in an effort to determine how metallation and metal oxidation state would affect the DNA cleavage activity unique to tatpp ligand and anticancer activity of [**P**]$^{4+}$ and [M**P**]$^{2+}$ overall, we aimed at preparing Re(I) tatpp analogues that we expected to show similar but not identical patterns of bioactivity due to the lower charge and differing coordination environment about the metal ion. In Chapter 2, we showed that the new analogues were found to be surprisingly reactive towards photooxidation and dimerization reactions that severely limit their progress to further bioactivity studies, while no such reactivity for precursor complex [**P**]$^{4+}$ and [M**P**]$^{2+}$is known.

In this chapter we aim at preparing structurally similar mixed metal Ru(II)-Re(I) tatpp analogues $[(phen)_2Ru(tatpp)Re(CO)_3(CH_3CN)]^{3+}$ - [**RuRe$_{CH3CN}$**]$^{3+}$ and $[(phen)_2Ru(tatpp)Re(CO)_3(PR_3)]^{3+}$ - [**RuRe$_{PR3}$**]$^{3+}$, where PR_3 = tris(hydroxymethyl) phosphine, which are in between [**P**]$^{4+}$ and [M**P**]$^{2+}$, in that they are +3 cation and have one Ru(II) and one Re(I) ion instead of one or two Ru(II) ions in [M**P**]$^{2+}$ and [**P**]$^{4+}$ respectively. The $Re(CO)_3L$ core on one end would allow us to follow the variations in the bioactivity, if any, due to Re functionality. The differing axial ligand in these analogues may also help delineate which properties are due to the overall complex composition or due to variation in L.

Although there have been numerous studies exploring the rich photophysical properties of Re(I) polypyridine complexes[99, 100], reports on their cytotoxicity are relatively few while in vivo toxicity has rarely been studied. This is probably due to the poor aqueous solubility as most of the success to date with water soluble $Re(CO)_3L$ polypyridine complexes has been with ones containing shorter N^N ligands wherein they are principally used in live cell imaging experiments to trace cellular targets due to their inherent luminescence.[101, 102] Water soluble Re(I) complexes with long N^N ligands have rarely been reported. We herein report on the synthesis, characterization and DNA cleavage activity of $[\mathbf{RuRe_{CH3CN}}]^{3+}$ and $[\mathbf{RuRe_{PR3}}]^{3+}$, as well as cytotoxicity and animal toxicity of water soluble Re(I) tatpp complex $[\mathbf{RuRe_{PR3}}]^{3+}$.

3.2 Experimental

3.2.1 General Methods

$Re(CO)_5Cl$ (Acros), $AgPF_6$ (Alfa Aesar), tris(hydroxymethyl)phosphine (Sigma Aldrich) were purchased and used as such. All solvents were reagent grade and used as received unless otherwise indicated. All ligands 9,11,20,22-tetraazatetrapyridopentacence (tatpp)[9], 11,12-diaminodipyridophenazinedadppz (dadppz)[11], 1,10-phenanthroline-5,6-dione[13], (phendione) were prepared as described in previous chapter. $[Ru(phen)_2]Cl_2$, $[Ru(phen)_2(phendione)]PF_6$, $[Ru(phen)_2(tatpp)][PF_6]_2$[103] were synthesized according to literature procedures. All synthesis were conducted under N_2 and in dark environment. ^1H NMR was recorded on JEOL Eclispse 500 MHz spectrometer and referenced to residual solvent peaks in ppm. FTIR spectra were recorded on Bruker Vector 22 FT-IR spectrometer as KBR pellets. ESI-HRMS data was recorded on a Shimadzu LCMS IT-TOF at the Schimadzu Center for Advanced Analytical Chemistry (SCAAC) at UTA. UV-Vis

spectra were obtained on a Hewlett-Packard HP8453A spectrophotometer in MeCN. NMR and IR annotations used: s= singlet, d = doublet, t = triplet, m = multiplet, br = broad

3.2.2 Synthesis

3.2.2.1 $[Ru(phen)_2(tatpp)(CH_3CN)(CO)_3Re][PF_6]_3$ - $[\mathbf{RuRe_{CH3CN}}]^{3+}$

A solution of 0.10 g (0.08 mmol) of $[Ru(phen)_2(tatpp)][PF_6]_2$, 0.03 g (0.09 mmol) of $Re(CO)_5Cl$ and 0.02 g (0.09 mmol) of $AgPF_6$ in 100 mL CH_3CN was heated to reflux for 12 h in dark. After cooling, the solution was filtered to remove AgCl and filtrate concentrated to minimum volume (~5 mL) by rotary evaporation. Crude product was then obtained by dropwise addition of a saturated solution of aqueous NH_4PF_6, collected by suction filtration and washed with 50 mL of water followed by 50 mL ethanol. This crude product was further purification by repeated metathesis reaction, as needed (~2x), between Cl^- and PF_6^- salts. Silica gel column chromatography purification procedure was deliberately avoided due to the irreversible adsorption of the complex on the column which resulted in considerably low yields.

Metathesis Reaction: The dropwise addition of the saturated solution of n-tetrabutylammonium chloride in CH_3CN to the saturated solution of $[RuRe_{CH3CN}]^{3+}$ in CH_3CN ((as PF_6^- salt from above) results in the precipitation of the complex as Cl^- salt, which is collected by filtration, washed with 10 mL acetone and air dried. The Cl^- salt of complex obtained was then dissolved in minimum amount of methanol and a saturated solution of aqueous ammonium hexafluorophosphate in methanol was added dropwise to obtain the product as PF_6^- salt, which is collected by filtration, washed with 50 mL water, followed by 50 mL ethanol and air dried to obtain the pure product as deep red brown solid. (0.09 g, 66 % yield, PF_6^- salt).

^{1}H NMR (500 MHz, CD_3CN, δ) 9.99 (2H, d, J = 8.3 Hz), 9.71 (2H, s,), 9.70 (2H, d, J = 9.15 Hz), 9.51 (2H, d, J = 5.2 Hz), 8.64 (4H, dd, J_1 = 12.3 Hz, J_2 = 8.3 Hz), 8.29 (4H, s,), 8.31-8.25 (8H, m), 8.15 (2H, d, J = 5.7 Hz), 8.03 (2H, d, J = 4.6 Hz), 7.82 (2H, dd, J_1 = 8.3 Hz, J_2 = 5.4 Hz), 7.71 (2H, dd, J_1 = 8.3 Hz, J_2 = 5.4 Hz), 7.65 (2H, dd, J_1 = 8.6 Hz, J_2 = 5.2 Hz). HRMS-ESI $[M\text{-}3PF_6]^{3+}$ calc. 420.0476, observed. 420.0464. $[M\text{-}2PF_6]^{2+}$ calc. 702.5578, observed. 702.5480. IR (υ_{CO}, KBR, cm^{-1}): 2018 (s), 1879 (br). Anal. Calcd for $C_{59}H_{33}F_{18}N_{13}O_3P_3ReRu.H_2O$: C, 41.39; H, 2.06; N, 10.63. Found: C, 41.15; H, 1.70; N, 10.27.

3.2.2.2 $[Ru(phen)_2(tatpq)][PF_6]_2$ - $[MQ]^{2+}$

0.06 g (0.06 mmol) of $[Ru(phen)_2(tatpp)]Cl_2$ – ([MP])Cl_2 was first dissolved in 5 mL EtOH, after which 95 mL H_2O and 0.15 g (0.66 mmol) of $(NH_4)_2S_2O_8$ was added and resulting solution was heated at reflux overnight. After cooling to room temperature, the resulting solution was concentrated to minimum volume (~5 mL) by rotary evaporation. Crude product was then obtained by dropwise addition of a saturated solution of aqueous NH_4PF_6, collected by suction filtration and washed with 50 mL of water, followed by 50 mL ethanol and dried in vacuo at 60 ºC. The product was further purified by one metathesis reaction as described previously. (88 % yield, Cl^- salt). ^{1}H NMR (PF_6^-salt, 500 MHz, CD_3CN, δ) 9.99 (2H, d, J = 8.6 Hz), 9.70 (2H, d, J = 7.5 Hz,), 9.37 (2H, d, J = 3.14 Hz), 9.51 (2H, d, J = 5.2 Hz), 8.63 (4H, dd, J_1 = 13.8 Hz, J_2 = 6.9 Hz), 8.40 (4H, dd, J_1 = 9.9 Hz, J_2 = 6.6 Hz), 8.27 (4H, s), 8.26 (2H, d, J = 5.2 Hz,), 8.22 (2H, d, J = 5.2 Hz,), 8.03 (2H, d, J = 4.1 Hz,) 7.88 (4H, dd, J_1 = 8.3 Hz, J_2 = 5.4 Hz), 7.69-7.63 (4H, m). HRMS-ESI $[M\text{-}2PF_6]^{2+}$ calc. 489.08, observed. 489.08. IR (υ_{CO}, KBR, cm^{-1}): 1704 (s). Anal. Calcd for $C_{54}H_{28}F_{12}N_{12}O_2P_2Ru.4.3H_2O$: C, 48.21; H, 2.74; N, 12.49. Found: C, 47.76; H, 2.29; N; 12.51

3.2.2.3 $[Ru(phen)_2(tatppq)(CH_3CN)(CO)_3Re][PF_6]_3$ - $[\mathbf{RuReQ_{CH3CN}}]^{3+}$

Photochemical oxidation route: A solution of 0.020 g (0.01 mmol) of $[RuRe_{CH3CN}]^{3+}$ in 40 mL CH_3CN was irradiated with LED light (470 $\pm$ 15 nm) for 15 days under continuous supply of air, after which, the deep red solution was filtered and the supernatant was dried under reduced pressure. The residue obtained was dissolved in minimum acetonitrile (~5 mL) and diethyl ether added dropwise to obtain the crude product which is washed with 15 mL THF, followed by 5 mL MeOH and air dried. The residue obtained is further purified by a metathesis reaction as described previously. (33 % yield, PF_6^- salt).

Chemical oxidation route: A solution of 0.08 g (0.06 mmol) of $[MQ]Cl_2$, 0.03 (0.07 mmol) of $Re(CO)_5Cl$ and 0.03 (0.13 mmol) of $AgPF_6$ in CH_3CN was heated at reflux overnight. After cooling, the solution was filtered to remove AgCl and solvent concentrated to minimum volume (~5 mL) under reduced pressure. To this, diethyl ether was added dropwise to yield a deep red solid, which was collected by suction filtration, washed with diethyl ether (30 mL) and air dried. (78 % yield, PF_6^- salt).

^{1}H NMR (500 MHz, CD_3CN, δ) 10.0 (2H, d, J = 8.3 Hz), 9.70 (2H, d, J = 8.6 Hz,), 9.63 (2H, d, J = 5.2 Hz), 8.64 (4H, dd, J_1 = 7.4 Hz, J_2 = 5.3 Hz), 8.40 (4H, dd, J_1 = 8.0 Hz, J_2 = 5.2 Hz), 8.29 (4H, s), 8.27 (2H, d, J = 5.2 Hz,), 8.21 (2H, d, J = 5.2 Hz,), 8.04 (2H, d, J = 5.2 Hz) 7.90 (4H, dd, J_1 = 8.0 Hz, J_2 = 5.2 Hz), 7.69-7.64 (4H, m). HRMS-ESI $[M-2PF6]^{2+}$ calc. 717.5407, observed. 717.5371, $[M-3PF_6]^{3+}$ calc. 430.0390, observed. 430.0391. IR (υ_{CO}, KBR, cm^{-1}): 2039 (s), 1920 (br). Anal. Calcd for $C_{59}H_{31}F_{18}N_{13}O_5P_3ReRu$: C, 41.10; H, 1.81; N, 10.56. Found: C, 41.25; H, 1.97; N, 10.31.

3.2.2.4 $[Re(CO)_3(phen)(P(CH_2OH)_3][PF_6]$ - $[Rephen_{PR3}]^+$

A mixture of 0.08 g (0.13 mmol) of $[Redione_{CH3CN}]^+$ and 0.12 g (1.0 mmol) of PR_3 was dissolved in 10 mL of CH_3COCH_3 and 10 mL of H_2O, and heated at reflux for 5 h. The resulting solution was concentrated to minimum volume (~5 mL) by rotary evaporation and diethyl ether added dropwise to obtain the precipitate which is collected by filtration, washed with 10 mL of H_2O and air dried to obtain the pure product as deep yellow solid (88 % yield). ^{1}H NMR (500 MHz, CD_3CN, δ) 9.44 (2H, d, J = 5.2 Hz), 8.80 (2H, d, J = 8.6 Hz), 8.20 (2H, s), 7.98 (4H, dd, J_1 = 8.6, J_2 = 5.2 Hz). HRMS-ESI $[M\text{-}PF_6]^+$: calc. 575.0382, observed. 575.0327. Anal. Calcd for $C_{18}H_{17}F_6N_2O_6P2Re$: C, 30.05; H, 2.38; N, 3.89. Found: C, 29.59; H, 2.43; N, 3.62.

3.2.2.5 $[Ru(phen)_2(tatpp)P(CH_2OH)_3(CO)_3Re][PF_6]_3$ - $[RuRe_{PR3}]^{3+}$

A solution of 0.08 g (0.05 mmol) of $[RuRe_{CH3CN}]^{3+}$ and 0.05 g (0.40 mmol) PR_3 in 10 mL of CH_3COCH_3 and 10mL H_2O was heated at reflux in dark overnight. The resulting solution was allowed to cool to room temperature after which saturated solution of aqueous NH_4PF_6 was added dropwise to precipitate the crude product. The precipitate formed was collected by suction filtration and purified by repeated metathesis reaction between PF_6^- and Cl^- salts as described previously to obtain the pure product as deep red brown solid. (0.05 g, 60 % yield, $PF6^-$ salt). ^{1}H NMR (500 MHz, CD_3CN, δ) 9.93 (2H, d, J = 8.1 Hz), 9.83 (2H, d, J = 6.3 Hz), 9.70 (2H, s,), 9.6 (2H, d, J = 4.6 Hz), 8.64 (4H, dd, J_1 = 12.01 Hz, J_2 = 8.61 Hz), 8.30 (2H, d, J = 5.8 Hz), 8.28 (2H, s), 8.18 (2H, dd, J_1 = 8.0 Hz, J_2 = 5.2 Hz), 8.15 (2H, d, J = 4.6 Hz), 8.03 (2H, d, J = 5.2 Hz), 7.82 (2H, dd, J_1 = 8.3 Hz, J_2 = 5.4 Hz), 7.71 (2H, dd, J_1 = 8.2 Hz, J_2 = 5.6 Hz), 7.65 (2H, dd, J_1 = 8.6 Hz, J_2 = 5.2 Hz), 3.9 (6H, d, J = 3.4 Hz), 3.2 (3H, s). HRMS-ESI $[M\text{-}3PF_6]^{3+}$ calc. 447.719, observed. 447.704. $[M\text{-}2PF_6]^{2+}$ calc. 744.059,

observed. 744.052. IR (U_{CO}, KBR, cm^{-1}): 2034 (s), 1917 (br). Anal. Calcd for $C_{60}H_{39}F_{18}N_{12}O_6P_4ReRu$: C, 40.55; H, 2.21; N, 9.46. Found: C, 39.92; H, 2.47; N, 9.24.

3.2.3 DNA Cleavage Assay

3.2.3.1 Reagents

Ethidium bromide (EtBr), glutathione (GSH), Tris-Cl, EDTA (ethylenediaminetetraacetic acid), trizma base, tris acetate, sodium phosphate, bromophenol blue, glycerol and agarose were purchased from Sigma Aldrich and used as received. Supercoiled pUC 19 DNA (0.1 μg/μL, 0.154 mM DNA base pairs) was purchased from Bayou Biolabs. 1X TAE buffer (40 mM Tris-acetate, 1 mM EDTA, pH 8.0), 6x bromophenol blue loading solution and sodium phosphate buffer (7.0 mM, pH 7.0) were prepared as per established procedures.

3.2.3.2 Preparation of Agrose gel

Agrose gel (1%) was prepared by dissolving 0.04 g of agrose in 40 mL of hot 1X TAE and poured into a casting tray fitted with comb to form the sample wells. The gel was left undisturbed to solidify (usually 20-30 min) before the comb is removed carefully. The solidified gel was then placed in the electrophoretic tank containing TAE buffer with 0.2 mM EtBr.

3.2.3.3 Preparation of Stock Solutions

GSH stock solution was prepared in phosphate buffer to have the final concentration of [GSH] = 100 x [Complex] mM. Due to poor aqueous solubility of $[RuRe_{CH3CN}]^{3+}$ stock solution was prepared in 100% DMSO to a [Complex] = 0.0641 mM. 8μL of this stock was used such that the final concentration of DMSO in the eppendorf upon incubation was 20%

(Table details incubation conditions). $[RuRe_{PR3}]^{3+}$ was dissolved in minimum water and made upto volume by phosphate buffer to final [Complex] = 0.0641 mM.

3.2.3.4 DNA Cleavage reaction

The DNA cleaving ability of $[RuRe_{CH3CN}]^{3+}$ and $[RuRe_{PR3}]^{3+}$) was studied by following the conversion of supercoiled DNA to the nicked circular or linear forms using agrose gel electrophoresis as described previously.[104]. In a typical cleavage experiment, 4 μL of supercoiled pUC19 DNA and the test compound was incubated separately with and without GSH in 7 mM sodium phosphate buffer (pH 7.0) for 12 hrs in dark (Table 2). To these, 12 μL of loading buffer containing 3% glycerol and 0.1% w/v bromophenol blue was added and 8 μL of this preparation was loaded into a well of 1% agrose gel submerged in TAE buffer. The gel was subjected to electrophoresis at 70 V for 90 min and cleavage products visualized using a UVPGDS 8000 gel analysis system.

For all the complexes examined, the first two lanes were controls containing just the DNA by itself and DNA with GSH. If DMSO was the solvent in complex stock preparation, an additional lane of DNA, GSH and DMSO with equivalent % DMSO was used as control. The detailed experiment is depicted in Table 2.

Table 2 Typical DNA cleavage assay incubation conditions. [DNA] =0.154 mM, [GSH] = 100 x [Complex], [complex] = 0.0128 mM

Eppendorf	**1**	**2**	**3**	**4**	**5**	**6**
DNA	4 µL	4 µL	4 µL	4 µL	4 µL	4 µL
GSH		8 µL		8 µL		8 µL
[P]Cl_4			8 µL	8 µL		
RuRe complex					8 µL	8 µL
Na_3PO_4 Buffer	36 µL	28 µL	28 µL	24 µL	28 µL	24 µL
Total Volume	40 µL	40 µL	40 µL	40 µL	40 µL	40 µL

3.2.4 Cytotoxicity Determination

3.2.4.1 Reagents

Growth medium RPMI-1640 and DMEM, supplements fetal bovine serum (FBS), penicillin/streptomycin solution (P/S) and BME Vitamins, 100x, trypsin-EDTA (1X), DMSO, 0.04% Trypan Blue (Sigma) and 3-(4,5-dimethylthiazol-2-yl)-2,5-diphenyltetrazolium bromide (MTT) were purchased from Sigma Aldrich. Phosphate buffered saline (PBS,1X, 10 mM) was prepared in lab.

3.2.4.2 Cell lines and culture details

Non-small cell lung carcinoma (NSCLC) H358 and HOP62, colon carcinoma (HCC 2998), and breast carcinoma (MCF7) lines were obtained from Dr. Macdonnell laboratory. HCC-2998 and HOP62 were cultured in RPMI-1640 medium supplemented with 10% FBS, 1.1% penicillin/streptomycin solution and 1x BME Vitamin (v/v). MCF7 cells were cultured in DMEM medium supplemented with 10% FBS, 1.1% penicillin/streptomycin solution and

1% L-glutamine (v/v). Cells were seeded and passaged as per the culturing protocol by ATCC and maintained at 37 °C in a humidified atmosphere of 5% CO_2.

3.2.4.3 MTT Assay to determine Cell viability

Cell viability and proliferation as affected by the test drug was assessed by MTT Cell Proliferation Assay. Briefly, cells were seeded into each well of a 96 well plate at a seeding density of ~ 2 x 10^4 cells/well containing 180 µL of growth medium, and left to incubate for 24 h before the cells are treated with increasing concentration of the test drug, $[RuRe_{PR3}]^{3+}$ and cisplatin as control. 100 mM drug stock solution is prepared previously in DMSO and diluted with Millipore water to get the working solutions with the final drug concentrations of 0.0175, 0.0315, 0.0625, 0.125, 0.25 and 0.50 mM. 20 µL of working solution/concentration was then added to the 180 µL of cell medium in 96 well plate leading to a final concentration of 1.75, 3.15, 6.25, 12.5, 25, 50 µM of drug/well with 4 replicate wells/concentration. The final concentration of DMSO in treated culture is > 0.1% at that point. The basic layout of the experiment in 96 well plate is shown in Table 3.

Table 3 Demonstration of a 96 well plate MTT experiment. For example, wells 1c-6c and 7c-12c are treatment lanes with increasing concentration of cisplatin and $[RuRe_{PR3}]Cl_3$ respectively, and wells 1c-1f demonstrate 4 replicate wells of 1.7 µM cisplatin and so on

Lane	**1**	**2**	**3**	**4**	**5**	**6**	**7**	**8**	**9**	**10**	**11**	**12**
a	Blank (no cells, growth medium only)											
b	Negative control (cells with growth medium and >0.1 % DMSO, no drug)											
c	1.7	3.1	6.2	12	25	50	1.7	3.1	6.2	12	25	50
d	Cisplatin (µM)						$[RuRe_{PR3}]Cl_3$ (µM)					
e												
f	1.7	3.1	6.2	12	25	50	1.7	3.1	6.2	12	25	50
g	Negative control (cells with growth medium and >0.1 % DMSO, no drug)											
h	Blank (no cells, growth medium only)											

After 96 h of incubation, 30 µL of MTT reagent (5 mg MTT/mL PBS) was added to each well of 96 well plate and incubated for 4 h during which MTT is converted to insoluble formazan in the mitochondria of living cells that allows direct measurement of cell viability in each well. After 4 h of MTT incubation, the medium is carefully removed and 120 µL of DMSO is added to each well to dissolve formazan. The plate is mounted on a plate shaker for 30 min and absorbance read at 570 nm on a microplate reader. The IC_{50}, which is the inhibitory concentration that reduces cell viability by 50%, was then determined by plotting a dose response curve of % viable cells against drug concentrations tested. The IC_{50} values reported for each cell line are from three separate experiments.

3.2.5 Animal Studies

3.2.5.1 Maximum Tolerable Dose (MTD)

The purpose of this study was to determine MTD, the maximum dose of the test drug that the animal can withstand without showing signs of sickness or morbidity and was determined as described previously.[55] In brief, 6 Male Balb/C Mice at 14 weeks of age were randomly allocated into 2 groups, a control and a treatment group of 3 mice/group. The treatment group received test drug $[RuRe_{PR3}]Cl_3$ at increasing concentration via IP injection for 5 consecutive days, while the control group received 30% H_2O:PBS. The drug concentrations administered were: 6.0 mg/mL (20 mg drug/kg mouse weight), 12.0 mg/mL (40 mg drug/kg mouse weight), 18.0 mg/mL (60 mg drug/kg mouse weight), 24.0 mg/mL (80 mg drug/kg mouse weight), 48.0 mg/mL (180 mg drug/kg mouse weight). To prepare each drug concentration, required amount of $[RuRe_{PR3}]Cl_3$ complex was dissolved in 30% millipore water and made upto volume by PBS. After IP injection, both the groups were closely monitored twice every day for signs of sickness or distress and a total of 24 h before the next higher dose is given (only if they survived the previous dose without toxicity).

All animal procedures were conducted in accordance to approved IACUC (Institutional Animal Care and Use Committee) protocol A08.018, dated 02/20/08 of UTA.

3.2.5.2 Renal clearance Study

This study was conducted to determine the renal clearance, if any, of the test drug. For this, two mice from treatment group after the 3rd dose of 18.0 mg/mL (60 mg drug/kg mouse weight) was administered were put in special cages designed to aid urine collection. One mice from control group was put in a separate cage after PBS administration. Minimal food was put in both cages to promote water consumption over a period of 24 h, after which,

urine is carefully collected with the help of minimum PBS (to wash off dried urine), and transferred into separate vials, filtered and submitted for Mass Spectrometry analysis.

3.2.5.3 Biodistribution Study

In order to follow the biodistribution of the test drug $[RuRe_{PR3}]Cl_3$ in the body tissues following IP injection, two mice from the treatment group after 72 h of the last dose of 48.0 mg/mL (160 mg/kg) administered and one mice from control group were euthanized by CO_2 and autopsied. The third mice from treatment group and two mice from control group were autopsied 2 weeks after the last dose of 48.0 mg/mL (180 mg/kg) administered. The body was visually inspected for precipitation or drug accumulation which should be apparent by the dark color of the complex and various organs such as liver, kidney, lungs and heart were collected and stored at -80 ºC immediately.

3.3 Results and Discussion:

3.3.1 Synthesis and Characterization

Complex $[RuRe_{CH3CN}]^{3+}$ and $[RuRe_{PR3}]^{3+}$ were prepared as depicted in Figure 3.1. A reaction between $[MP](PF_6)_2$, prepared by literature method[103], and $Re(CO)_5Cl$ in refluxing MeCN in the presence of $AgPF_6$ results in the formation of $[RuRe_{CH3CN}]^{3+}$ in moderate yield (66%). This complex was readily soluble in MeCN or $(CH_3)_2CO$ as PF_6^- salt and methanol as Cl^- salt, but poorly soluble in H_2O which was unexpected given the free solubility of the precursor complex $[MP]Cl_2$ in H_2O. Additionally visible light irradiation (470 $\pm$ 15 nm) of this complex in MeCN (PF_6^- salt) under aerobic conditions also produced the quinone analogue $[RuReQ_{CH3CN}]^{3+}$, while no such oxidation was observed for $[MP](PF_6)_2$ even after prolonged irradiation of over 6 d in air. In fact harsh conditions such as peroxydisulfate oxidation of $[MP]Cl_2$ in refluxing EtOH and H_2O can drive the reaction to obtain the respective quinone

$[MQ]^{2+}$ (Yield 88%). It is unequivocally a photoxidation process because no changes in ^{1}H NMR was observed unless the sample is irradiated continuously or O_2 is removed.

In Chapter 2, we reported on the similar photoactivity of complex $[ReP_{CH3CN}]^{2+}$, however, it is noteworthy that with $Ru(phen)_2$ present, the stability is considerably improved in that, the photooxidation of $[RuRe_{CH3CN}]^{3+}$ requires considerably longer reaction time of 3 days versus 30 min as in $[ReP_{CH3CN}]^{2+}$, for an NMR scale reaction (1.0 mg/mL CD_3CN). The complexity and slowness of this process is further supported by the considerably low yield of only 33%. Alternatively, $[RuReQ_{CH3CN}]^{3+}$ was obtained in high yield (78%) by the chemical oxidation of $[MP]^{2+}$ to $[MQ]^{2+}$ followed by Re coordination in refluxing MeCN in presence of $Re(CO)_5Cl$ (Fig 3.1).

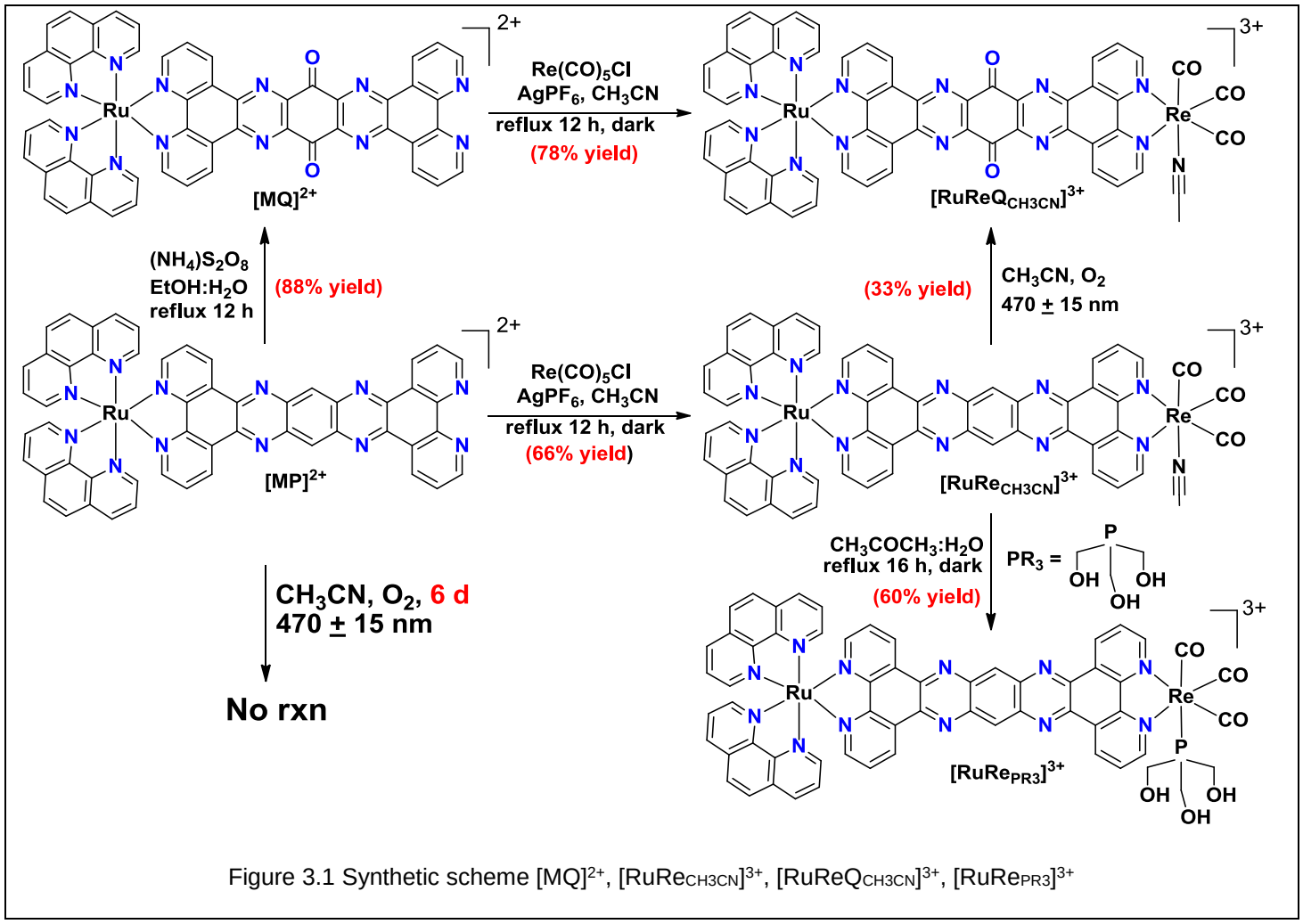

Figure 3.1 Synthetic scheme $[MQ]^{2+}$, $[RuRe_{CH3CN}]^{3+}$, $[RuReQ_{CH3CN}]^{3+}$, $[RuRe_{PR3}]^{3+}$

The phosphine derivative, $[RuRe_{PR3}]^{3+}$ was obtained in 60% yield by a reaction of $[RuRe_{CH3CN}]^{3+}$ with excess PR_3 in 1:1 $(CH_3)_2CO:H_2O$. The structures of $[RuRe_{CH3CN}]^{3+}$, $[RuReQ_{CH3CN}]^{3+}$, $[MQ]^{2+}$, $[RuRe_{PR3}]^{3+}$ and $[Rephen_{PR3})]^{+}$ were confirmed by ^1H NMR, IR, ESI-HRMS and CHN. The overlaid ^1H NMR spectra of $[MP]^{2+}$ with Zn(II) ions, $[RuRe_{CH3CN}]^{3+}$ and $[RuRe_{PR3}]^{3+}$ in d_3-acetonitrile is shown in Figure 3.2 and is assigned based on the peak integrals and coupling constants, as well as by the comparison with $[MP]^{2+}$, $[P]^{4+}$ and $[ReP_{CH3CN}]^{2+}$ which helped identifying the phen peaks on tatpp associated with Ru (H_a, H_b, H_c) and Re ($H_{a'}$, $H_{b'}$, $H_{c'}$) centers. Clearly Re coordination shifts the resonances of $H_{c'}$, H_c, H_d and $H_{a'}$ protons downfield relative to their position in $[MP]^{2+}$, of which the most noticeable shift is in the position of $H_{a'}$, which is observed at 9.51 and 9.55 ppm in $[RuRe_{CH3CN}]^{3+}$ and $[RuRe_{PR3}]^{3+}$ but leaves the other protons relatively unaffected, except a small upfield shift of H_a and $H_{b'}$ (Fig 3.2).

For quinone analogues $[MQ]^{2+}$ and $[RuReQ_{CH3CN}]^{3+}$, the most diagnostic difference, other than the missing singlet for H_d proton, in a small upfield shift of H_2 proton by ~0.06 ppm such that it overlaps with H_7 and collectively appears as a multiplet is of note (Fig 3.3). Similar overlap in the ^1H NMR of complex $[(phen)_2Ru(tatpq)Ru(phen)_2]^{4+}$ is reported which is the chemical oxidation product of $[P]^{4+}$.[80]

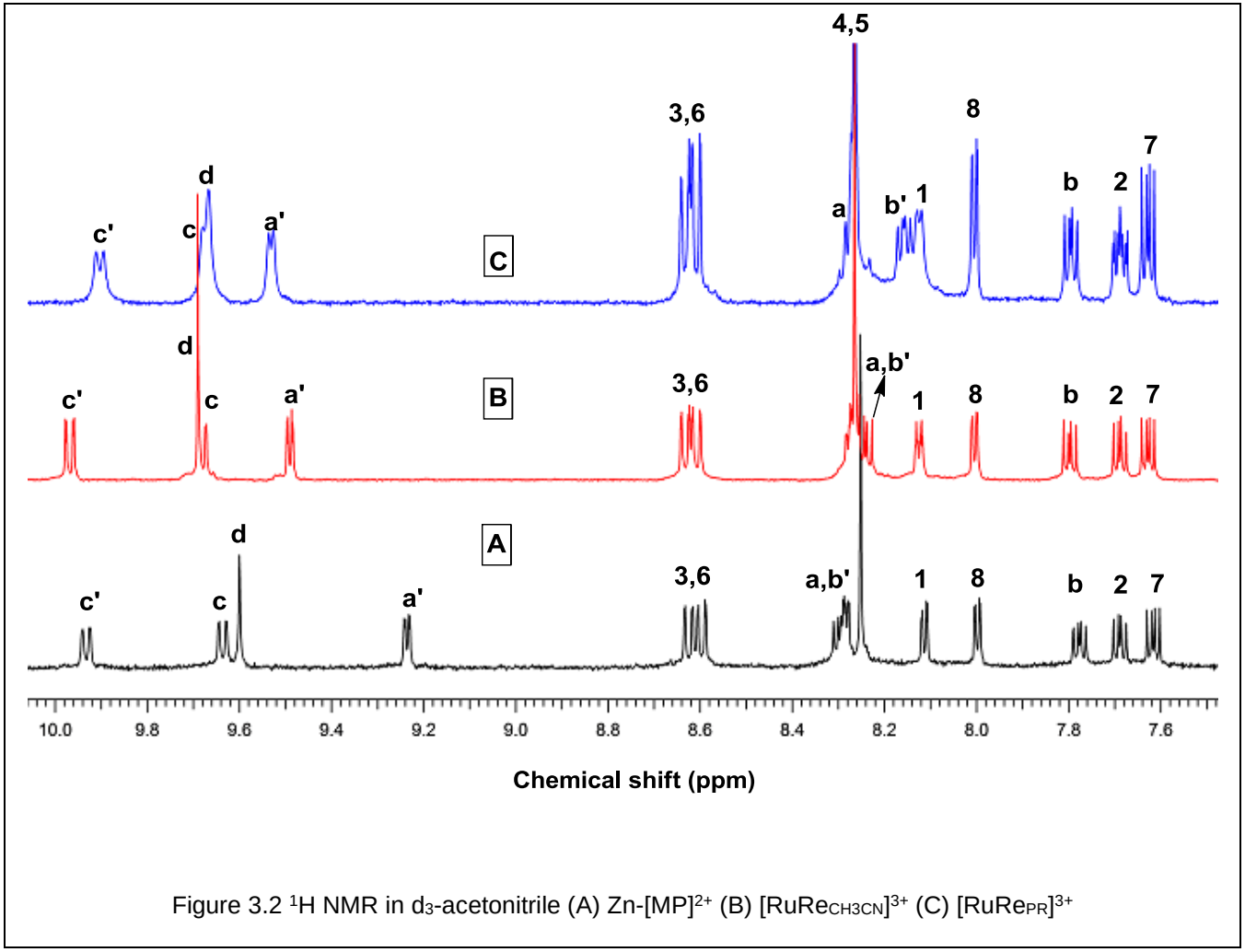

Figure 3.2 ^{1}H NMR in d_3-acetonitrile (A) Zn-$[MP]^{2+}$ (B) $[RuRe_{CH3CN}]^{3+}$ (C) $[RuRe_{PR}]^{3+}$

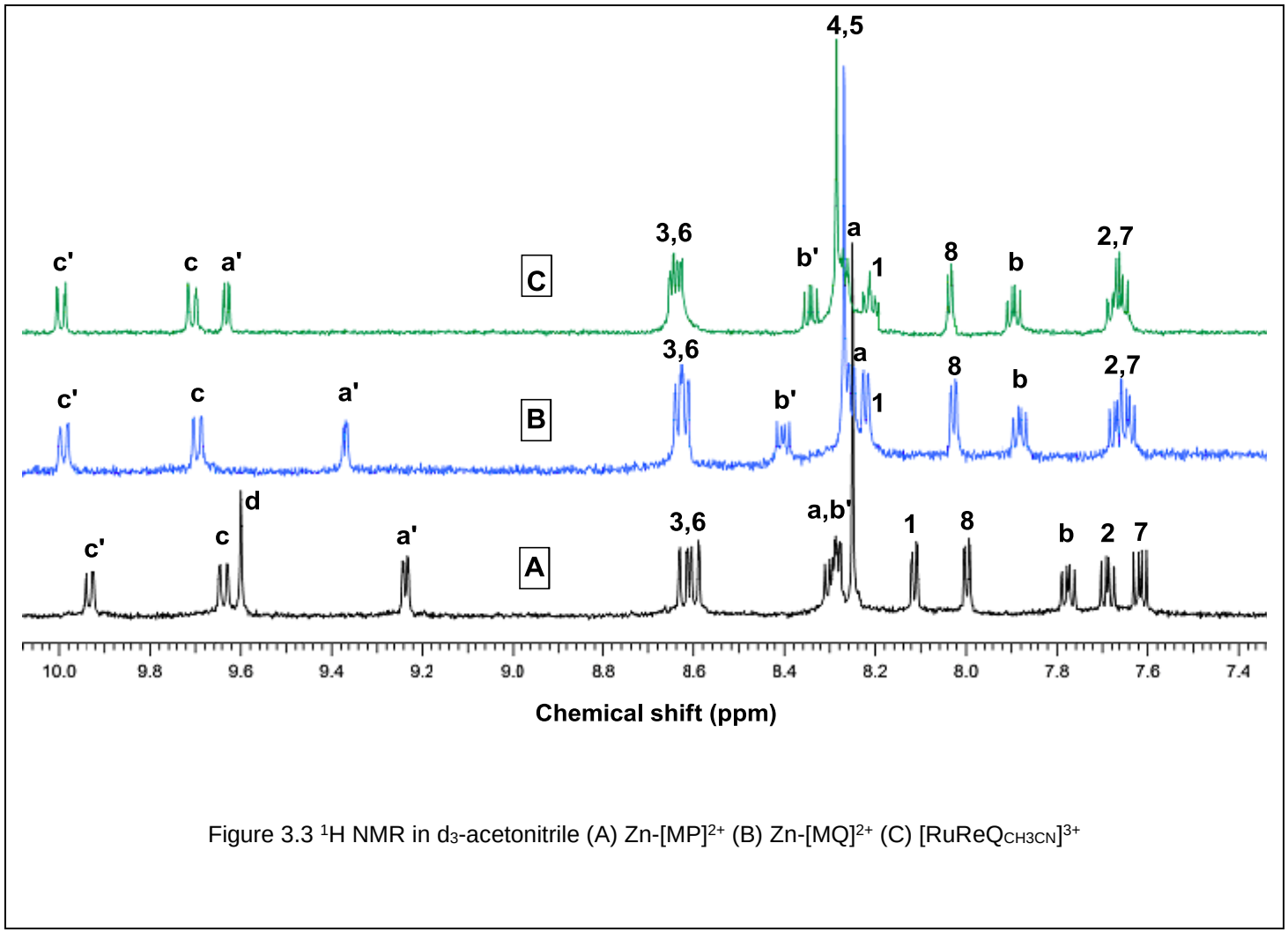

Figure 3.3 ^{1}H NMR in d_3-acetonitrile (A) Zn-$[MP]^{2+}$ (B) Zn-$[MQ]^{2+}$ (C) $[RuReQ_{CH3CN}]^{3+}$

The IR spectra of $[RuRe_{CH3CN}]^{3+}$, $[RuRe_{PR3}]^{3+}$ and $[RuReQ_{CH3CN}]^{3+}$ complexes show characteristic υ_{CO} absorptions in the range of 1870-2050 cm^{-1} confirming the attachment of $Re(CO)_3$ moiety, and a separate ketonic stretch at 1704 and 1708 cm^{-1} in $[MQ]^{2+}$ and $[RuReQ_{CH3CN}]^{3+}$ respectively. The ESI-HRMS spectra for all five complexes show peaks consistent with parent ions $[M\text{-}PF_6]^+$, $[M\text{-}2PF_6]^{2+}$ and $[M\text{-}3PF_6]^{3+}$ (where applicable) and in high agreement with calculated values. The formation of all five complexes is further supported by CHN analysis.

3.3.2 DNA cleavage

The DNA cleaving ability of tatpp complexes $[RuRe_{CH3CN}]^{3+}$ and $[RuRe_{PR3}]^{3+}$ to the nicked circular or linear forms was studied using supercoiled pUC 19 DNA as the target and agrose gel electrophoresis mobility assay as the sieving process (Fig 3.4). Complex $[ReP_{CH3CN}]^{2+}$and [ReP] were also tested, although they appear to precipitate out due to poor solubility and thus the results are inconclusive for these complexes and thus are included in the appendix for archival purposes.

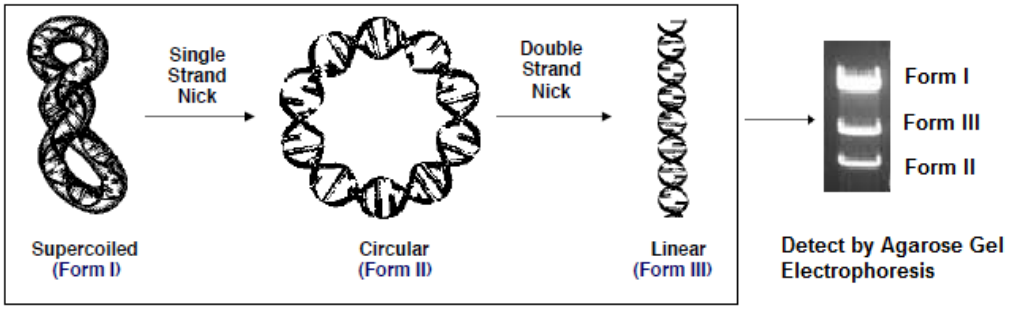

Figure 3.4 Confirmations of plasmid DNA, supercoiled (Form I), circular (Form II) and linear (Form III) and detection by agrose gel electrophoresis

The results of the assays for complex $[RuRe_{CH3CN}]Cl_3$ and $[RuRe_{PR3}]Cl_3$ are depicted in Fig 3.5. For both gels, lanes 1-2 are controls for DNA and GSH, while lane 3 in top gel is a control for DNA, GSH, and DMSO and as expected, little or no cleavage is observed in any of these. Complex $[P]Cl_4$ was used as a positive control since it is an effective DNA cleaving agent in presence of GSH. This is also seen in Lanes 4-5 (top gel) and lanes 3-4 (bottom gel) in that the cleavage activity is enhanced with added reductant. Similarly for complex $[RuRe_{CH3CN}]Cl_3$ and $[RuRe_{PR3}]Cl_3$, DNA cleavage is only observed when GSH present (Lane 7 and 6 respectively) which strongly support the role of redox activity of tatpp in the cleavage reaction here.

Lane	1	2	3	4	5	6	7
DNA	+	+	+	+	+	+	+
GSH			+		+		+
DMSO		+	+	+	+	+	+
$[P]Cl_4$				+	+		
$[RuRe_{CH3CN}]Cl_3$						+	+

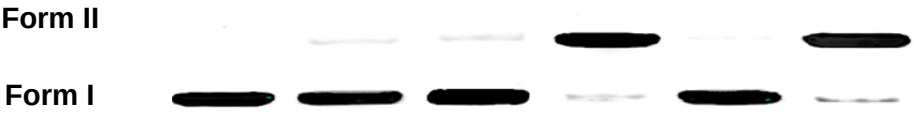

Lane	1	2	3	4	5	6
DNA	+	+	+	+	+	+
GSH		+		+		+
$[P]Cl_4$			+	+		
$RuRe_{PR3}]Cl_3$					+	+

Figure 3.5 DNA cleavage of supercoiled pUC19 DNA (Form I) to nicked circular (Form II) by complex $[RuRe_{CH3CN}]Cl_3$ (top) and $[RuRe_{PR3}]Cl_3$ at 25ºC in 7mM Na_3PO_4 buffer (pH 7.0) after 12 h of incubation where [DNA] =0.154 mM, [GSH] = 100 x [Complex], [Complex] = 0.0128 mM, DMSO = 20%

Additionally, it is noteworthy that although the cleavage activity by $[RuRe_{PR3}]Cl_3$ is comparable to that of $[P]Cl_4$ (lanes 4 and 6, bottom gel), cleavage induced by $[RuRe_{CH3CN}]Cl_3$ is relatively greater. While we are unsure but this could be related to the lability of acetonitrile ligand as many well-known metallopharmaceuticals are known to function via adduct formation with DNA upon loss of labile ligand(s), with cisplatin as one of them. Therefore, two processes, generation of reactive intermediate upon in situ reduction by GSH (as in $[P]^{4+}$) and adduct formation via loss of labile acetonitrile ligand (unlike $[P]^{4+}$), might be responsible for greater cleavage activity in this case, however further studies would be needed to warrant this assumption. Nonetheless, comparable cleavage induced by substitutionally inert $[RuRe_{PR3}]Cl_3$ and $[P]Cl_4$ provides a good basis to support the assumption just made above.

Even though it is clear that $[RuRe_{CH3CN}]Cl_3$ induces greater DNA cleavage relative to $[P]Cl_4$ or $[RuRe_{PR3}]Cl_3$ which may have important implications therapeutically, however, it is the poor water solubility that puts it at a disadvantage and limits its cell culture studies since cells cannot survive the amount of DMSO (>10%) needed to keep it in solution. For this reason, only the $[RuRe_{PR3}]Cl_3$ complex was screened for cytotoxicity against 4 different cancer cell lines: lung carcinomas (H358 and HOP62), colon carcinoma (HCC2998), and breast carcinoma (MCF7) as discussed in the next section.

3.3.3 Cytotoxicity and Animal Studies Results

The IC_{50} values obtained are depicted in the form of bar graph in Fig 3.6. Cisplatin was used as positive control. The data with individual IC_{50s} for each cell line along with SD's is summarized in Table 4.

From the data obtained, we observe that complex $[RuRe_{PR3}]Cl_3$ exhibits higher cytotoxicity of 8 µM against H358 cells and comparable IC_{50} of 55 µM against HOP62 cells in comparison to respective values of 15 µM and 50 µM for the parent drug $[P]Cl_4$[42, 105], indicating minimal difference due to added Re functionality, but this trend did not continue as we examined the other two cell lines. This is evident from the noticeably high IC_{50} of >50 µM of complex $[RuRe_{PR3}]Cl_3$ against HCC2998 and MCF7 cells. For complex $[P]Cl_4$, we have previously reported on the regression of tumor growth and doubled survival time in H358 NSCLC xenograft mouse models. In the present case, given the high cytotoxicity of $[RuRe_{PR3}]Cl_3$ in H358 cells, subsequent studies will be needed to show whether this improvement may result in an increased efficacy in vivo.

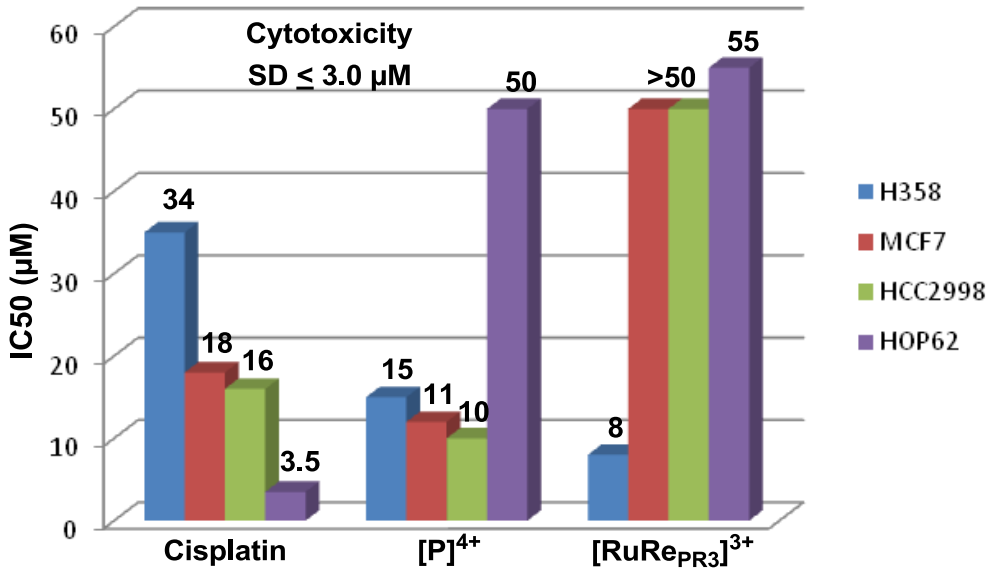

Figure 3.6 Cytotoxicity results of complex $[RuRe_{PR3}]Cl_3$

MTD was determined as outlined in the experimental section. Throughout the duration of study, mice were monitored closely for signs of sickness such as pain or distress as well as loss in body weight or impaired mobility, plus an additional two weeks after the last dose of 160 mg/kg was administered, but no notable difference in behavior or health of treatment group compared to control was seen and thus an MTD of >160 mg/kg was assigned for $[RuRe_{PR3}]Cl_3$ which is equivalent to that reported for $[P]Cl_4$, while cisplatin and $[MP]Cl_2$ have relatively very low MTDs of <20 mg/kg[106] and <40 mg/kg respectively.[42] Comparative IC_{50s} and MTD values are summarized in Table 4.

Table 4 IC_{50s} and MTD values summarized

	H358	**MCF7**	**HCC2998**	**HOP62**	**MTD**
Complex	**IC_{50} (μM)**				**(mg/kg)**
Cisplatin	35 ± 2.1	15 ± 4.0	16 ± 1.5	3.5 ± 1.2	20
$[P]^{4+}$	15 + 1.8	11 + 1.5	10 + 3.0	50 ± 1.9	>160
$[RuRe_{PR3}]^{3+}$	8.0 + 3.0	> 50	>50	55 ± 2.1	>160

Since the treated mice showed no abnormality, we speculate that $[RuRe_{PR3}]Cl_3$ might be excreted in urine and feces, in view of the earlier report by Dwyer and coworkers on the high stability of RPC $[Ru(phen)_3]^{2+}$ in vivo and renal drug clearance almost entirely.[24] In the present case, although we are yet to prove this, substantial body clearance however was apparent in the notable dark red color of the urine collected over a period of 24 h.

Furthermore, biodistribution profile of the test drug in the animal tissues after the course of MTD study, as determined by visual inspection, appeared to be very different for the mice autopsied at two different time frames. For the mice incised 72 h after the last

dose of 48 mg/mL (180 mg/kg) was administered, we noticed heavy staining of the entire intraperitoneal cavity including precipitation of the unadsorbed complex in liver and heart by the dark red black color, whereas the mice incised 12 days after the last dose of 48 mg/mL (10 mg/kg) administered appeared to be all clear (Fig 3.7). Although we are yet to determine %heavy metal in the various organs of the autopsied mice collected at respective time frames, this observation strongly indicates gradual body clearance. Dr. Yadav in our lab also reported no significant accumulation of complex $[P]Cl_4$ in any organ of mice[55] which were administered a single dose of 33.3 mg/kg, thus, it is reasonable to assume that initial build up in the present case is possibly a consequence of heavy drug dosage administration as part of MTD experiment.

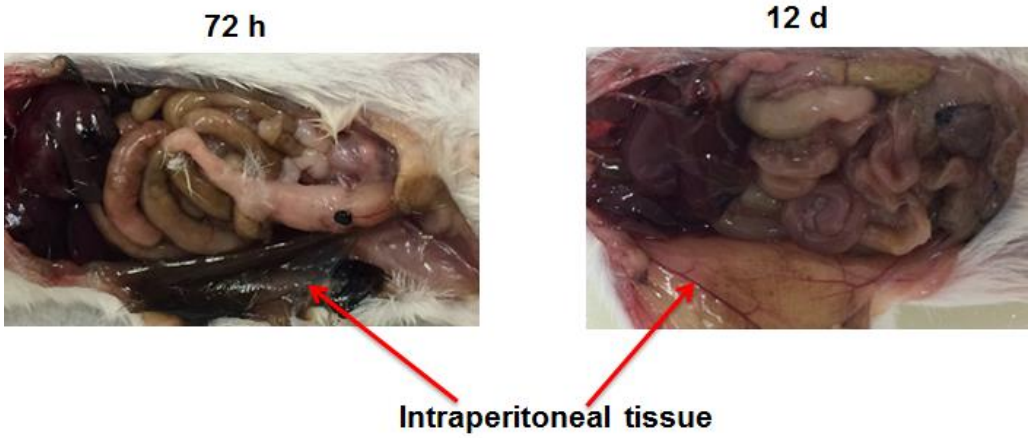

Figure 3.7 Biodistribution (visual inspection)

3.4 Conclusion

Two novel heterobimetallic Ru(II)-Re(I)tatpp complexes $[RuRe_{CH3CN}]^{3+}$ and $[RuRe_{PR3}]^{3+}$ have been prepared and characterized by ^{1}H NMR, IR, HRMS as well as CHN, and their DNA cleavage activity examined. It is found that while complex $[RuRe_{PR3}]^{3+}$ demonstrate comparable DNA cleavage activity in regards to $[P]^{4+}$, $[RuRe_{CH3CN}]^{3+}$ is by far more effective, indicating that substituent's at axial position may have pronounced effect in their observed biological activity. While we are yet to prove this, we speculate that greater DNA cleavage by $[RuRe_{CH3CN}]Cl_3$ may be related to the lability of acetonitrile ligand.

Photooxidation of complex $[RuRe_{CH3CN}]^{3+}$ is also examined to show that this complex is less reactive than homometallic Re(I)tatpp complex $[ReP_{CH3CN}]^{2+}$ but will undergo photooxidation to the quinone analogue $[RuReQ_{CH3CN}]^{3+}$ after prolonged irradiation in air but then in relatively low yield (33 %), while no such activity is observed for complex $[P]^{4+}$ or $[MP]^{2+}$. Alternatively, high yield synthetic route (78%) to $[RuReQ_{CH3CN}]^{3+}$ via chemical oxidation of $[MP]^{2+}$ to $[MQ]^{2+}$ analogue followed by Re coordination is also reported. The formation of both the complexes, $[MQ]^{2+}$ and $[RuReQ_{CH3CN}]^{3+}$ is supported by ^{1}H NMR, IR, HRMS as well as CHN.

Due to the poor aqueous solubility of $[RuRe_{CH3CN}]^{3+}$, further biological studies were conducted with $[RuRe_{PR3}]^{3+}$ and found that while the IC_{50s} for H358 and HOP62 cell lines are comparable to that reported for $[P]^{4+}$, similar activity is not seen with other two cell lines tested. In future, further cytotoxicity screening of $[RuRe_{PR3}]^{3+}$ against various malignant and non-malignant cell lines would be required to understand the activity pattern.

Dose escalation toxicity studies in mice reveal that like $[P]^{4+}$, $[RuRe_{PR3}]^{3+}$ is safe at levels up to 160 mg drug/kg mouse with no obvious side effects, when administered

via IP injection. Biodistribution analysis reveal gradual body clearance, possibly in urine, as apparent from the color of the urine collected from treated mice as well as visual inspection of mice autopsied at two different time frames.

Chapter 4

UNEXPECTED LUMINESCENCE OF HETEROBIMETALLIC Ru(II)-Re(I) TATPP ANALOGUES : LUMINESCENT PROBES TO DETERTMINE CELLULAR LOCALIZATION

4.1 Introduction

RPCs represent extensively studied class of transition metals complexes due to their excellent stability in aqueous environments and their propensity to non-covalently bind a number of biological substrates. Perhaps the best known example is the molecular 'light switch', $[(phen)_2Ru(dppz)]^{2+}$, shown in Figure 4.1, which Barton and co-workers showed binding to duplex DNA via a combination of intercalation and electrostatics and a considerable enhancement of the complex luminescence upon binding.[107] Since then, a number of RPCs have been examined for their potential as biological stains or fluorophores, photoactivated DNA cleavage agents, heavy metals tags, and potential anti-tumor agents.

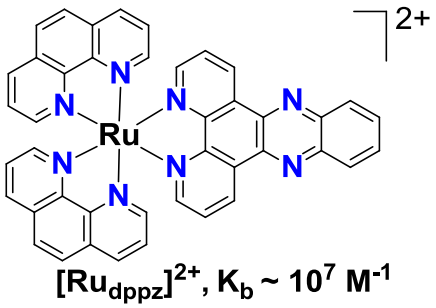

Figure 4.1 Structure of $[(phen)_2Ru(dppz)]^{2+}$

Ultimately, not much is known about the cellular target(s) or mechanism(s) by which any RPCs function in live cells. Numerous studies of compound cytotoxicity do not

probe the potential mode of action.[108]. A number of groups have used the inherent luminescence of the RPCs and confocal microscopic imaging to determine RPC localization or colocalization with known organelle dyes. These and related studies have revealed a wide assortment of potential targets including: nuclear DNA[109, 110], mitochondria[26, 27, 111,47] cytoplasm[112], endoplasmic reticulum[50], plasma membranes,[49] and/or changing cell morphology, cell-cell contacts, or cell-matrix contacts.[43] Granted in all of these various studies, different RPCs were under examination and the breadth of cellular structures targeted reveal that relatively minor structural changes appear to have major consequences in the structures targeted. Furthermore, not all the RPCs studied are particularly cytotoxic, at least in a potentially therapeutic way and where the data is available, most of the more potent RPCs show little to no selectivity for malignant over normal cells.[20] For those with demonstrable cytotoxic activity, preferential localization in a given organelle suggests this is the site of biological activity, although it does not prove it. In fact, it seems likely that many RPCs share some common cellular targets, such as the mitochondria, and some basal level of cytotoxicity.

We recently reported that RPCs, $[MP]^{2+}$ and $[P]^{4+}$ are potential chemotherapeutic drugs due to their unique DNA cleavage activity, antitumor properties and relatively low toxicity in vivo and in vitro.[61] We postulate that all RPCs may have some ability to poison mitochondrial function, which leads to non-discriminate cell cytotoxicity, whereas $[MP]^{2+}$ and $[P]^{4+}$, with their additional unique DNA cleavage activity display a more selective and targeted cytotoxicity against malignant cell lines. While we would like to map the cellular distribution of $[MP]^{2+}$ and $[P]^{4+}$ using confocal microscopy, but unfortunately, these tatpp-based complexes are non-luminescent due to excited state deactivation to a low-lying ligand-centered triplet on the tatpp ligand.[80, 113] This is due to the electron transfer from inherently luminescent "$^3MLCT_{prox}$" state (also referred to as bright state), in which the

promoted electron resides on the proximal phen part of the bridge (Figure 4.2) as in **[Ru(phen)$_3$]$^{2+}$**, to lower energy "^{3}MLCT$_{dist}$" state (also referred as dark state) involving population of distal phenazine like central part of the bridge. The significance of this charge separated (CS) state is illustrated in Jablonski diagram shown in Figure 4.2. The long extended structure of tatpp bridge further makes the availability of low lying ^{3}LC states low enough in energy to deactivate the CS state by energy transfer (ET) thus making ^{3}LC as the lowest excited state of the system that decays to ground state non-radiatively.[113, 114]

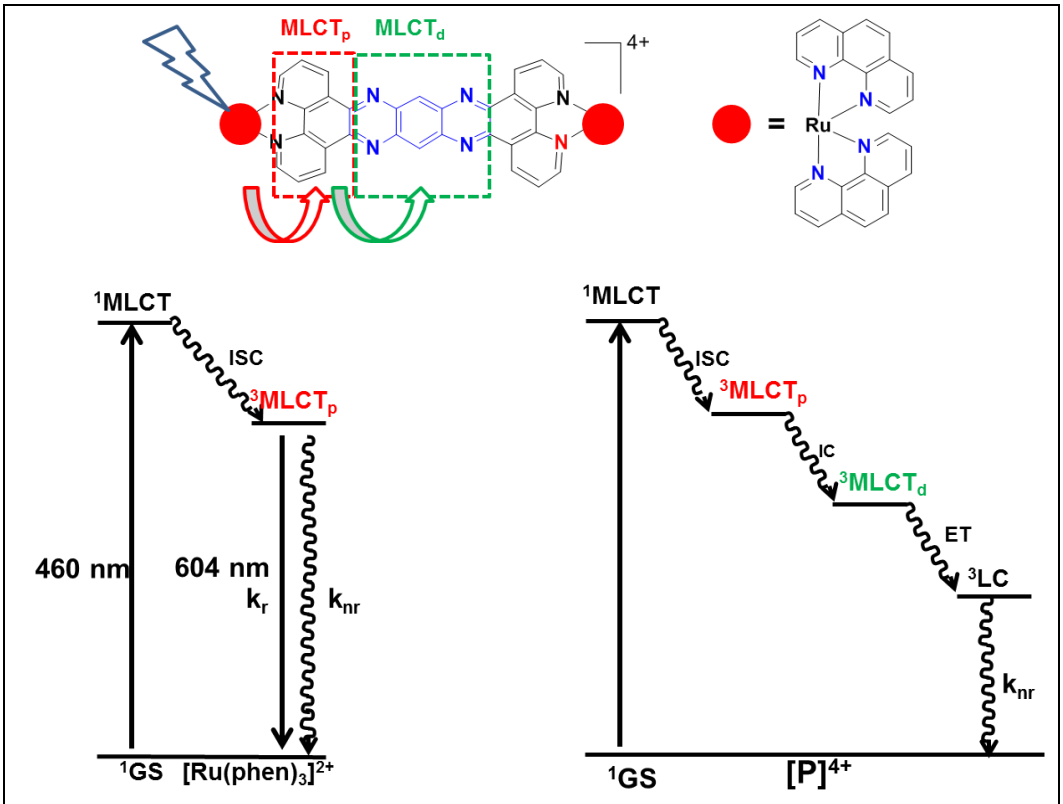

Figure 4.2 Jablonski diagram **[Ru(phen)$_3$]$^{2+}$** and **[P]$^{4+}$** where MLCT$_p$ and MLCT$_d$ denotes metal to ligand charge transfer proximal and distal states respectively. MLCT$_d$ state is absent in **[Ru(phen)$_3$]$^{2+}$** and thus emission arises from luminescent bright state, MLCT$_p$. LC is ligand centered state and ET denotes energy transfer. ISC = intersystem crossing, IC = internal conversion, k_r = radiative decay rate constant, k_{nr} = nonradiative decay rate constant

However to our surprise, we have observed that addition of a $\{Re(CO)_3L\}^+$ unit to one end of $[MP]^{2+}$ to form hybrid heterobimetallic complexes, where L is CH_3CN and PR_3 ($R = CH_2OH$) gives resulting complexes $[RuRe_{CH3CN}]^{3+}$ and $[RuRe_{PR3}]^{3+}$ that are luminescent at 604 nm due to the Re functionality. This is unusual and unexpected because for this to happen the ^{3}LC state in these compounds should be high up in energy so as to provide a channel for ^{3}MLCTprox (bright state) as the emitting state at 604 nm. Such unusual observation is not comprehensible at this point. The proposed Jablonski diagram for this surprising "turn on" luminescence due to Re functionality is shown in Figure 4.3.

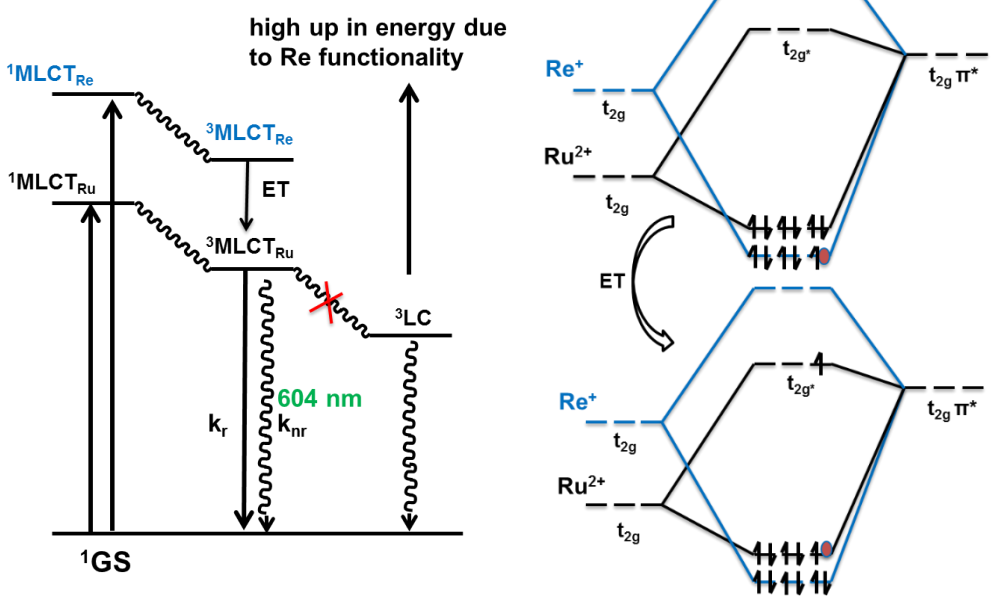

Figure 4.3 Proposed Jablonski for surprising "turn on" luminescence of $[RuRe_L]^{3+}$ where L is CH_3CN and PR_3 ($R = CH_2OH$) due to Re functionality (PF_6^- salts).

We have shown in Chapter 3, that both $[RuRe_{CH3CN}]^{3+}$ and $[RuRe_{PR3}]^{3+}$ are functional DNA cleaving agents with $[RuRe_{PR3}]^{3+}$ also demonstrating comparable cytotoxicity to $[P]^{4+}$ against H358 and HOP62 cells and thus may be a useful therapeutic in its own right. While the underlying photophysics of these complexes are yet to be completely established, the luminescence of $[RuRe_{PR3}]^{3+}$ may allow us to track its localization in cells and to thereby function as a 'fluorescent-tagged' analogue of $[P]^{4+}$. However, to be able to do that, we needed to first establish the purity of $[RuRe_{CH3CN}]^{3+}$ and $[RuRe_{PR3}]^{3+}$ by high performance liquid chromatography (HPLC) in order to rule out possible involvement of minor impurities (if any) in the observed luminescence. This chapter focusses on representative HPLC purity studies that we initially conducted in collaboration with Prof. Daniel W. Armstrong lab (UTA) to show that these complexes are not only pure but are certainly fluorescent. Cellular colocalization studies of $[RuRe_{PR3}]^{3+}$ complex conducted by Adam S. Dayoub (graduate student, Macdonnell group) to demonstrate nuclear accumulation in H358 lung carcinoma cells are also presented.

4.2 Experimental

HPLC grade H_2O, MeCN and MeOH, TFA were purchased from Sigma Aldrich. Reverse phase C_{18} column (250 x 4.6 mm) was obtained from AZYP, LLC. Complex solution was prepared by dissolving 1.0 mg complex (PF_6^-) salt in 1.0 ml MeCN and stored in amber HPLC vials. Chromatographic separation was performed on an Agilent© 1260 HPLC system equipped with a degasser, quaternary pump, autosampler, and a diode array detector and separation monitored at 450 nm unless otherwise noted. Flow rate of 1mL/min and injection volume of 1 µL was used unless otherwise indicated. Preparative scale separation was carried on a Shimadzu© preparative LC system using a 21.2 x 250 mm C_{18} column, flow rate of 19.0 mL/min and injection volume 2.0 mL. Emission

measurements were obtained on a Jobin Yvon Horiba Fluoromax-3. For confocal microscopy studies, H358 lung carcinoma cells were cultured, and passaged as detailed in Chapter 3. Cells were treated with 20 µM of $[RuRe_{PR3}]^{3+}$ (Cl^- salt) for 8, 12 and 24 h. After each analysis period, cells were prepared for staining and fluorescent probing. Propidium Iodide (PI) was used as a nuclear stain as follows: Media was removed from cover slip and washed 2x with PBS, cells were fixed with ice cold methanol for 10 min, cell membranes were permeabilized with 1 ml of 0.25% Triton/PBS for 10 min in a 37˚C incubator, 300 µL of 1% PI/PBS solution was administered for 10 min in a 37°C incubator and lastly 1 ml of 3% Bovine Serum Albumin was used as a blocking agent for 30 min in a 37°C incubator. The cover slip was adhered to a microscope slide and scanned using a Zeiss axioplane fluorescent microscope at 488 nm excitation and an emission band path of 585-615 nm. The nuclear stains were then pseudo-colored red and colocalized with $[RuRe_{PR3}]^{3+}$ emissions. Images taken at 60x oil immersion.

4.3 Results and Discussion

4.3.1 HPLC purity analysis $[RuRe_{CH3CN}]^{3+}$

The reverse phase analytical scale HPLC chromatogram of a ^{1}H NMR clean $[RuRe_{CH3CN}]^{3+}$ sample is shown in Figure 4.4 and %Purity as determined by peak area analysis was found to be 88%.

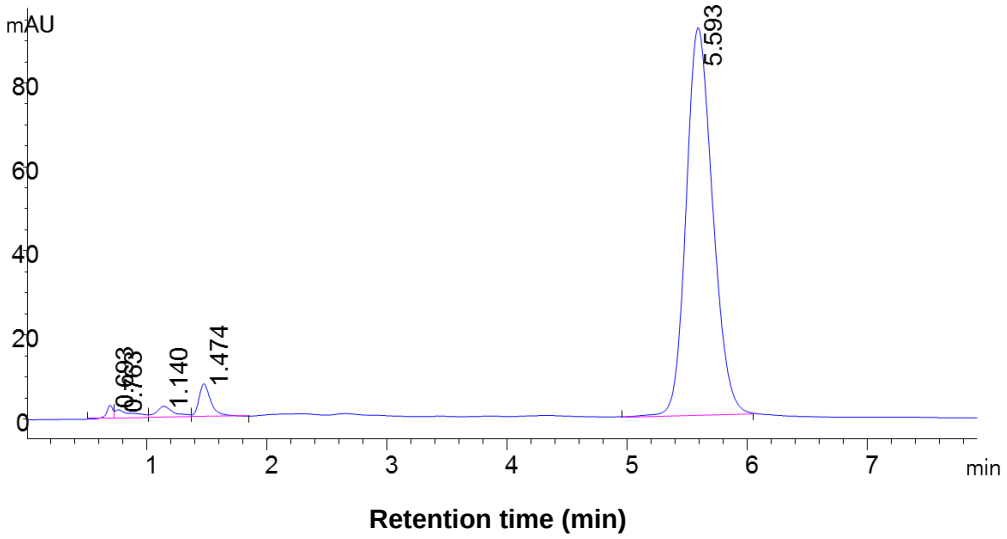

Figure 4.4 Analytical scale reverse phase HPLC chromatographic separation of $[RuRe_{CH3CN}](PF_6)_3$ – 1.0 mg complex in 1.0 mL MeCN, mobile phase: 65:35 MeCN:H_2O with 0.1 %TFA

Therefore to obtain pure complex free of trace impurities, prep scale HPLC separation was performed using the conditions outlined in the experimental section while keeping the mobile phase of 65:35 MeCN:H_2O with 0.1 %TFA. The eluent peak between 5.4-5.8 min was collected with the aid of fraction collector and rotovaped to dryness (~16% recovery). While the fluorescence spectra of the isolated fraction in MeCN still showed emission at 604 nm, the ^{1}H NMR spectra revealed some irregularities (Figure 4.5) thereby introducing uncertainty in fluorescence measurements. Although the reason for such a behavior is unknown, however, a plausible explanation might be related to the lability of axial ligand in $[RuRe_{CH3CN}]^{3+}$ complex. Additionally low % recovery after separation was disappointing given the difficulty involved in long 10 step synthesis of $[RuRe_{CH3CN}]^{3+}$.

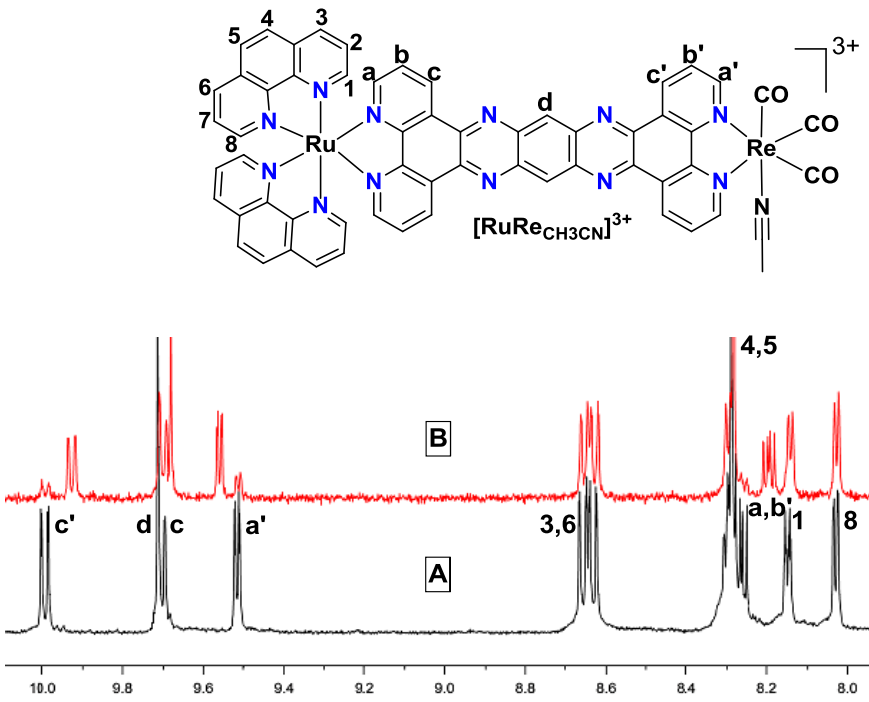

Figure 4.5 ^{1}H NMR [RuRe$_{CH3CN}$](PF$_6$)$_3$ in d3-acetonitrile (A) before HPLC (B) after HPLC preparatory scale separation

4.3.2 HPLC purity analysis [RuRe$_{PR3}$]$^{3+}$ and Fluorescence

The reverse phase analytical scale HPLC chromatogram of a ^{1}H NMR, HRMS and CHN clean sample of [RuRe$_{PR3}$]$^{3+}$ is shown in Figure 4.6. The %Purity as determined by peak area analysis was found to be 50% which was questionable given the fact that the sample was also pure by CHN.

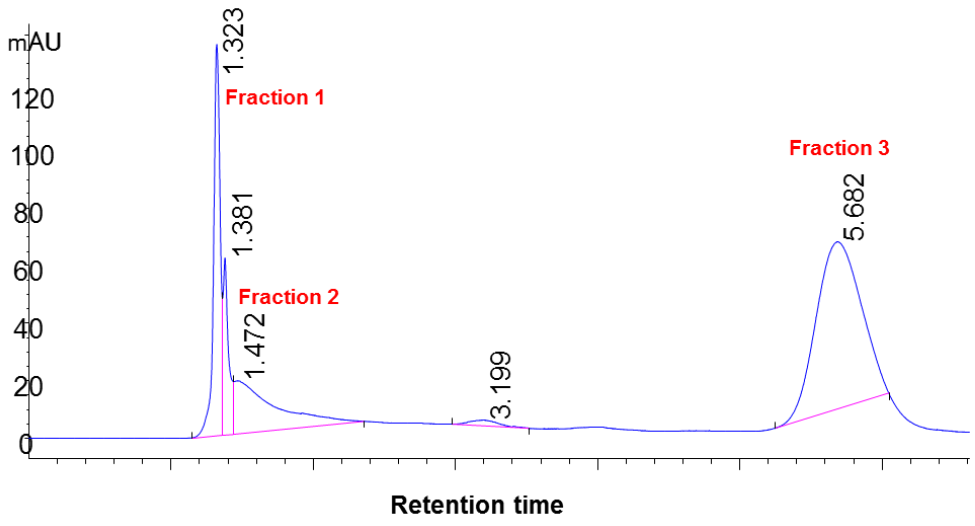

Figure 4.6 Analytical scale reverse phase HPLC chromatographic separation of $[RuRe_{PR3}]Cl_3$: 1.0 mg in 1.0 mL MeOH, mobile phase: 45:55 MeOH:H_2O with 0.1%TFA

Nonetheless prep scale HPLC was performed using 45:55 MeOH:H_2O and 0.1%TFA. Three fractions (1, 2 and 3) were collected separately and fluorescence measurements of the eluted fractions soon after elution were recorded as is, with 45:55 MeOH:H_2O with 0.1% TFA as blank. The data reveal that all the three fractions are fluorescent at ~604 nm, however, the ^1H NMR of the first two fractions recorded after drying by rotary evaporation was broad thus making identification of the species difficult, but the third fraction was pure $[RuRe_{PR3}]^{3+}$ as shown in Figure 4.7.

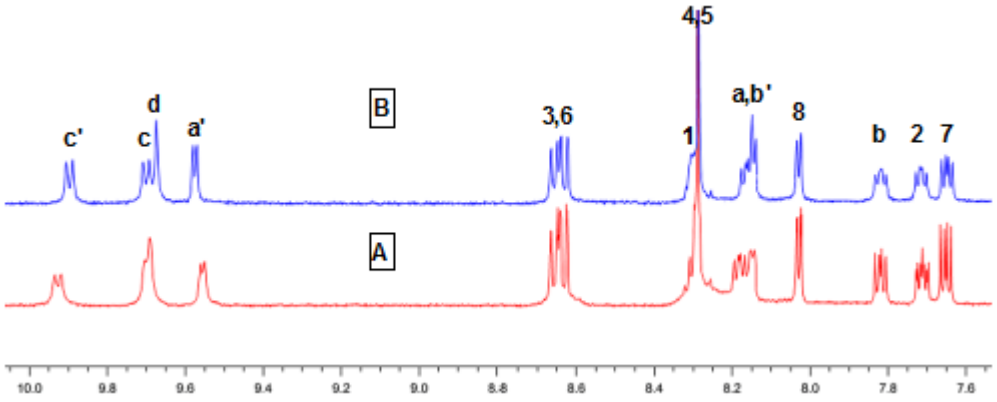

Figure 4.7 ^{1}H NMR $[RuRe_{PR3}]^{3+}$ in d_3-acetonitrile (A) before (B) after prep scale HPLC

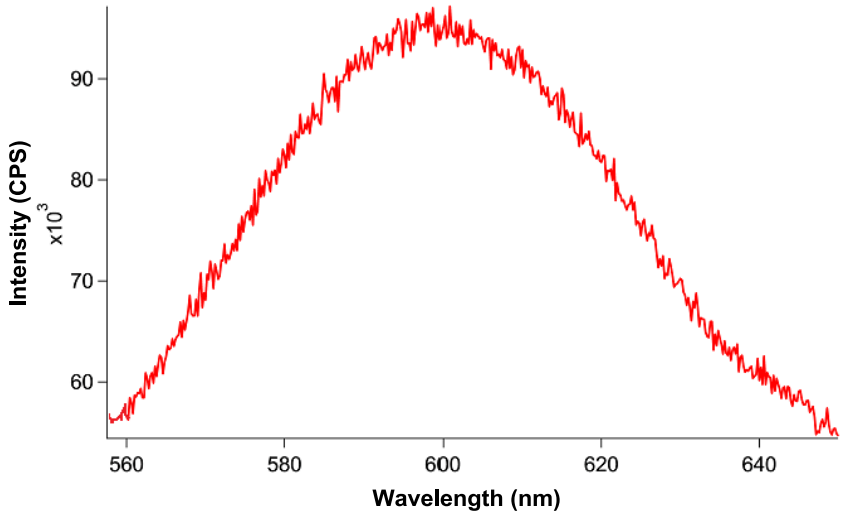

Figure 4.8 Emission spectrum of fraction 3 (HPLC) of $[RuRe_{PR3}]^{3+}$ (~40μM in MeCN, λ_{ex} = 467 nm)

While the prep scale chromatographic separation in conjunction with the ^{1}H NMR and emission data reveal that complex $[RuRe_{PR3}]^{3+}$ is fluorescent, however, low %purity and recovery from HPLC even with a CHN clean sample does indicate that some reactivity is occurring during the separation process and thus further studies are underway to probe the possible reactive species that may be involved.

4.3.3 Cellular localization studies by confocal microscopy

In order to allow better understanding as to what cellular compartments $[RuRe_{PR3}]^{3+}$ complex would be targeting in vivo, we studied the pattern of uptake and localization by making use of its inherent fluorescence via confocal microscopy in both fixed and live H358 cells. The auto-fluorescence from H358 cells treated with $[RuRe_{PR3}]^{3+}$ (Cl^- salt) indicated variable patterns of uptake and localization depending on the time frame we look at (Figure 4.9). After 8 h of inoculation, the emission originated from cytoplasmic regions of the cells indicating generalized cytoplasmic staining (Figure 4.9A). In 12 h, the emission seem to originate exclusively from the perinuclear regions of the cytoplasm that is likely mitochondria as is evident from the circular ring pattern (Figure 4.9B). After 24 h however, the emission originates almost entirely from the center of the cell (Figure 4.9C), which is very similar to emission from cells stained with propidium iodide (PI) (Figure 4.9D), a known nuclear DNA stain. High degree of overlay observed on colocalization with PI (Figure 4.9E) strongly indicate that the complex is ending up in the nucleus of the cell. It is of note that PI does not interfere with the fluorescence of $[RuRe_{PR3}]^{3+}$ in the cell which excited at 488 nm and emitted at ~530 nm using a lambda search stack, while PI emission is at 590 nm. Understanding of how these compounds would be truly functioning in vivo is a complex issue and would require a detailed study to obtain a complete picture, however, cell imaging data allows us to correlate our findings from the study so far. The complex is

making its way to the nucleus and probably inducing cell death via DNA cleavage pathway as supported by the results of our in vitro cleavage assay discussed in Chapter 3.

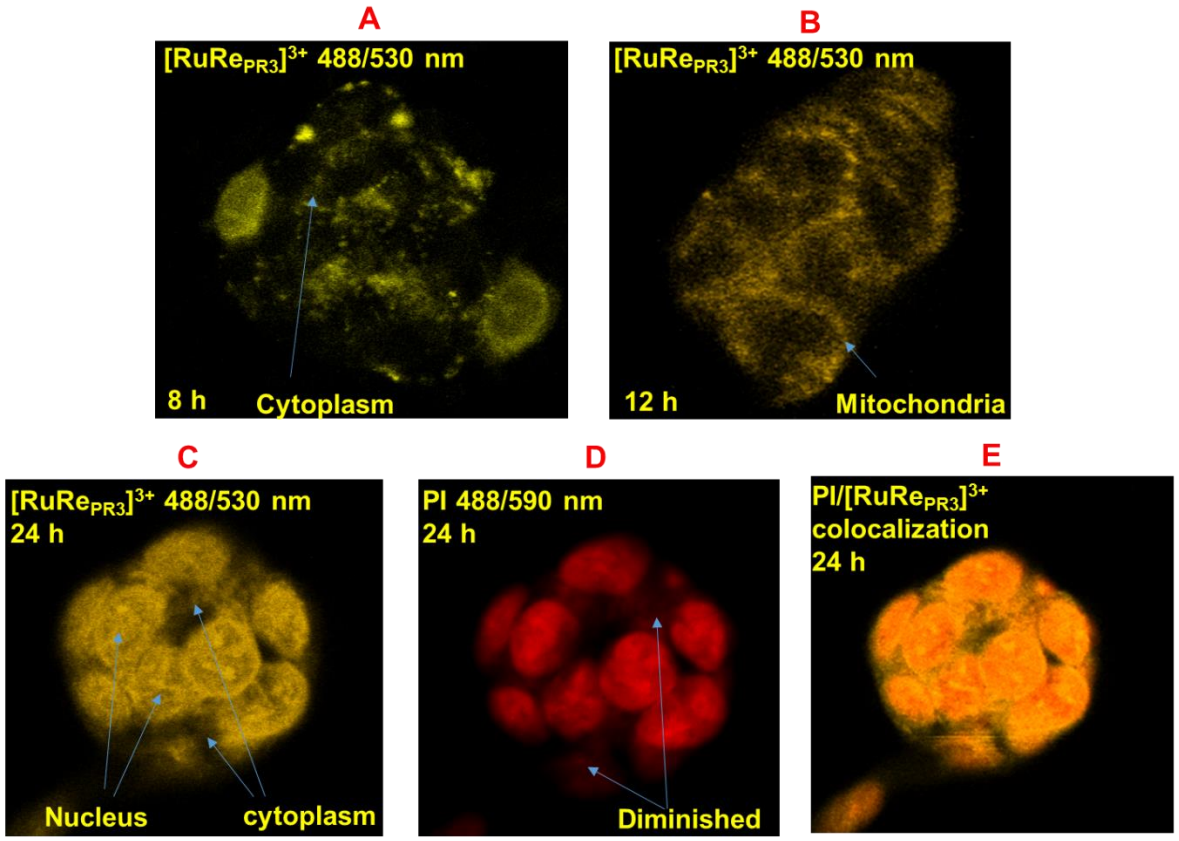

Figure 4.9 Laser scanning confocal microscopy cell images of H358 lung carcinoma cells treated with $[RuRe_{PR3}]Cl_3$ complex (20 μM)[115]

4.4 Conclusion

In this chapter, we investigated the purity of hybrid complexes $[RuRe_{CH3CN}]^{3+}$ and $[RuRe_{PR3}]^{3+}$ by reverse phase HPLC analysis and performed prep scale separation to isolate the pure compounds free of trace impurities. The % purity of $[RuRe_{CH3CN}]^{3+}$ is found to be ~88 % and the isolated complex after HPLC is fluorescent at ~604 nm due to Re functionality. The emission data is inconclusive though due to the presence of few extra proton peaks in the ^{1}H NMR of isolated $[RuRe_{CH3CN}]^{3+}$. The reason for this is unknown but may have to do with the lability of acetonitrile ligand. The % purity of a ^{1}H NMR, HRMS and CHN clean sample of $[RuRe_{PR3}]^{3+}$ as determined by HPLC is found to be ~50%, which is questionable, however, the isolated fraction after HPLC separation is pure by ^{1}H NMR and fluorescent with emission max at 604 nm. $[RuRe_{PR3}]^{3+}$ was thus taken forward as a fluorescent tagged derivative of $[P]^{4+}$ and confocal microscopy studies were probed to determine its localization in H358 cells. The results indicate that the complex initially localizes in the cytoplasmic and mitochondrial regions of the cells but ends up almost entirely in the nucleus after 24 h. This observation is in agreement with the results of our in vitro DNA cleavage assay thereby suggesting that the complex may be inducing cell death via DNA cleavage mechanism discussed earlier.

APPENDIX A

Crystallographic Data

Crystal data and structure refinement for C20 H10 F6 N3 O6 P Re,[6a].

Identification code	pooja1m	
Empirical formula	C20 H10 F6 N3 O6 P Re	
Formula weight	719.48	
Temperature	100(2) K	
Wavelength	0.71073 Å	
Crystal system	Monoclinic	
Space group	P2(1)/c	
Unit cell dimensions	a = 8.2176(13) Å	□= 90°.
	b = 16.747(3) Å	□= 116.008(6)°.
	c = 17.720(3) Å	□ = 90°.
Volume	2191.7(6) $Å^3$	
Z	4	
Density (calculated)	2.180 Mg/m^3	
Absorption coefficient	5.714 mm^{-1}	
F(000)	1372	
Crystal size	0.20 x 0.15 x 0.05 mm^3	
Theta range for data collection	1.76 to 28.29°.	
Index ranges	-10<=h<=10, -22<=k<=22, -23<=l<=23	
Reflections collected	21334	
Independent reflections	5444 [R(int) = 0.0381]	
Completeness to theta = 28.29°	100.0 %	
Absorption correction	Semi-empirical from equivalents	
Max. and min. transmission	0.745 and 0.466	
Refinement method	Full-matrix least-squares on F^2	
Data / restraints / parameters	5444 / 0 / 334	
Goodness-of-fit on F^2	1.039	
Final R indices [I>2sigma(I)]	R1 = 0.0339, wR2 = 0.0823	
R indices (all data)	R1 = 0.0433, wR2 = 0.0891	
Largest diff. peak and hole	3.492 and -0.736 $e.Å^{-3}$	

Atomic coordinates (x 10^4) and equivalent isotropic displacement parameters ($Å^2$x 10^3) for C20 H10 F6 N3 O6 P Re, **[6a]**. U(eq) is defined as one third of the trace of the orthogonalized U^{ij} tensor.

	x	y	z	U(eq)
Re	2525(1)	7231(1)	34(1)	16(1)
O(1)	457(5)	7212(2)	-1895(2)	34(1)
O(2)	3254(5)	9026(2)	40(2)	28(1)
O(3)	5932(4)	6941(2)	-205(2)	28(1)
O(4)	3813(4)	5360(2)	3540(2)	25(1)
O(5)	2987(4)	4130(2)	2422(2)	27(1)
O(6)	148(4)	7234(2)	233(2)	21(1)
N(1)	2373(4)	5967(2)	278(2)	17(1)
N(2)	3602(5)	7142(2)	1394(2)	18(1)
N(3)	-2281(6)	9225(3)	593(3)	40(1)
C(1)	4686(6)	7062(2)	-89(3)	19(1)
C(2)	2862(5)	8351(2)	13(2)	15(1)
C(3)	1239(6)	7224(2)	-1178(3)	22(1)
C(4)	1969(5)	5376(3)	-298(3)	21(1)
C(5)	1867(6)	4583(2)	-104(2)	20(1)
C(6)	2177(5)	4391(2)	705(3)	22(1)
C(7)	2634(5)	4987(2)	1306(2)	17(1)
C(8)	2748(5)	5772(2)	1077(2)	15(1)
C(9)	3033(5)	4794(2)	2191(2)	18(1)
C(10)	3549(5)	5497(2)	2827(3)	20(1)
C(11)	3734(5)	6300(2)	2524(2)	19(1)
C(12)	4313(6)	6938(3)	3077(2)	23(1)
C(13)	4539(7)	7675(3)	2777(3)	29(1)
C(14)	4187(6)	7754(2)	1942(3)	25(1)
C(15)	3369(5)	6419(2)	1688(2)	17(1)
C(16)	-629(6)	7873(2)	348(3)	22(1)

C(17)	-1006(6)	7933(3)	1043(3)	32(1)
C(18)	-1810(7)	8629(3)	1148(3)	41(1)
C(19)	-1945(7)	9178(3)	-79(3)	37(1)
C(20)	-1142(6)	8524(3)	-224(3)	28(1)
P	8256(2)	5493(1)	2435(1)	28(1)
F(1)	6660(3)	5471(2)	1495(2)	37(1)
F(2)	7686(4)	6380(2)	2536(2)	41(1)
F(3)	9840(4)	5522(2)	3368(2)	47(1)
F(4)	8824(4)	4603(2)	2324(2)	49(1)
F(5)	9627(4)	5822(2)	2080(2)	48(1)
F(6)	6873(4)	5148(2)	2778(2)	39(1)

Bond lengths [Å] and angles [°] for C20 H10 F6 N3 O6 P Re, **[6a]**.

Re-C(2)	1.899(4)
Re-C(1)	1.903(4)
Re-C(3)	1.934(4)
Re-O(6)	2.131(3)
Re-N(1)	2.175(3)
Re-N(2)	2.178(4)
O(1)-C(3)	1.145(5)
O(2)-C(2)	1.170(5)
O(3)-C(1)	1.148(5)
O(4)-C(10)	1.207(5)
O(5)-C(9)	1.192(5)
O(6)-C(16)	1.306(5)
N(1)-C(8)	1.350(5)
N(1)-C(4)	1.355(5)
N(2)-C(14)	1.346(5)
N(2)-C(15)	1.365(5)
N(3)-C(18)	1.333(7)

N(3)-C(19)	1.338(7)
C(4)-C(5)	1.384(6)
C(4)-H(4)	0.9300
C(5)-C(6)	1.381(5)
C(5)-H(5)	0.9300
C(6)-C(7)	1.387(5)
C(6)-H(6)	0.9300
C(7)-C(8)	1.391(5)
C(7)-C(9)	1.490(5)
C(8)-C(15)	1.457(5)
C(9)-C(10)	1.554(6)
C(10)-C(11)	1.480(6)
C(11)-C(12)	1.386(6)
C(11)-C(15)	1.390(5)
C(12)-C(13)	1.389(6)
C(12)-H(12)	0.9300
C(13)-C(14)	1.384(6)
C(13)-H(13)	0.9300
C(14)-H(14)	0.9300
C(16)-C(17)	1.400(6)
C(16)-C(20)	1.421(6)
C(17)-C(18)	1.391(7)
C(17)-H(17)	0.9300
C(18)-H(18)	0.9300
C(19)-C(20)	1.359(6)
C(19)-H(19)	0.9300
C(20)-H(20)	0.9300
P-F(2)	1.592(3)
P-F(3)	1.595(3)
P-F(4)	1.599(3)
P-F(1)	1.606(3)
P-F(5)	1.609(3)

P-F(6)	1.613(3)
C(2)-Re-C(1)	89.60(17)
C(2)-Re-C(3)	89.85(15)
C(1)-Re-C(3)	87.39(18)
C(2)-Re-O(6)	98.79(14)
C(1)-Re-O(6)	171.21(15)
C(3)-Re-O(6)	95.17(16)
C(2)-Re-N(1)	170.71(13)
C(1)-Re-N(1)	90.90(15)
C(3)-Re-N(1)	99.44(14)
O(6)-Re-N(1)	80.39(11)
C(2)-Re-N(2)	95.57(13)
C(1)-Re-N(2)	99.75(15)
C(3)-Re-N(2)	171.03(15)
O(6)-Re-N(2)	76.97(12)
N(1)-Re-N(2)	75.20(12)
C(16)-O(6)-Re	125.0(3)
C(8)-N(1)-C(4)	118.8(3)
C(8)-N(1)-Re	115.9(2)
C(4)-N(1)-Re	125.3(3)
C(14)-N(2)-C(15)	117.7(4)
C(14)-N(2)-Re	126.1(3)
C(15)-N(2)-Re	115.2(3)
C(18)-N(3)-C(19)	120.3(4)
O(3)-C(1)-Re	176.2(4)
O(2)-C(2)-Re	173.2(4)
O(1)-C(3)-Re	178.8(4)
N(1)-C(4)-C(5)	122.3(4)
N(1)-C(4)-H(4)	118.8
C(5)-C(4)-H(4)	118.8
C(6)-C(5)-C(4)	118.6(4)

C(6)-C(5)-H(5)	120.7
C(4)-C(5)-H(5)	120.7
C(5)-C(6)-C(7)	119.6(4)
C(5)-C(6)-H(6)	120.2
C(7)-C(6)-H(6)	120.2
C(6)-C(7)-C(8)	119.2(4)
C(6)-C(7)-C(9)	120.8(4)
C(8)-C(7)-C(9)	120.0(3)
N(1)-C(8)-C(7)	121.4(3)
N(1)-C(8)-C(15)	116.4(3)
C(7)-C(8)-C(15)	122.1(3)
O(5)-C(9)-C(7)	122.6(4)
O(5)-C(9)-C(10)	119.8(4)
C(7)-C(9)-C(10)	117.6(3)
O(4)-C(10)-C(11)	123.5(4)
O(4)-C(10)-C(9)	118.8(4)
C(11)-C(10)-C(9)	117.6(3)
C(12)-C(11)-C(15)	119.3(4)
C(12)-C(11)-C(10)	120.1(4)
C(15)-C(11)-C(10)	120.6(4)
C(11)-C(12)-C(13)	118.5(4)
C(11)-C(12)-H(12)	120.8
C(13)-C(12)-H(12)	120.8
C(14)-C(13)-C(12)	119.5(4)
C(14)-C(13)-H(13)	120.2
C(12)-C(13)-H(13)	120.2
N(2)-C(14)-C(13)	122.7(4)
N(2)-C(14)-H(14)	118.6
C(13)-C(14)-H(14)	118.6
N(2)-C(15)-C(11)	122.3(4)
N(2)-C(15)-C(8)	116.0(3)
C(11)-C(15)-C(8)	121.8(4)

O(6)-C(16)-C(17)	120.5(4)
O(6)-C(16)-C(20)	122.0(4)
C(17)-C(16)-C(20)	117.4(4)
C(18)-C(17)-C(16)	118.6(5)
C(18)-C(17)-H(17)	120.7
C(16)-C(17)-H(17)	120.7
N(3)-C(18)-C(17)	122.0(4)
N(3)-C(18)-H(18)	119.0
C(17)-C(18)-H(18)	119.0
N(3)-C(19)-C(20)	121.5(5)
N(3)-C(19)-H(19)	119.2
C(20)-C(19)-H(19)	119.2
C(19)-C(20)-C(16)	120.0(4)
C(19)-C(20)-H(20)	120.0
C(16)-C(20)-H(20)	120.0
F(2)-P-F(3)	90.07(17)
F(2)-P-F(4)	179.47(17)
F(3)-P-F(4)	90.36(17)
F(2)-P-F(1)	89.55(16)
F(3)-P-F(1)	179.58(19)
F(4)-P-F(1)	90.03(17)
F(2)-P-F(5)	90.90(18)
F(3)-P-F(5)	90.08(16)
F(4)-P-F(5)	88.78(18)
F(1)-P-F(5)	89.77(15)
F(2)-P-F(6)	90.05(16)
F(3)-P-F(6)	90.53(16)
F(4)-P-F(6)	90.27(18)
F(1)-P-F(6)	89.63(16)
F(5)-P-F(6)	178.87(18)

Anisotropic displacement parameters ($Å^2 x\ 10^3$) for C20 H10 F6 N3 O6 P Re, **[6a]**. The anisotropic displacement factor exponent takes the form: $-2\pi^2[h^2 a^{*2} U^{11} + ... + 2 h k a^* b^* U^{12}]$

	U^{11}	U^{22}	U^{33}	U^{23}	U^{13}	U^{12}
Re	18(1)	12(1)	17(1)	1(1)	9(1)	1(1)
O(1)	43(2)	32(2)	19(2)	2(1)	7(2)	4(2)
O(2)	40(2)	16(2)	32(2)	1(1)	20(1)	-1(1)
O(3)	31(2)	26(2)	31(2)	2(1)	18(1)	4(1)
O(4)	28(2)	31(2)	20(1)	2(1)	13(1)	-2(1)
O(5)	32(2)	23(2)	30(2)	5(1)	18(1)	7(1)
O(6)	22(2)	17(2)	26(2)	0(1)	12(1)	2(1)
N(1)	22(2)	15(2)	15(2)	2(1)	11(1)	0(1)
N(2)	20(2)	16(2)	21(2)	-2(1)	11(1)	-3(1)
N(3)	33(2)	34(2)	52(3)	-14(2)	17(2)	3(2)
C(1)	20(2)	17(2)	20(2)	2(2)	10(2)	2(2)
C(2)	21(2)	11(2)	10(2)	1(1)	5(1)	6(2)
C(3)	26(2)	16(2)	24(2)	3(2)	12(2)	0(2)
C(4)	22(2)	23(2)	17(2)	-1(2)	8(2)	2(2)
C(5)	24(2)	17(2)	21(2)	-2(2)	11(2)	3(2)
C(6)	21(2)	19(2)	25(2)	3(2)	10(2)	2(2)
C(7)	17(2)	16(2)	20(2)	2(2)	9(2)	4(2)
C(8)	14(2)	14(2)	18(2)	0(1)	8(2)	1(1)
C(9)	14(2)	21(2)	24(2)	-3(2)	11(2)	2(2)
C(10)	18(2)	21(2)	25(2)	-1(2)	11(2)	-1(2)
C(11)	19(2)	19(2)	20(2)	2(2)	10(2)	3(2)
C(12)	29(2)	22(2)	18(2)	-1(2)	12(2)	0(2)
C(13)	41(3)	21(2)	26(2)	-9(2)	16(2)	-10(2)
C(14)	30(2)	18(2)	26(2)	-4(2)	12(2)	-6(2)
C(15)	15(2)	18(2)	19(2)	-2(2)	8(2)	2(2)

C(16)	18(2)	20(2)	26(2)	-5(2)	7(2)	-1(2)
C(17)	28(2)	40(3)	26(2)	-5(2)	12(2)	-1(2)
C(18)	37(3)	59(4)	38(3)	-25(3)	25(2)	-9(3)
C(19)	28(2)	25(3)	52(3)	-4(2)	12(2)	3(2)
C(20)	26(2)	24(2)	34(2)	-2(2)	14(2)	3(2)
P	22(1)	43(1)	21(1)	-2(1)	10(1)	6(1)
F(1)	26(1)	54(2)	27(1)	-2(1)	9(1)	2(1)
F(2)	39(2)	40(2)	45(2)	-6(1)	19(1)	2(1)
F(3)	34(2)	77(2)	24(1)	-2(1)	9(1)	16(2)
F(4)	56(2)	52(2)	40(2)	0(1)	23(2)	25(2)
F(5)	27(2)	86(3)	33(2)	0(2)	16(1)	-2(2)
F(6)	38(2)	47(2)	41(2)	6(1)	24(1)	5(1)

Hydrogen coordinates (x 10^4) and isotropic displacement parameters (Å^{2}x 10^3) for C20 H10 F6 N3 O6 P Re, **[6a]**.

	x	y	z	U(eq)
H(4)	1752	5509	-844	25
H(5)	1596	4188	-511	24
H(6)	2080	3864	847	26
H(12)	4546	6873	3637	27
H(13)	4924	8114	3135	35
H(14)	4361	8249	1751	29
H(17)	-726	7517	1427	38
H(18)	-2024	8681	1619	50
H(19)	-2268	9601	-456	44
H(20)	-929	8503	-698	33

Crystal data and structure refinement for [6b]$^+$

Identification code	dione_ch3cn
Empirical formula	$C_{19}H_{12}F_6N_4O_5PRe$
Formula weight	707.50
Temperature/K	296(2)
Crystal system	N/A
Space group	C2/c
a/Å	26.126(5)
b/Å	14.264(3)
c/Å	15.529(3)
α/°	90.00
β/°	121.737(2)
γ/°	90.00
Volume/Å^3	4921.8(16)
Z	8
ρ_{calc}g/cm^3	1.910
μ/mm^{-1}	5.085
F(000)	2704.0
Crystal size/mm^3	0.20 × 0.15 × 0.03
Radiation	MoKα (λ = 0.71073)
2Θ range for data collection/°	3.4 to 56.76
Index ranges	-34 ≤ h ≤ 34, -19 ≤ k ≤ 19, -20 ≤ l ≤ 20
Reflections collected	23789
Independent reflections	6147 [R_{int} = 0.0353, R_{sigma} = N/A]
Data/restraints/parameters	6147/36/327
Goodness-of-fit on F^2	1.051
Final R indexes [I>=2σ (I)]	R_1 = 0.0783, wR_2 = 0.2237
Final R indexes [all data]	R_1 = 0.1099, wR_2 = 0.2527
Largest diff. peak/hole / e Å^{-3}	4.47/-1.29

Fractional Atomic Coordinates (×10^4) and Equivalent Isotropic Displacement Parameters (Å^2×10^3) for $[6b]^+$. U_{eq} is defined as 1/3 of of the trace of the orthogonalised U_{IJ} tensor.

Atom	***x***	***y***	***z***	**U(eq)**
Re1	1053.6(2)	8688.8(3)	0.1(3)	87.4(3)
P1	2884.4(15)	9445.2(19)	4383(2)	85.0(8)
F1	3280(6)	9907(12)	5401(9)	227(7)
F2	2348(5)	9911(8)	4393(8)	178(5)
F3	2492(6)	8903(9)	3394(8)	171(4)
F4	3458(5)	8940(8)	4426(11)	161(4)
F5	2975(6)	10257(7)	3832(8)	161(3)
F6	2807(7)	8597(7)	4934(10)	164(4)
O1	3526(5)	11238(6)	2634(9)	124(4)
O2	3981(4)	9463(8)	2888(8)	130(3)
O3	-222(5)	9479(10)	-968(10)	161(4)
O4	502(7)	6756(12)	-692(15)	221(8)
O5	970(7)	8983(11)	-1984(11)	166(5)
N1	1555(3)	9999(5)	620(5)	69.6(17)
N2	1998(3)	8279(5)	808(5)	68.8(17)
N3	1128(4)	8512(6)	1430(8)	83(2)
C1	2206(5)	7418(7)	904(7)	76(2)
C2	2814(6)	7180(7)	1457(9)	93(3)
C3	3217(5)	7891(8)	1939(8)	83(3)
C4	3013(5)	8801(6)	1849(8)	72(2)
C5	2400(4)	8983(6)	1299(6)	61.9(18)
C6	2161(5)	9912(6)	1174(6)	69(2)
C7	2534(5)	10699(7)	1615(7)	77(2)
C8	2261(7)	11576(8)	1433(10)	97(4)
C9	1674(7)	11642(8)	878(10)	97(3)
C10	1310(6)	10857(8)	472(9)	95(3)

C11	3448(5)	9598(8)	2367(8)	88(3)
C12	3191(5)	10563(8)	2226(8)	91(3)
C13	267(7)	9177(12)	-584(12)	119(4)
C14	708(6)	7460(12)	-427(12)	131(5)
C15	995(8)	8863(12)	-1272(9)	131(6)
C16	1143(6)	8397(9)	2162(12)	93(3)
C17	1178(7)	8252(12)	3122(11)	123(4)
N4	224(7)	7564(16)	4030(18)	200(9)
C18	197(9)	6811(15)	4210(20)	174(10)
C19	155(12)	5900(20)	4330(20)	203(10)

Anisotropic Displacement Parameters ($Å^2 \times 10^3$) for $[6b]^+$. The Anisotropic displacement factor exponent takes the form: $-2\pi^2[h^2a^{*2}U_{11}+2hka^*b^*U_{12}+\ldots]$.

Atom	**U_{11}**	**U_{22}**	**U_{33}**	**U_{23}**	**U_{13}**	**U_{12}**
Re1	72.9(3)	99.8(4)	80.2(3)	-19.43(19)	33.9(3)	-0.32(19)
P1	121(2)	66.8(14)	89.7(17)	0.8(12)	70.7(17)	6.3(14)
F1	236(13)	302(18)	147(8)	-87(10)	104(9)	-96(13)
F2	215(11)	180(10)	208(10)	49(8)	159(10)	81(9)
F3	182(11)	213(11)	126(7)	-60(7)	87(8)	-65(8)
F4	129(8)	153(7)	229(13)	-9(7)	112(9)	13(6)
F5	235(8)	125(6)	179(7)	20(5)	146(6)	-1(5)
F6	226(9)	129(6)	175(7)	27(5)	132(7)	3(5)
O1	134(8)	100(6)	128(8)	-38(5)	63(7)	-53(5)
O2	70(5)	142(8)	149(8)	-21(6)	37(5)	-23(5)
O3	126(7)	185(9)	156(8)	-33(6)	65(6)	25(6)
O4	162(12)	157(11)	310(20)	-117(14)	102(13)	-67(10)
O5	171(9)	193(8)	134(8)	6(6)	81(7)	53(7)
N1	77(5)	68(4)	72(4)	6(3)	45(4)	12(3)
N2	77(5)	64(4)	71(4)	-2(3)	43(4)	-3(3)

N3	74(5)	86(5)	97(6)	-7(4)	50(5)	-9(4)
C1	85(6)	68(5)	76(5)	-9(4)	42(5)	-5(4)
C2	112(8)	63(5)	123(9)	11(5)	75(7)	19(5)
C3	74(6)	92(7)	85(6)	5(5)	44(5)	7(5)
C4	79(6)	74(5)	75(5)	5(4)	48(5)	1(4)
C5	72(5)	66(4)	51(4)	3(3)	35(4)	-3(4)
C6	90(6)	69(5)	65(5)	-3(4)	52(5)	-2(4)
C7	101(7)	71(5)	76(5)	-2(4)	58(5)	-11(5)
C8	147(12)	61(5)	113(9)	-15(5)	90(9)	-18(6)
C9	137(11)	64(6)	117(9)	17(6)	86(9)	25(7)
C10	122(9)	93(8)	86(7)	13(6)	65(7)	26(7)
C11	84(7)	98(7)	83(6)	-11(5)	46(6)	-18(5)
C12	110(8)	85(7)	83(6)	-9(5)	54(6)	-28(6)
C13	102(7)	128(8)	119(8)	-24(6)	53(6)	20(6)
C14	93(9)	130(12)	154(13)	-58(10)	53(9)	-28(8)
C15	133(13)	199(16)	47(5)	11(7)	37(7)	58(10)
C16	87(7)	89(7)	121(10)	-10(7)	69(7)	-8(6)
C17	145(12)	131(11)	137(11)	-13(9)	103(10)	-26(9)
N4	106(11)	174(17)	300(20)	-25(17)	96(13)	-18(11)
C18	131(15)	102(12)	230(20)	-10(13)	50(14)	-37(11)
C19	180(13)	194(13)	202(13)	7(9)	77(9)	-2(9)

Bond Lengths for [6b]$^{+}$.

Atom	Atom	Length/Å	Atom	Atom	Length/Å
Re1	C13	1.889(15)	N2	C1	1.319(12)
Re1	C15	1.916(14)	N2	C5	1.361(12)
Re1	C14	1.923(15)	N3	C16	1.128(16)
Re1	N3	2.140(11)	C1	C2	1.394(15)
Re1	N2	2.178(8)	C2	C3	1.366(15)
Re1	N1	2.193(8)	C3	C4	1.383(13)

P1	F1	1.510(11)	C4	C5	1.387(14)
P1	F5	1.529(9)	C4	C11	1.506(14)
P1	F3	1.534(10)	C5	C6	1.433(13)
P1	F6	1.554(10)	C6	C7	1.406(13)
P1	F2	1.557(9)	C7	C8	1.394(16)
P1	F4	1.632(10)	C7	C12	1.474(15)
O1	C12	1.229(12)	C8	C9	1.310(18)
O2	C11	1.201(13)	C9	C10	1.387(19)
O3	C13	1.172(16)	C11	C12	1.496(16)
O4	C14	1.110(18)	C16	C17	1.459(19)
O5	C15	1.085(18)	N4	C18	1.12(3)
N1	C10	1.344(13)	C18	C19	1.32(4)
N1	C6	1.352(12)			

Bond Angles for [6b]$^{+}$

Atom	Atom	Atom	Angle/˚	Atom	Atom	Atom	Angle/˚
C13	Re1	C15	88.9(7)	C1	N2	C5	118.2(9)
C13	Re1	C14	88.6(7)	C1	N2	Re1	126.1(7)
C15	Re1	C14	89.7(8)	C5	N2	Re1	115.6(6)
C13	Re1	N3	91.4(6)	C16	N3	Re1	176.9(10)
C15	Re1	N3	179.1(7)	N2	C1	C2	124.4(9)
C14	Re1	N3	91.1(6)	C3	C2	C1	117.2(9)
C13	Re1	N2	172.6(5)	C2	C3	C4	119.7(10)
C15	Re1	N2	94.6(6)	C3	C4	C5	119.8(9)
C14	Re1	N2	97.9(5)	C3	C4	C11	120.8(10)
N3	Re1	N2	85.0(3)	C5	C4	C11	119.4(9)
C13	Re1	N1	98.3(5)	N2	C5	C4	120.6(8)
C15	Re1	N1	92.7(6)	N2	C5	C6	116.9(8)
C14	Re1	N1	172.7(5)	C4	C5	C6	122.4(8)

N3	Re1	N1	86.4(3)	N1	C6	C7	121.1(9)
N2	Re1	N1	75.0(3)	N1	C6	C5	116.8(8)
F1	P1	F5	91.9(8)	C7	C6	C5	122.1(9)
F1	P1	F3	175.5(8)	C8	C7	C6	117.9(11)
F5	P1	F3	92.3(6)	C8	C7	C12	123.2(10)
F1	P1	F6	88.8(8)	C6	C7	C12	118.9(9)
F5	P1	F6	177.9(7)	C9	C8	C7	119.7(11)
F3	P1	F6	86.9(7)	C8	C9	C10	121.8(11)
F1	P1	F2	85.8(7)	N1	C10	C9	120.4(12)
F5	P1	F2	95.0(6)	O2	C11	C12	121.2(10)
F3	P1	F2	95.4(7)	O2	C11	C4	121.4(11)
F6	P1	F2	87.0(7)	C12	C11	C4	117.5(10)
F1	P1	F4	92.4(8)	O1	C12	C7	120.0(12)
F5	P1	F4	87.1(6)	O1	C12	C11	120.2(12)
F3	P1	F4	86.2(7)	C7	C12	C11	119.8(9)
F6	P1	F4	90.9(7)	O3	C13	Re1	178.4(14)
F2	P1	F4	177.3(7)	O4	C14	Re1	179(2)
C10	N1	C6	119.1(9)	O5	C15	Re1	178(2)
C10	N1	Re1	125.4(8)	N3	C16	C17	178.7(14)
C6	N1	Re1	115.5(6)	N4	C18	C19	174(3)

Hydrogen Atom Coordinates (Å×10^4) and Isotropic Displacement Parameters (Å^2×10^3) for [6b]$^+$

Atom	*x*	*y*	*z*	U(eq)
H1	1928	6938	581	91
H2	2941	6564	1495	111
H3	3627	7763	2327	99
H8	2495	12112	1705	116
H9	1495	12231	752	116

H10	894	10924	95	114
H17A	1525	7879	3562	185
H17B	822	7935	3000	185
H17C	1210	8848	3434	185
H19A	-132	5801	4532	305
H19B	540	5666	4850	305
H19C	26	5582	3709	305

Crystal data and structure refinement for C21 H13 Cl N3 O9 Re, $[6c]^+$

Identification code	pooja3_0m_a
Empirical formula	C21 H13 Cl N3 O9 Re
Formula weight	672.99
Temperature	296(2) K
Wavelength	0.71073 Å
Crystal system	Triclinic
Space group	P -1
Unit cell dimensions	a = 13.8293(5) Å □= 103.9000(5)°.
	b = 14.4788(5) Å □= 112.7060(5)°.
	c = 14.6580(5) Å □ = 109.8240(5)°.
Volume	2302.40(14) $Å^3$
Z	4
Density (calculated)	1.942 Mg/m^3
Absorption coefficient	5.452 mm^{-1}
F(000)	1296
Crystal size	0.380 x 0.323 x 0.088 mm^3
Theta range for data collection	2.505 to 28.282°.
Index ranges	-18<=h<=18, -19<=k<=19, -19<=l<=19
Reflections collected	25015
Independent reflections	11404 [R(int) = 0.0224]
Completeness to theta = 25.000°	99.9 %
Absorption correction	Numerical
Max. and min. transmission	0.710 and 0.310
Refinement method	Full-matrix least-squares on F^2
Data / restraints / parameters	11404 / 36 / 633
Goodness-of-fit on F^2	1.134
Final R indices [I>2sigma(I)]	R1 = 0.0449, wR2 = 0.1182
R indices (all data)	R1 = 0.0601, wR2 = 0.1275

Extinction coefficient	n/a
Largest diff. peak and hole	4.832 and -2.332 e.Å^{-3}

Atomic coordinates (x 10^4) and equivalent isotropic displacement parameters (Å^{2}x 10^3) for C21 H13 Cl N3 O9 Re, **[6c]$^+$**. U(eq) is defined as one third of the trace of the orthogonalized U^{ij} tensor.

	x	y	z	U(eq)
Re(1)	1964(1)	336(1)	2774(1)	60(1)
Cl(1)	3581(2)	4152(1)	6955(1)	66(1)
O(1)	2873(8)	1483(5)	7711(5)	120(2)
O(2)	5170(6)	2087(5)	8120(4)	102(2)
O(3)	1361(6)	-1857(4)	2888(5)	109(2)
O(4)	-576(6)	-660(7)	843(5)	141(3)
O(5)	2751(7)	-370(5)	1159(6)	128(3)
O(6)	4227(5)	3634(4)	7419(5)	102(2)
O(7)	3058(6)	3682(4)	5819(4)	94(2)
O(8)	4346(5)	5284(4)	7396(6)	112(2)
O(9)	2650(7)	3970(6)	7192(6)	119(2)
N(1)	1579(4)	902(4)	4041(4)	57(1)
N(2)	3647(4)	1050(3)	4313(4)	51(1)
N(3)	2440(4)	1957(4)	2797(4)	57(1)
C(1)	560(6)	928(5)	3885(7)	71(2)
C(2)	352(8)	1190(6)	4730(9)	90(3)
C(3)	1153(8)	1378(6)	5747(8)	85(2)
C(4)	2208(7)	1360(5)	5939(6)	66(2)
C(5)	2407(5)	1156(4)	5066(5)	51(1)
C(6)	3091(8)	1529(5)	7007(6)	78(2)
C(7)	4337(8)	1764(5)	7206(5)	78(2)
C(8)	4508(6)	1591(4)	6246(5)	62(2)
C(9)	3547(5)	1252(4)	5210(4)	50(1)

C(10)	5611(7)	1755(5)	6339(7)	81(2)
C(11)	5695(6)	1568(6)	5419(7)	79(2)
C(12)	4713(6)	1213(5)	4428(6)	65(2)
C(13)	1584(6)	-1038(6)	2836(6)	76(2)
C(14)	392(8)	-276(7)	1566(6)	94(3)
C(15)	2473(8)	-93(6)	1770(6)	87(2)
C(16)	2080(7)	2095(7)	1874(6)	81(2)
C(17)	2366(9)	3097(9)	1866(8)	98(3)
C(18)	3024(8)	4013(8)	2812(9)	84(2)
C(19)	3382(7)	3880(6)	3760(7)	78(2)
C(20)	3092(6)	2863(5)	3725(5)	65(2)
C(21)	3375(11)	5141(9)	2833(11)	121(4)
Re(2)	1043(1)	5906(1)	8382(1)	61(1)
Cl(2)	2862(2)	8820(1)	6514(2)	70(1)
O(10)	5328(5)	7735(4)	7275(5)	85(2)
O(11)	3484(6)	6078(4)	5297(4)	87(2)
O(12)	-56(5)	7286(5)	7594(5)	95(2)
O(13)	1267(10)	6944(8)	10576(7)	157(4)
O(14)	-1431(6)	4050(6)	7564(7)	125(2)
O(15)	4116(6)	9482(5)	7275(6)	121(2)
O(16)	2479(6)	9311(5)	5834(5)	101(2)
O(17)	2616(6)	7764(4)	5873(5)	103(2)
O(18)	2224(8)	8670(7)	7052(7)	142(3)
N(4)	2780(4)	7066(3)	8742(4)	50(1)
N(5)	1108(4)	5258(4)	6913(4)	53(1)
N(6)	1919(5)	4969(4)	8946(4)	61(1)
C(22)	3611(6)	7963(5)	9672(5)	60(1)
C(23)	4711(6)	8638(5)	9866(5)	66(2)
C(24)	4982(5)	8404(5)	9063(5)	62(2)
C(25)	4126(5)	7488(4)	8066(5)	50(1)
C(26)	3041(4)	6840(4)	7937(4)	42(1)
C(27)	4370(6)	7215(5)	7177(6)	58(1)

C(28)	3362(6)	6253(5)	6085(5)	62(2)
C(29)	2254(5)	5564(4)	6029(4)	54(1)
C(30)	2104(5)	5860(4)	6924(4)	46(1)
C(31)	1365(6)	4593(5)	5121(5)	64(2)
C(32)	388(7)	3981(5)	5120(5)	71(2)
C(33)	260(6)	4322(5)	6009(5)	64(2)
C(34)	355(6)	6757(6)	7882(6)	70(2)
C(35)	1186(10)	6544(8)	9748(8)	98(3)
C(36)	-494(8)	4761(7)	7904(10)	104(3)
C(37)	1343(7)	3873(6)	8471(7)	78(2)
C(38)	1835(7)	3261(6)	8800(7)	81(2)
C(39)	2978(7)	3730(6)	9636(6)	72(2)
C(40)	3588(8)	4848(6)	10112(5)	86(2)
C(41)	3047(7)	5430(6)	9760(6)	76(2)
C(42)	3576(9)	3083(7)	9996(6)	96(3)

Bond lengths [Å] and angles [°] for C21 H13 Cl N3 O9 Re, **[6c]**$^{+}$.

Re(1)-C(14)	1.901(8)
Re(1)-C(13)	1.913(8)
Re(1)-C(15)	1.924(9)
Re(1)-N(1)	2.175(5)
Re(1)-N(2)	2.184(4)
Re(1)-N(3)	2.199(5)
Cl(1)-O(7)	1.397(5)
Cl(1)-O(9)	1.417(7)
Cl(1)-O(8)	1.418(6)
Cl(1)-O(6)	1.432(5)
O(1)-C(6)	1.190(8)
O(2)-C(7)	1.217(8)
O(3)-C(13)	1.150(9)

O(4)-C(14)	1.159(9)
O(5)-C(15)	1.144(10)
N(1)-C(5)	1.351(7)
N(1)-C(1)	1.353(8)
N(2)-C(12)	1.345(8)
N(2)-C(9)	1.348(7)
N(3)-C(20)	1.333(8)
N(3)-C(16)	1.340(8)
C(1)-C(2)	1.372(11)
C(1)-H(1)	0.9300
C(2)-C(3)	1.360(12)
C(2)-H(2)	0.9300
C(3)-C(4)	1.386(11)
C(3)-H(3)	0.9300
C(4)-C(5)	1.394(8)
C(4)-C(6)	1.463(10)
C(5)-C(9)	1.459(8)
C(6)-C(7)	1.529(12)
C(7)-C(8)	1.493(10)
C(8)-C(9)	1.397(7)
C(8)-C(10)	1.407(11)
C(10)-C(11)	1.368(11)
C(10)-H(10)	0.9300
C(11)-C(12)	1.365(10)
C(11)-H(11)	0.9300
C(12)-H(12)	0.9300
C(16)-C(17)	1.373(12)
C(16)-H(16)	0.9300
C(17)-C(18)	1.354(13)
C(17)-H(17)	0.9300
C(18)-C(19)	1.369(11)
C(18)-C(21)	1.526(11)

C(19)-C(20)	1.371(9)
C(19)-H(19)	0.9300
C(20)-H(20)	0.9300
C(21)-H(21A)	0.9600
C(21)-H(21B)	0.9600
C(21)-H(21C)	0.9600
Re(2)-C(35)	1.894(9)
Re(2)-C(36)	1.914(8)
Re(2)-C(34)	1.912(7)
Re(2)-N(4)	2.175(5)
Re(2)-N(5)	2.181(5)
Re(2)-N(6)	2.207(5)
Cl(2)-O(18)	1.392(7)
Cl(2)-O(16)	1.403(5)
Cl(2)-O(15)	1.427(7)
Cl(2)-O(17)	1.429(5)
O(10)-C(27)	1.212(7)
O(11)-C(28)	1.210(7)
O(12)-C(34)	1.162(8)
O(13)-C(35)	1.155(10)
O(14)-C(36)	1.156(9)
N(4)-C(22)	1.339(7)
N(4)-C(26)	1.360(7)
N(5)-C(30)	1.349(7)
N(5)-C(33)	1.352(7)
N(6)-C(41)	1.333(9)
N(6)-C(37)	1.349(9)
C(22)-C(23)	1.370(10)
C(22)-H(22)	0.9300
C(23)-C(24)	1.369(9)
C(23)-H(23)	0.9300
C(24)-C(25)	1.402(8)

C(24)-H(24)	0.9300
C(25)-C(26)	1.382(7)
C(25)-C(27)	1.466(8)
C(26)-C(30)	1.468(7)
C(27)-C(28)	1.529(9)
C(28)-C(29)	1.475(9)
C(29)-C(31)	1.388(8)
C(29)-C(30)	1.396(8)
C(31)-C(32)	1.341(10)
C(31)-H(31)	0.9300
C(32)-C(33)	1.378(10)
C(32)-H(32)	0.9300
C(33)-H(33)	0.9300
C(37)-C(38)	1.357(9)
C(37)-H(37)	0.9300
C(38)-C(39)	1.355(11)
C(38)-H(38)	0.9300
C(39)-C(40)	1.377(10)
C(39)-C(42)	1.506(9)
C(40)-C(41)	1.369(9)
C(40)-H(40)	0.9300
C(41)-H(41)	0.9300
C(42)-H(42A)	0.9600
C(42)-H(42B)	0.9600
C(42)-H(42C)	0.9600

C(14)-Re(1)-C(13)	89.8(3)
C(14)-Re(1)-C(15)	89.3(4)
C(13)-Re(1)-C(15)	88.7(3)
C(14)-Re(1)-N(1)	96.6(3)
C(13)-Re(1)-N(1)	91.7(3)
C(15)-Re(1)-N(1)	174.1(3)

C(14)-Re(1)-N(2)	171.4(3)
C(13)-Re(1)-N(2)	88.5(2)
C(15)-Re(1)-N(2)	99.1(3)
N(1)-Re(1)-N(2)	75.03(18)
C(14)-Re(1)-N(3)	92.2(3)
C(13)-Re(1)-N(3)	176.9(2)
C(15)-Re(1)-N(3)	93.6(3)
N(1)-Re(1)-N(3)	85.72(18)
N(2)-Re(1)-N(3)	89.23(17)
O(7)-Cl(1)-O(9)	108.0(4)
O(7)-Cl(1)-O(8)	110.3(4)
O(9)-Cl(1)-O(8)	109.7(4)
O(7)-Cl(1)-O(6)	109.6(4)
O(9)-Cl(1)-O(6)	108.4(4)
O(8)-Cl(1)-O(6)	110.8(3)
C(5)-N(1)-C(1)	118.0(6)
C(5)-N(1)-Re(1)	115.3(4)
C(1)-N(1)-Re(1)	126.4(5)
C(12)-N(2)-C(9)	118.8(5)
C(12)-N(2)-Re(1)	126.5(4)
C(9)-N(2)-Re(1)	114.5(4)
C(20)-N(3)-C(16)	115.6(6)
C(20)-N(3)-Re(1)	122.5(4)
C(16)-N(3)-Re(1)	121.9(5)
N(1)-C(1)-C(2)	121.8(7)
N(1)-C(1)-H(1)	119.1
C(2)-C(1)-H(1)	119.1
C(3)-C(2)-C(1)	120.1(8)
C(3)-C(2)-H(2)	119.9
C(1)-C(2)-H(2)	119.9
C(2)-C(3)-C(4)	119.6(8)
C(2)-C(3)-H(3)	120.2

C(4)-C(3)-H(3)	120.2
C(3)-C(4)-C(5)	117.8(7)
C(3)-C(4)-C(6)	122.3(7)
C(5)-C(4)-C(6)	119.9(7)
N(1)-C(5)-C(4)	122.4(6)
N(1)-C(5)-C(9)	115.5(5)
C(4)-C(5)-C(9)	122.1(6)
O(1)-C(6)-C(4)	122.8(9)
O(1)-C(6)-C(7)	119.6(8)
C(4)-C(6)-C(7)	117.6(6)
O(2)-C(7)-C(8)	120.7(9)
O(2)-C(7)-C(6)	121.3(8)
C(8)-C(7)-C(6)	118.0(6)
C(9)-C(8)-C(10)	118.0(6)
C(9)-C(8)-C(7)	119.6(6)
C(10)-C(8)-C(7)	122.3(6)
N(2)-C(9)-C(8)	121.8(6)
N(2)-C(9)-C(5)	117.1(5)
C(8)-C(9)-C(5)	121.0(6)
C(11)-C(10)-C(8)	119.0(6)
C(11)-C(10)-H(10)	120.5
C(8)-C(10)-H(10)	120.5
C(12)-C(11)-C(10)	120.0(7)
C(12)-C(11)-H(11)	120.0
C(10)-C(11)-H(11)	120.0
N(2)-C(12)-C(11)	122.4(7)
N(2)-C(12)-H(12)	118.8
C(11)-C(12)-H(12)	118.8
O(3)-C(13)-Re(1)	179.1(7)
O(4)-C(14)-Re(1)	178.4(8)
O(5)-C(15)-Re(1)	178.4(8)
N(3)-C(16)-C(17)	123.1(8)

N(3)-C(16)-H(16)	118.4
C(17)-C(16)-H(16)	118.4
C(18)-C(17)-C(16)	120.9(7)
C(18)-C(17)-H(17)	119.6
C(16)-C(17)-H(17)	119.6
C(17)-C(18)-C(19)	116.5(7)
C(17)-C(18)-C(21)	122.3(9)
C(19)-C(18)-C(21)	121.2(9)
C(18)-C(19)-C(20)	120.4(8)
C(18)-C(19)-H(19)	119.8
C(20)-C(19)-H(19)	119.8
N(3)-C(20)-C(19)	123.5(7)
N(3)-C(20)-H(20)	118.2
C(19)-C(20)-H(20)	118.2
C(18)-C(21)-H(21A)	109.5
C(18)-C(21)-H(21B)	109.5
H(21A)-C(21)-H(21B)	109.5
C(18)-C(21)-H(21C)	109.5
H(21A)-C(21)-H(21C)	109.5
H(21B)-C(21)-H(21C)	109.5
C(35)-Re(2)-C(36)	88.8(5)
C(35)-Re(2)-C(34)	89.0(3)
C(36)-Re(2)-C(34)	91.5(3)
C(35)-Re(2)-N(4)	98.4(3)
C(36)-Re(2)-N(4)	172.5(3)
C(34)-Re(2)-N(4)	90.7(2)
C(35)-Re(2)-N(5)	173.3(3)
C(36)-Re(2)-N(5)	97.0(4)
C(34)-Re(2)-N(5)	94.1(2)
N(4)-Re(2)-N(5)	75.60(17)
C(35)-Re(2)-N(6)	92.4(3)
C(36)-Re(2)-N(6)	91.3(3)

C(34)-Re(2)-N(6)	176.9(2)
N(4)-Re(2)-N(6)	86.35(17)
N(5)-Re(2)-N(6)	84.18(18)
O(18)-Cl(2)-O(16)	109.9(4)
O(18)-Cl(2)-O(15)	111.1(5)
O(16)-Cl(2)-O(15)	109.2(4)
O(18)-Cl(2)-O(17)	106.6(5)
O(16)-Cl(2)-O(17)	110.2(4)
O(15)-Cl(2)-O(17)	109.9(4)
C(22)-N(4)-C(26)	117.6(5)
C(22)-N(4)-Re(2)	126.6(4)
C(26)-N(4)-Re(2)	115.9(3)
C(30)-N(5)-C(33)	117.5(5)
C(30)-N(5)-Re(2)	115.8(4)
C(33)-N(5)-Re(2)	126.7(5)
C(41)-N(6)-C(37)	115.1(6)
C(41)-N(6)-Re(2)	123.3(4)
C(37)-N(6)-Re(2)	121.7(5)
N(4)-C(22)-C(23)	123.7(6)
N(4)-C(22)-H(22)	118.2
C(23)-C(22)-H(22)	118.2
C(24)-C(23)-C(22)	118.9(6)
C(24)-C(23)-H(23)	120.6
C(22)-C(23)-H(23)	120.6
C(23)-C(24)-C(25)	119.3(6)
C(23)-C(24)-H(24)	120.4
C(25)-C(24)-H(24)	120.4
C(26)-C(25)-C(24)	118.4(5)
C(26)-C(25)-C(27)	120.4(5)
C(24)-C(25)-C(27)	121.2(5)
N(4)-C(26)-C(25)	122.2(5)
N(4)-C(26)-C(30)	116.1(5)

C(25)-C(26)-C(30)	121.7(5)
O(10)-C(27)-C(25)	122.4(6)
O(10)-C(27)-C(28)	119.4(6)
C(25)-C(27)-C(28)	118.2(5)
O(11)-C(28)-C(29)	122.0(6)
O(11)-C(28)-C(27)	120.0(6)
C(29)-C(28)-C(27)	118.0(5)
C(31)-C(29)-C(30)	118.3(6)
C(31)-C(29)-C(28)	121.7(6)
C(30)-C(29)-C(28)	120.0(5)
N(5)-C(30)-C(29)	122.2(5)
N(5)-C(30)-C(26)	116.6(5)
C(29)-C(30)-C(26)	121.2(5)
C(32)-C(31)-C(29)	119.5(6)
C(32)-C(31)-H(31)	120.2
C(29)-C(31)-H(31)	120.2
C(31)-C(32)-C(33)	120.2(6)
C(31)-C(32)-H(32)	119.9
C(33)-C(32)-H(32)	119.9
N(5)-C(33)-C(32)	122.3(6)
N(5)-C(33)-H(33)	118.9
C(32)-C(33)-H(33)	118.9
O(12)-C(34)-Re(2)	179.0(7)
O(13)-C(35)-Re(2)	178.9(9)
O(14)-C(36)-Re(2)	176.5(10)
N(6)-C(37)-C(38)	123.9(7)
N(6)-C(37)-H(37)	118.1
C(38)-C(37)-H(37)	118.1
C(39)-C(38)-C(37)	121.1(7)
C(39)-C(38)-H(38)	119.5
C(37)-C(38)-H(38)	119.5
C(38)-C(39)-C(40)	115.8(6)

C(38)-C(39)-C(42)	122.8(7)
C(40)-C(39)-C(42)	121.3(7)
C(41)-C(40)-C(39)	121.0(7)
C(41)-C(40)-H(40)	119.5
C(39)-C(40)-H(40)	119.5
N(6)-C(41)-C(40)	123.2(7)
N(6)-C(41)-H(41)	118.4
C(40)-C(41)-H(41)	118.4
C(39)-C(42)-H(42A)	109.5
C(39)-C(42)-H(42B)	109.5
H(42A)-C(42)-H(42B)	109.5
C(39)-C(42)-H(42C)	109.5
H(42A)-C(42)-H(42C)	109.5
H(42B)-C(42)-H(42C)	109.5

Anisotropic displacement parameters ($Å^2 x\ 10^3$) for C21 H13 Cl N3 O9 Re, **[6c]$^+$**. The anisotropic displacement factor exponent takes the form: $-2\pi^2[h^2 a^{*2} U^{11} + ... + 2 h k a^* b^* U^{12}]$

	U^{11}	U^{22}	U^{33}	U^{23}	U^{13}	U^{12}
Re(1)	57(1)	48(1)	40(1)	8(1)	14(1)	10(1)
Cl(1)	72(1)	47(1)	66(1)	22(1)	18(1)	34(1)
O(1)	213(8)	110(5)	86(4)	56(4)	100(5)	89(5)
O(2)	135(4)	83(3)	62(3)	39(2)	21(3)	56(3)
O(3)	109(5)	53(3)	118(5)	28(3)	40(4)	19(3)
O(4)	80(4)	150(6)	70(4)	32(4)	-11(3)	-2(4)
O(5)	167(7)	86(4)	107(5)	6(4)	99(5)	27(4)
O(6)	99(3)	69(3)	108(4)	38(3)	16(3)	54(3)
O(7)	143(5)	86(4)	71(3)	37(3)	54(3)	73(4)
O(8)	100(4)	64(3)	134(4)	39(3)	20(3)	48(3)

O(9)	177(6)	142(5)	143(6)	96(5)	117(5)	116(5)
N(1)	53(3)	46(2)	59(3)	24(2)	23(2)	17(2)
N(2)	49(2)	42(2)	47(2)	17(2)	17(2)	15(2)
N(3)	53(3)	66(3)	49(3)	29(2)	23(2)	25(2)
C(1)	53(4)	63(4)	92(5)	38(4)	34(3)	23(3)
C(2)	80(5)	61(4)	149(8)	52(5)	71(6)	35(4)
C(3)	109(6)	58(4)	124(7)	45(4)	85(6)	42(4)
C(4)	96(5)	45(3)	70(4)	29(3)	51(4)	36(3)
C(5)	62(3)	38(2)	51(3)	22(2)	28(3)	22(2)
C(6)	133(7)	53(3)	58(4)	28(3)	52(4)	50(4)
C(7)	122(6)	44(3)	44(3)	22(3)	19(4)	41(4)
C(8)	70(4)	38(3)	49(3)	18(2)	10(3)	22(3)
C(9)	55(3)	31(2)	43(3)	14(2)	14(2)	13(2)
C(10)	63(4)	59(4)	79(5)	29(3)	4(3)	25(3)
C(11)	58(4)	74(4)	97(6)	42(4)	29(4)	31(3)
C(12)	61(4)	59(3)	79(4)	35(3)	39(3)	28(3)
C(13)	67(4)	54(4)	58(4)	8(3)	16(3)	8(3)
C(14)	79(5)	89(5)	57(4)	25(4)	12(4)	14(4)
C(15)	92(5)	63(4)	60(4)	5(3)	33(4)	14(4)
C(16)	82(5)	101(6)	64(4)	44(4)	36(4)	42(4)
C(17)	116(7)	149(9)	107(7)	99(7)	78(6)	88(7)
C(18)	104(6)	108(6)	132(7)	85(6)	93(6)	81(5)
C(19)	94(5)	68(4)	101(6)	48(4)	61(5)	49(4)
C(20)	73(4)	59(4)	62(4)	29(3)	32(3)	35(3)
C(21)	171(9)	122(7)	190(10)	114(7)	133(8)	111(7)
Re(2)	64(1)	65(1)	78(1)	42(1)	44(1)	39(1)
Cl(2)	75(1)	56(1)	104(1)	46(1)	52(1)	41(1)
O(10)	75(3)	81(3)	121(4)	49(3)	65(3)	39(3)
O(11)	132(5)	88(3)	82(3)	44(3)	74(4)	66(3)
O(12)	101(4)	104(4)	122(5)	64(4)	62(4)	76(4)
O(13)	255(11)	174(8)	141(7)	85(6)	155(8)	127(8)
O(14)	87(3)	115(4)	176(5)	72(4)	68(3)	46(3)

O(15)	87(4)	77(4)	140(6)	28(4)	25(4)	30(3)
O(16)	126(5)	99(4)	131(5)	78(4)	73(4)	78(4)
O(17)	112(4)	57(3)	130(5)	42(3)	46(4)	48(3)
O(18)	168(7)	171(7)	176(7)	104(6)	135(7)	96(6)
N(4)	62(3)	45(2)	48(2)	24(2)	26(2)	30(2)
N(5)	50(3)	45(2)	54(3)	23(2)	16(2)	25(2)
N(6)	65(3)	66(3)	71(3)	43(3)	40(3)	37(3)
C(22)	76(4)	52(3)	46(3)	23(3)	24(3)	33(3)
C(23)	78(4)	47(3)	47(3)	14(3)	17(3)	26(3)
C(24)	50(3)	48(3)	72(4)	27(3)	21(3)	20(3)
C(25)	55(3)	43(3)	59(3)	28(2)	27(3)	30(2)
C(26)	48(3)	38(2)	44(2)	21(2)	21(2)	25(2)
C(27)	68(4)	53(3)	81(4)	40(3)	46(3)	38(3)
C(28)	90(5)	60(3)	68(4)	38(3)	51(4)	52(3)
C(29)	70(4)	48(3)	48(3)	23(2)	24(3)	40(3)
C(30)	50(3)	41(2)	52(3)	25(2)	22(2)	28(2)
C(31)	78(4)	59(3)	49(3)	19(3)	21(3)	42(3)
C(32)	73(4)	48(3)	57(4)	11(3)	8(3)	32(3)
C(33)	55(3)	47(3)	71(4)	25(3)	15(3)	26(3)
C(34)	73(4)	73(4)	84(5)	39(4)	47(4)	46(4)
C(35)	144(8)	105(6)	110(7)	62(6)	96(7)	79(6)
C(36)	74(5)	91(6)	181(10)	77(6)	78(6)	47(5)
C(37)	67(4)	63(4)	99(5)	43(4)	36(4)	29(3)
C(38)	86(5)	67(4)	98(5)	48(4)	44(5)	41(4)
C(39)	105(6)	82(5)	59(4)	43(4)	48(4)	63(4)
C(40)	98(5)	85(5)	50(4)	22(3)	10(4)	55(5)
C(41)	84(5)	64(4)	62(4)	24(3)	22(4)	37(4)
C(42)	143(8)	98(6)	72(5)	44(4)	46(5)	88(6)

Hydrogen coordinates (x 10^4) and isotropic displacement parameters ($Å^2$x 10^3) for C21 H13 Cl N3 O9 Re, **[6c]**$^+$.

	x	y	z	U(eq)
H(1)	-15	765	3186	86
H(2)	-337	1238	4606	108
H(3)	993	1518	6311	102
H(10)	6272	1987	7016	97
H(11)	6420	1683	5469	95
H(12)	4784	1080	3810	78
H(16)	1615	1483	1208	97
H(17)	2104	3148	1201	118
H(19)	3826	4483	4431	93
H(20)	3366	2802	4383	78
H(21A)	2953	5073	2104	182
H(21B)	4221	5525	3120	182
H(21C)	3172	5535	3290	182
H(22)	3430	8137	10217	71
H(23)	5265	9244	10532	79
H(24)	5725	8849	9178	74
H(31)	1446	4369	4517	77
H(32)	-206	3325	4518	85
H(33)	-432	3894	5985	77
H(37)	562	3516	7884	94
H(38)	1381	2508	8445	97
H(40)	4379	5213	10682	104
H(41)	3489	6184	10105	91
H(42A)	3002	2324	9607	144
H(42B)	3895	3300	10768	144
H(42C)	4214	3213	9845	144

APPENDIX B

UV-Vis Spectroscopic Data

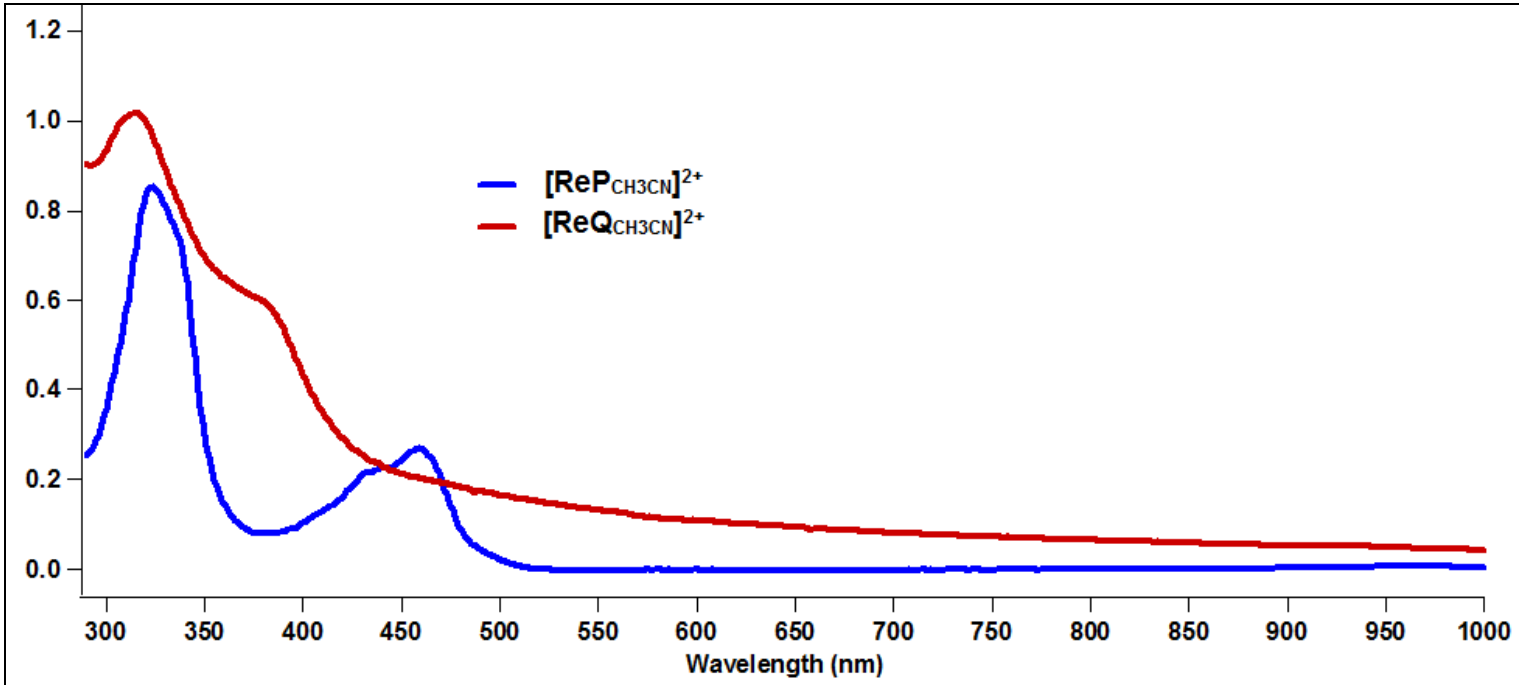

Figure 4.10 UV-Vis spectra of **[ReP$_{CH3CN}$]$^{2+}$ and [ReQ$_{CH3CN}$]$^{2+}$ in MeCN (**15 µM)

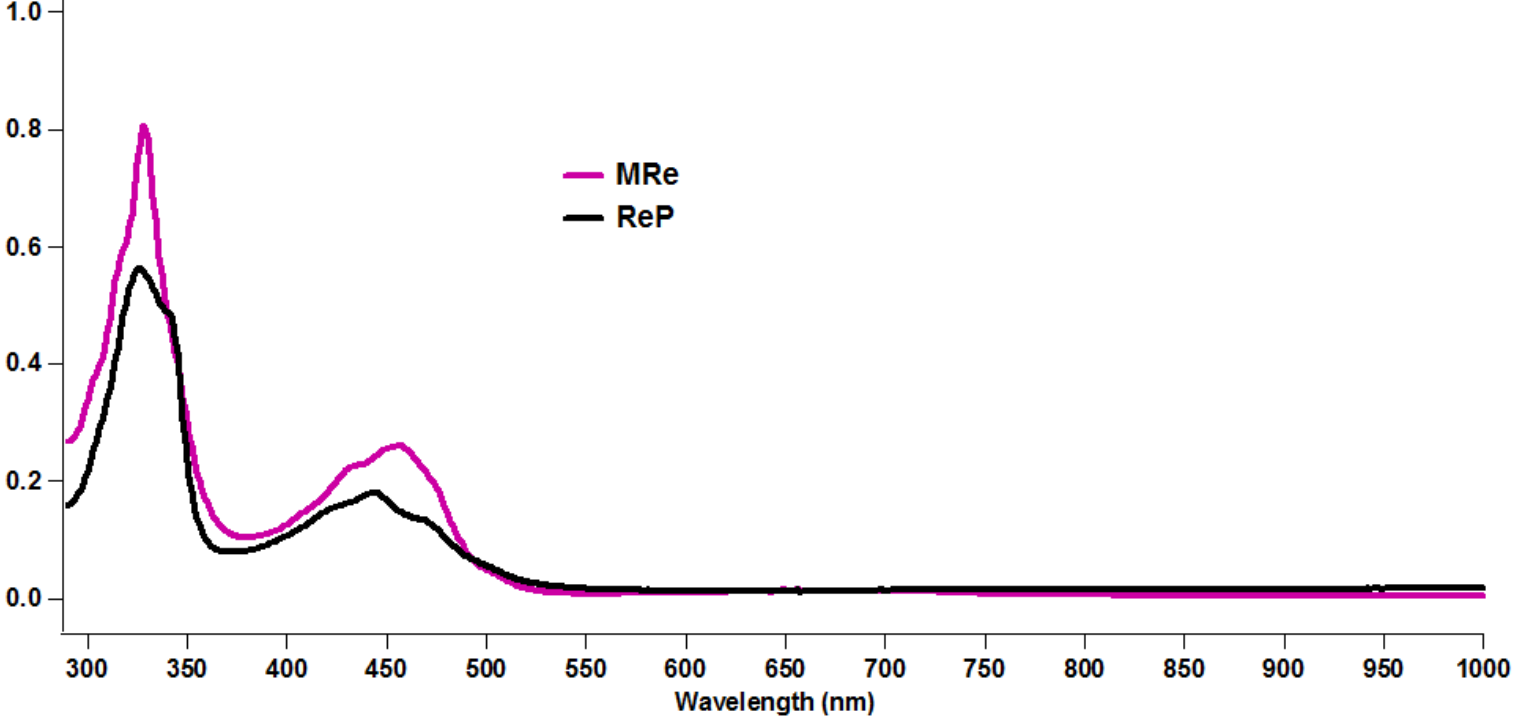

Figure 4.11 UV-Vis spectra of MRe and [**ReP**] in dichloromethane (15 µM)

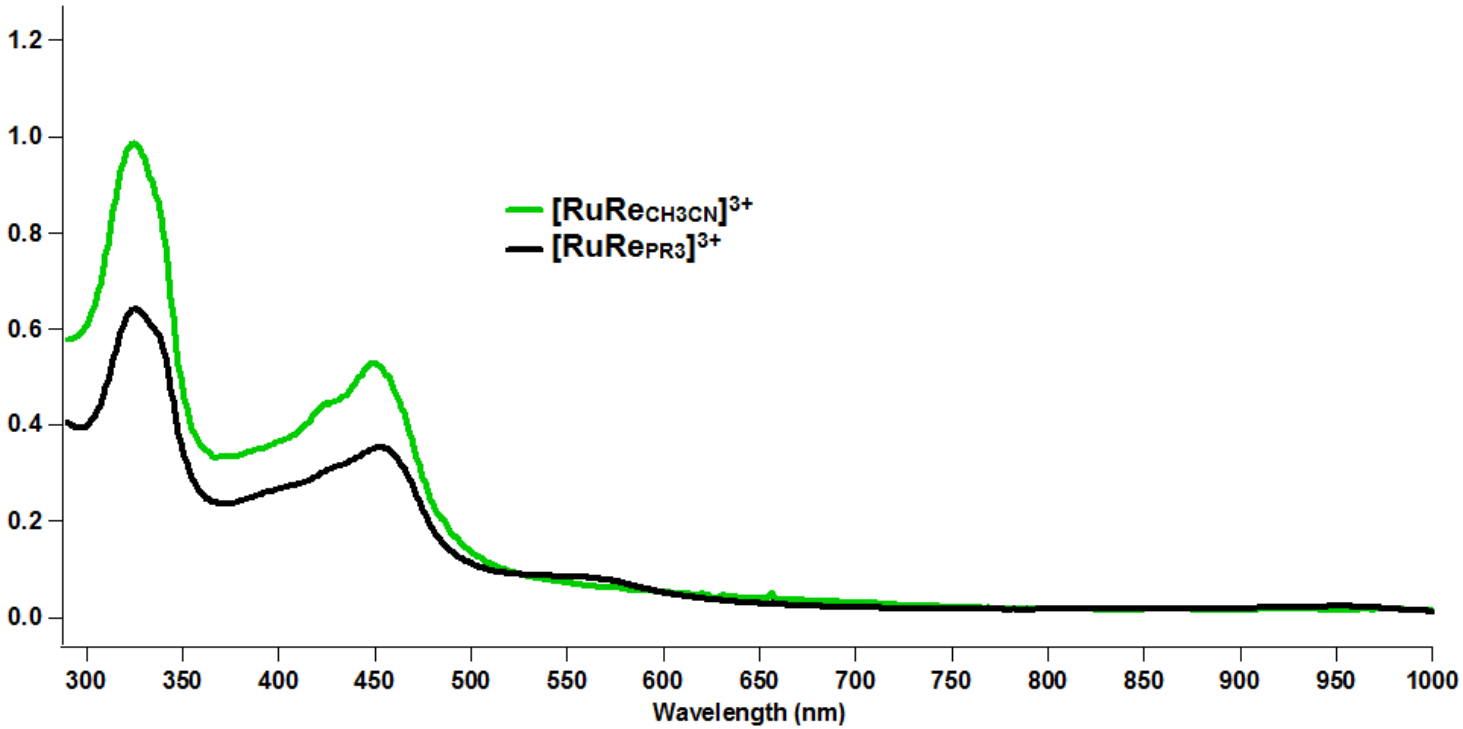

Figure 4.12 UV-Vis spectra of **[RuRe$_{CH3CN}$]$^{3+}$** (15 µM) and **[RuRe$_{PR3}$]$^{3+}$ (**20 µM) **in MeCN**

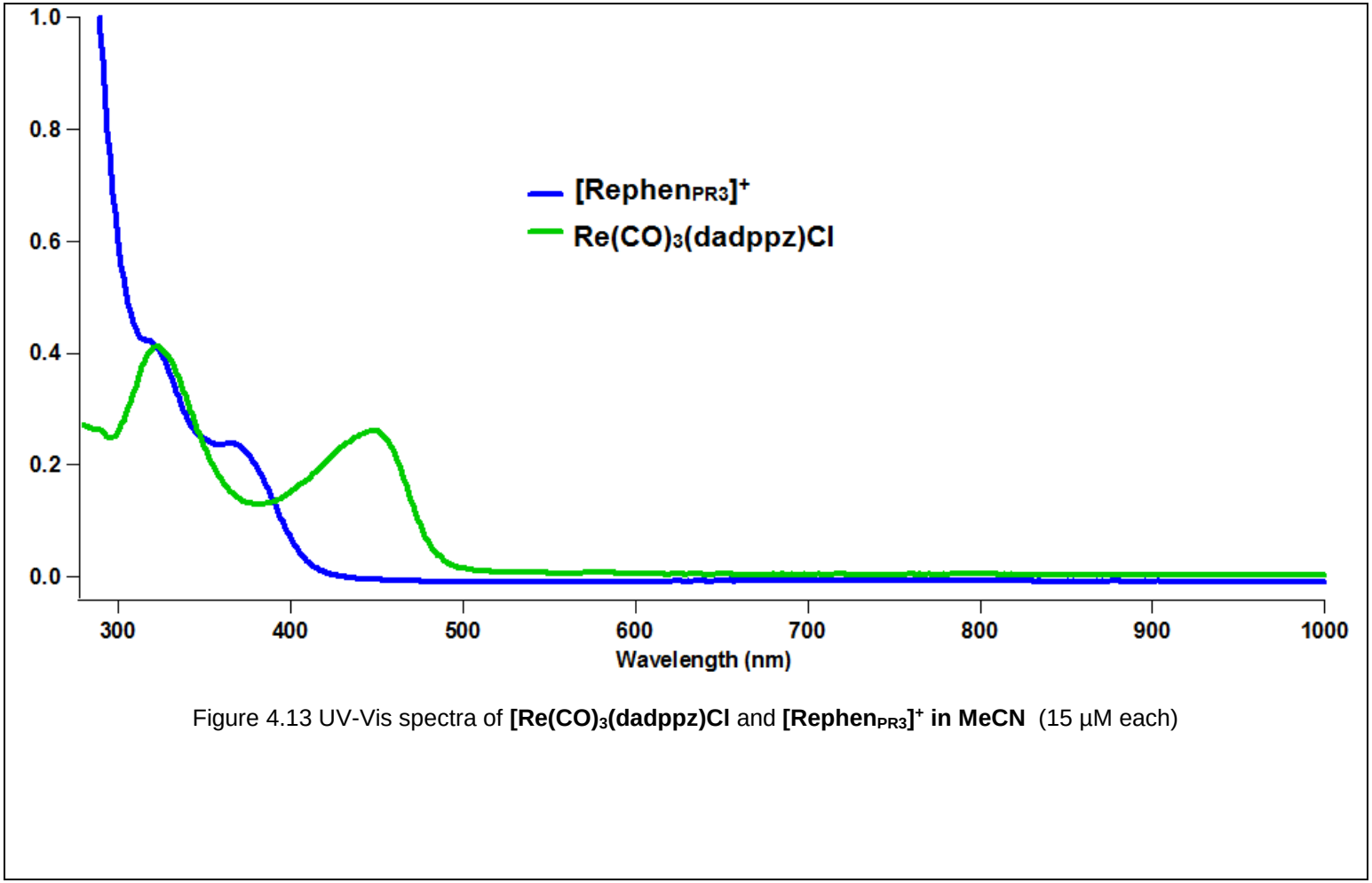

Figure 4.13 UV-Vis spectra of **[Re(CO)$_3$(dadppz)Cl** and **[Rephen$_{PR3}$]$^{+}$ in MeCN** (15 µM each)

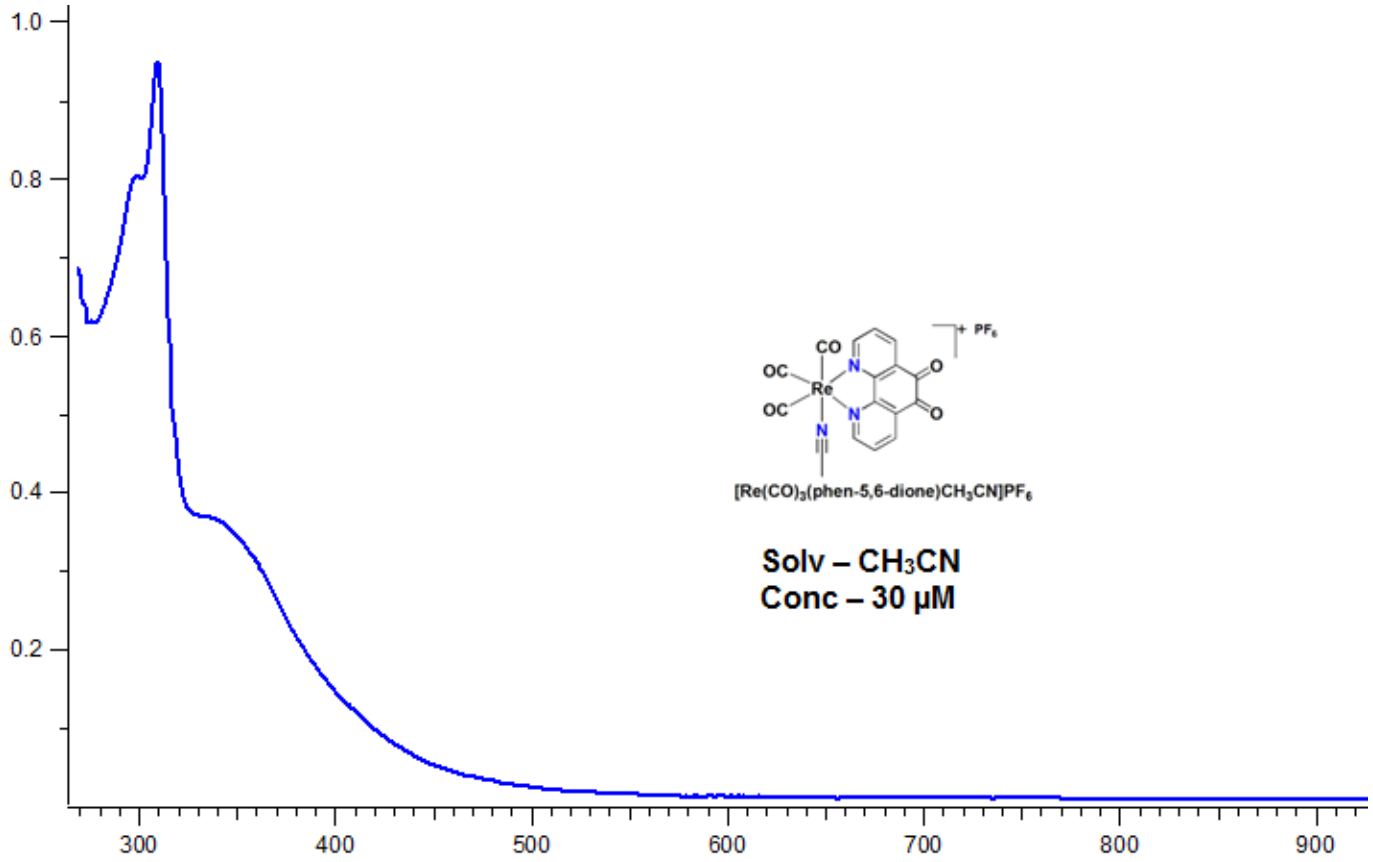

Figure 4.14 UV-Vis spectra of **[Redione$_{CH3CN}$]$^{+}$ in MeCN** (30 µM)

APPENDIX C

HPLC, Fluorescence and DNA Cleavage Data

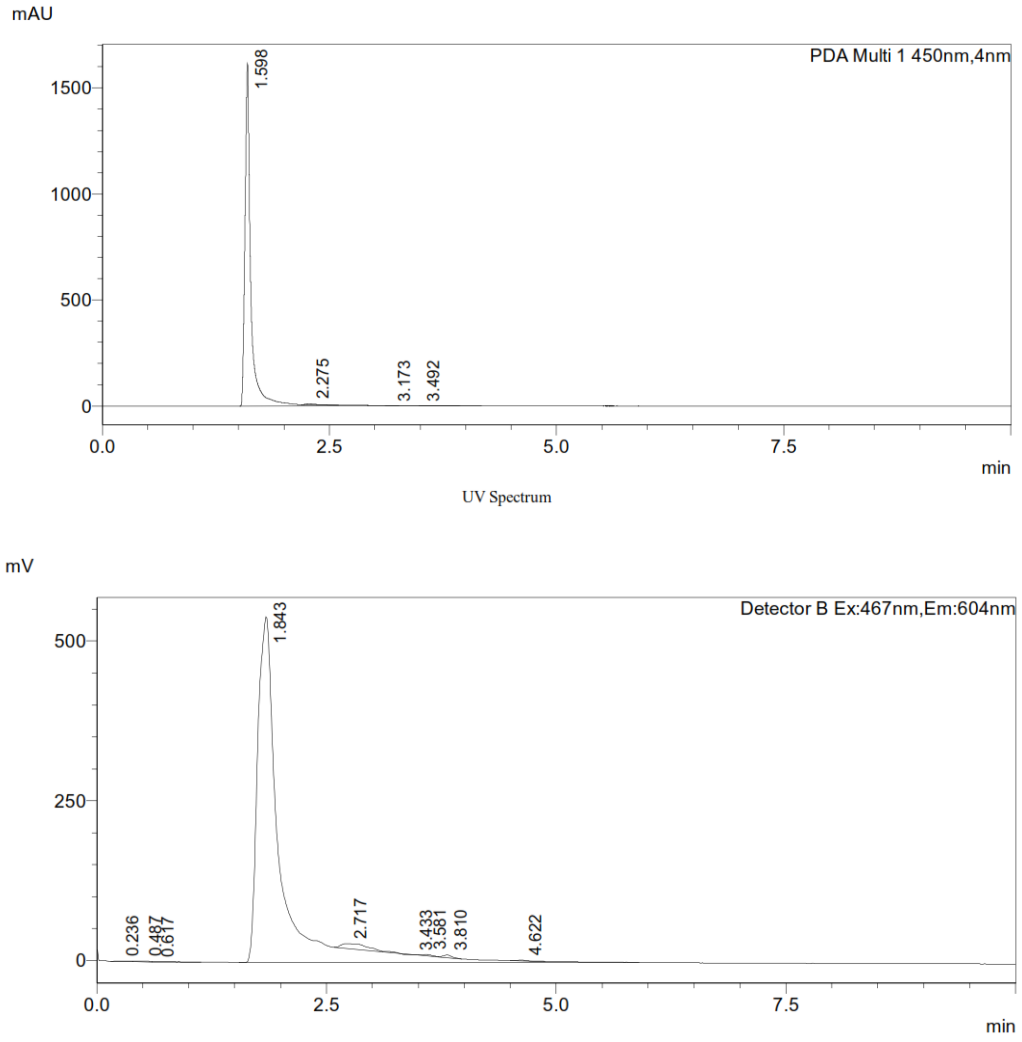

Figure 4.15 **[RuRe$_{PR3}$]Cl$_3$** HPLC-UV spectra (1.0 mg complex dissolved in 1.0 ml H_2O, Mobile phase: 99:1 MeOH:H_2O (Top), UV-Fluorescence spectra (bottom) This HPLC (UVVis-LC-FL) is coupled to a fluorescence detector and thus provides simultaneous fluorescence determination of separated analytes

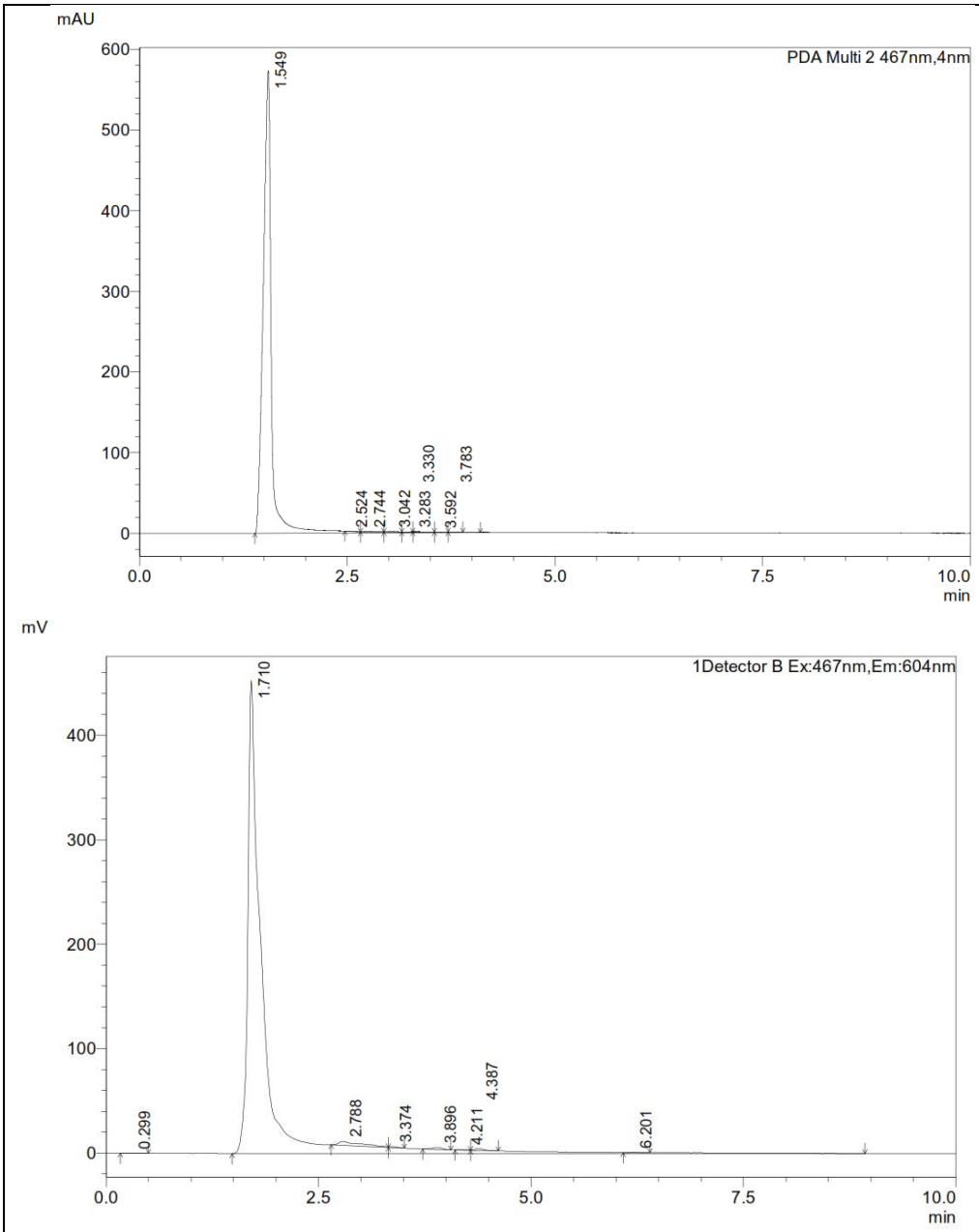

Figure 4.16 **[RuRe$_{PR3}$]Cl$_3$** HPLC-UV spectra (1.0 mg complex dissolved in 1.0 ml H_2O, Mobile phase: 90:10 MeOH:H_2O (Top), UV-Fluorescence spectra (bottom). This HPLC (UVVis-LC-FL) is coupled to a fluorescence detector and thus provides simultaneous fluorescence determination of separated analytes

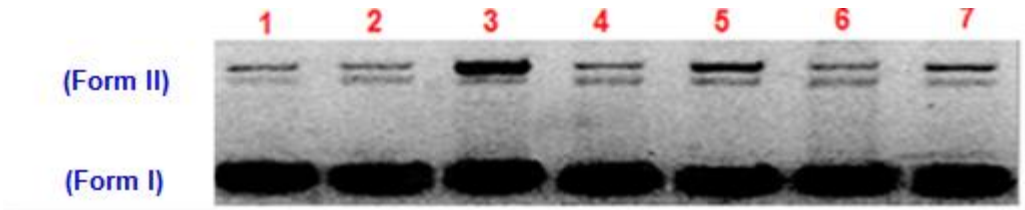

DNA	+	+	+	+	+	+	+
GSH			+		+		+
DMSO (20%)	+	+	+	+	+	+	+
$[P]^{4+}$		+	+				
$[ReP_{CH3CN}]^{2+}$				+	+		
ReP						+	+

Figure 4.17 DNA Cleavage assay $[ReP_{CH3CN}]^{2+}$and [ReP]

REFERENCES

1. Twombly, R., Cancer Surpasses Heart Disease as Leading Cause of Death for All But the Very Elderly. *Journal of the National Cancer Institute* **2005,** *97* (5), 330-331.

2. Rahib, L.; Smith, B. D.; Aizenberg, R.; Rosenzweig, A. B.; Fleshman, J. M.; Matrisian, L. M., Projecting Cancer Incidence and Deaths to 2030: The Unexpected Burden of Thyroid, Liver, and Pancreas Cancers in the United States. *Cancer Research* **2014,** *74* (11), 2913-2921.

3. Witschi, H., A Short History of Lung Cancer. *Toxicol. Sci.* **2001,** *64* (1), 4-6.

4. Siegel, R.; Naishadham, D.; Jemal, A., Cancer statistics, 2013. *CA: A Cancer Journal for Clinicians* **2013,** *63* (1), 11-30.

5. Dasari, S.; Bernard Tchounwou, P., Cisplatin in cancer therapy: Molecular mechanisms of action. *Eur. J. Pharmacol.* **2014,** *740*, 364-378.

6. Zamble, D. B.; Lippard, S. J., Cisplatin and DNA repair in cancer chemotherapy. *Trends Biochem. Sci* **1995,** *20* (10), 435-439.

7. Curran, W. J., New Chemotherapeutic Agents: Update of Major Chemoradiation Trials in Solid Tumors. *Oncology* **2002,** *63(suppl 2)* (Suppl. 2), 29-38.

8. O'Dwyer, P. J.; Stevenson, J. P.; Johnson, S. W., Clinical Status of Cisplatin, Carboplatin, and Other Platinum-Based Antitumor Drugs. In *Cisplatin*, Verlag Helvetica Chimica Acta: 2006; pp 29-69.

9. Rosenberg, B., Platinum Complexes for the Treatment of Cancer: Why the Search Goes On. In *Cisplatin*, Verlag Helvetica Chimica Acta: 2006; pp 1-27.

10. McWhinney, S. R.; Goldberg, R. M.; McLeod, H. L., Platinum Neurotoxicity Pharmacogenetics. *Molecular cancer therapeutics* **2009,** *8* (1), 10-16.

11. Temel, J. S.; Greer, J. A.; Admane, S.; Gallagher, E. R.; Jackson, V. A.; Lynch, T. J.; Lennes, I. T.; Dahlin, C. M.; Pirl, W. F., Longitudinal Perceptions of Prognosis and Goals

of Therapy in Patients With Metastatic Non–Small-Cell Lung Cancer: Results of a Randomized Study of Early Palliative Care. *Journal of Clinical Oncology* **2011,** *29* (17), 2319-2326.

12. Younes, R. N.; Pereira, J. R.; Fares, A. L.; Gross, J. L., Chemotherapy beyond first-line in stage IV metastatic non-small cell lung cancer. *Revista da Associação Médica Brasileira* **2011,** *57*, 686-691.

13. Hambley, T. W., Chemistry. Metal-based therapeutics. *Science* **2007,** *318* (5855), 1392-3.

14. Pieper, T.; Borsky, K.; Keppler, B., Non-Platinum Antitumor Compounds. In *Metallopharmaceuticals I*, Clarke, M.; Sadler, P., Eds. Springer Berlin Heidelberg: 1999; Vol. 1, pp 171-199.

15. Bratsos, I.; Jedner, S.; Gianferrara, T.; Alessio, E., Ruthenium Anticancer Compounds: Challenges and Expectations. *CHIMIA International Journal for Chemistry* **2007,** *61* (11), 692-697.

16. Bergamo, A.; Sava, G., Ruthenium complexes can target determinants of tumour malignancy. *Dalton Transactions* **2007,** (13), 1267-1272.

17. Sava, G.; Clerici, K.; Capozzi, I.; Cocchietto, M.; Gagliardi, R.; Alessio, E.; Mestroni, G.; Perbellini, A., Reduction of lung metastasis by ImH[trans-RuCl4(DMSO)Im]: mechanism of the selective action investigated on mouse tumors. *Anti-Cancer Drugs* **1999,** *10* (1), 129.

18. Alessio, E.; Mestroni, G.; Bergamo, A.; Sava, G., Ruthenium antimetastatic agents. *Curr. Top. Med. Chem.* **2004,** *4* (15), 1525-1535.

19. Groessl, M.; Reisner, E.; Hartinger, C. G.; Eichinger, R.; Semenova, O.; Timerbaev, A. R.; Jakupec, M. A.; Arion, V. B.; Keppler, B. K., Structure−Activity Relationships for NAMI-A-type Complexes (HL)[trans-$RuCl_4$L(S-dmso)ruthenate(III)] (L = Imidazole,

Indazole, 1,2,4-Triazole, 4-Amino-1,2,4-triazole, and 1-Methyl-1,2,4-triazole): Aquation, Redox Properties, Protein Binding, and Antiproliferative Activity. *J. Med. Chem.* **2007,** *50* (9), 2185-2193.

20. Dwyer, F. P.; Mayhew, E.; Roe, E. M. F.; Shulman, A., Inhibition of Landschütz Ascites Tumour Growth by Metal Chelates Derived from 3,4,7,8-Tetramethyl-1,10-phenanthroline. *British Journal of Cancer* **1965,** *19* (1), 195-199.

21. Dwyer, F. P.; Gyarfas, E. C.; Rogers, W. P.; Koch, J. H., Biological Activity of Complex Ions. *Nature* **1952,** *170* (4318), 190-191.

22. Dwyer, F. P.; Gyarfas, E. C.; Wright, R. D.; Shulman, A., Effect of Inorganic Complex Ions on Transmission at a Neuromuscular Junction. *Nature* **1957,** *179* (4556), 425-426.

23. Shulman, A.; Dwyer, F. P., CHAPTER 9 - Metal Chelates in Biological Systems. In *Chelating Agents and Metal Chelates*, Mellor, F. P. D. P., Ed. Academic Press: 1964; pp 383-439.

24. Koch, J. H. R., W.P.; Dwyer, F.P.; Gyarfas, E.C, The Metabollic Fate of Tris-1,10-Phenanthroline Ruthenium-106 (II) Perchlorate, a compound with Anticholinesterase and Curare-Like Activity. *Australian Journal of Biological Sciences* **1957,** (10), 342-350.

25. H Koch, J.; C Gyarfas, E.; Dwyer, F., Biological Activity of Complex Ions Mechanism of Inhibition of Acetylcholinesterase. *Australian Journal of Biological Sciences* **1956,** *9* (3), 371-381.

26. Pisani, M. J.; Fromm, P. D.; Mulyana, Y.; Clarke, R. J.; Korner, H.; Heimann, K.; Collins, J. G.; Keene, F. R., Mechanism of cytotoxicity and cellular uptake of lipophilic inert dinuclear polypyridylruthenium(II) complexes. *ChemMedChem* **2011,** *6* (5), 848-58.

27. Pisani, M. J.; Weber, D. K.; Heimann, K.; Collins, J. G.; Keene, F. R., Selective mitochondrial accumulation of cytotoxic dinuclear polypyridyl ruthenium(ii) complexes. *Metallomics* **2010,** *2* (6), 393-396.

28. Shulman, A.; Laycock, G. A., Action of 1,10-phenanthroline transition metal chelates on P388 mouse lymphocyte leukaemic cells. *Chem. Biol. Interact.* **1977,** *16* (1), 89-99.

29. White, D. O.; Harris, A. W.; Cheyne, I. M.; Shew, M., Actions of metal chelates of substituted 1,10-phenanthrolines on viruses and cells. 3. Actions on cultured cells. *Aust J Exp Biol Med Sci* **1969,** *47* (1), 81-9.

30. Butler, H. M.; Hurse, A.; Thursky, E.; Shulman, A., BACTERICIDAL ACTION OF SELECTED PHENANTHROLINE CHELATES AND RELATED COMPOUNDS. *Aust J Exp Biol Med* **1969,** *47* (5), 541-552.

31. Shulman, A.; White, D. O., Virostatic activity of 1,10-phenanthroline transition metal chelates: A structure-activity analysis. *Chem. Biol. Interact.* **1973,** *6* (6), 407-413.

32. Johann, T. W.; Barton, J. K., Recognition of DNA by Octahedral Coordination Complexes. *Philosophical Transactions of the Royal Society of London A: Mathematical, Physical and Engineering Sciences* **1996,** *354* (1706), 299-324.

33. Chow, C. S.; Barton, J. K., [12] Transition metal complexes as probes of nucleic acids. In *Methods Enzymol.*, Academic Press: 1992; Vol. Volume 212, pp 219-242.

34. Murphy, C. J.; Barton, J. K., Ruthenium complexes as luminescent reporters of DNA. *Methods Enzymol.* **1993,** *226*, 576-94.

35. Erkkila, K. E.; Odom, D. T.; Barton, J. K., Recognition and Reaction of Metallointercalators with DNA. *Chem. Rev.* **1999,** *99* (9), 2777-2796.

36. Wilhelmsson, L. M.; Esbjörner, E. K.; Westerlund, F.; Nordén, B.; Lincoln, P., Meso Stereoisomer as a Probe of Enantioselective Threading Intercalation of Semirigid Ruthenium Complex [μ-(11,11'-bidppz)$(phen)_4Ru_2]^{4+}$. *The Journal of Physical Chemistry B* **2003,** *107* (42), 11784-11793.

37. Rajput, C. C., Dinuclear monointercalating RuII complexes that display high affinity binding to duplex and quadruplex DNA. *Chemistry : a European journal* **2006,** *12* (17), 4611-4619.

38. Hiort, C.; Lincoln, P.; Norden, B., DNA binding of .DELTA.- and .LAMBDA.-$[Ru(phen)_2DPPZ]^{2+}$. *JACS* **1993,** *115* (9), 3448-3454.

39. Lincoln, P.; Norden, B., Binuclear ruthenium(II) phenanthroline compounds with extreme binding affinity for DNA. *Chem. Commun.* **1996,** (18), 2145-2146.

40. Satyanarayana, S.; Dabrowiak, J. C.; Chaires, J. B., Tris(phenanthroline)ruthenium(II) enantiomer interactions with DNA: Mode and specificity of binding. *Biochemistry* **1993,** *32* (10), 2573-2584.

41. Aldrich-Wright, J.; Brodie, C.; Glazer, E. C.; Luedtke, N. W.; Elson-Schwab, L.; Tor, Y., Symmetrical dinuclear complexes with high DNA affinity based on [Ru(dpq)2(phen)]2+. *Chem. Commun.* **2004,** (8), 1018-1019.

42. Alatrash, N. Redox Active Lipophilic Ruthenium Complexes As Potential Anti-cancer Drugs. University of Texas at Arlington, 2015.

43. Schatzschneider, U.; Niesel, J.; Ott, I.; Gust, R.; Alborzinia, H.; Wolfl, S., Cellular uptake, cytotoxicity, and metabolic profiling of human cancer cells treated with ruthenium(II) polypyridyl complexes $[Ru(bpy)_2(N\text{--}N)]Cl_2$ with N--N=bpy, phen, dpq, dppz, and dppn. *ChemMedChem* **2008,** *3* (7), 1104-9.

44. Jonas, S. K.; Riley, P. A., The effect of ligands on the uptake of iron by cells in culture. *Cell Biochem. Funct.* **1991,** *9* (4), 245-53.

45. McKeage, M. J.; Berners-Price, S. J.; Galettis, P.; Bowen, R. J.; Brouwer, W.; Ding, L.; Zhuang, L.; Baguley, B. C., Role of lipophilicity in determining cellular uptake and antitumour activity of gold phosphine complexes. *Cancer Chemother Pharmacol* **2000,** *46* (5), 343-50.

46. Puckett, C. A.; Barton, J. K., Mechanism of cellular uptake of a ruthenium polypyridyl complex. *Biochemistry* **2008,** *47* (45), 11711-6.

47. Puckett, C. A.; Barton, J. K., Methods to explore cellular uptake of ruthenium complexes. *J. Am. Chem. Soc.* **2007,** *129* (1), 46-7.

48. Svensson, F. R.; Matson, M.; Li, M.; Lincoln, P., Lipophilic ruthenium complexes with tuned cell membrane affinity and photoactivated uptake. *Biophys. Chem.* **2010,** *149* (3), 102-6.

49. Zava, O.; Zakeeruddin, S. M.; Danelon, C.; Vogel, H.; Gratzel, M.; Dyson, P. J., A cytotoxic ruthenium tris(bipyridyl) complex that accumulates at plasma membranes. *Chembiochem* **2009,** *10* (11), 1796-800.

50. Gill, M. R.; Cecchin, D.; Walker, M. G.; Mulla, R. S.; Battaglia, G.; Smythe, C.; Thomas, J. A., Targeting the endoplasmic reticulum with a membrane-interactive luminescent ruthenium(ii) polypyridyl complex. *Chemical Science* **2013,** *4* (12), 4512-4519.

51. Hergueta-Bravo, A.; Jiménez-Hernández, M. E.; Montero, F.; Oliveros, E.; Orellana, G., Singlet Oxygen-Mediated DNA Photocleavage with Ru(II) Polypyridyl Complexes. *The Journal of Physical Chemistry B* **2002,** *106* (15), 4010-4017.

52. K.R, S. G.; Mathew, B. B.; Sudhamani, C. N.; Naik, H. S. B., Mechanism of DNA Binding and Cleavage. *Biomedicine and Biotechnology* **2014,** *2* (1), 1-9.

53. Knoll, J. D.; Turro, C., Control and utilization of ruthenium and rhodium metal complex excited states for photoactivated cancer therapy. *Coord. Chem. Rev.* **2015,** *282–283*, 110-126.

54. Fitzsimons, M. P.; Barton, J. K., Design of a Synthetic Nuclease: DNA Hydrolysis by a Zinc-Binding Peptide Tethered to a Rhodium Intercalator. *JACS* **1997,** *119* (14), 3379-3380.

55. Yadav, A. *Investigation of Redox Active Ruthenium (II) Polypyridyl Complexes as Potential Anti-cancer Drugs*; The University of Texas at Arlington: Arlington, Texas, 2008.

56. Janaratne, T. K. Investigation of Ru(II) Polypyridyl Dimers as Potential Chemotherapeutic Agents. University of Texas at Arlington, 2006.

57. Tacconi, N. R.; Chitakunye, R.; Macdonnell, F. M.; Lezna, R. O., The role of monomers and dimers in the reduction of ruthenium(II) complexes of redox-active tetraazatetrapyridopentacene ligand. *J. Phys. Chem. A* **2008,** *112* (3), 497-507.

58. de Tacconi, N. R.; Lezna, R. O.; Konduri, R.; Ongeri, F.; Rajeshwar, K.; MacDonnell, F. M., Influence of pH on the photochemical and electrochemical reduction of the dinuclear ruthenium complex, $[(phen)_2Ru(tatpp)Ru(phen)_2)Cl_4$, in water: proton-coupled sequential and concerted multi-electron reduction. *Chemistry* **2005,** *11* (15), 4327-39.

59. de Tacconi, N. R.; Lezna, R. O.; Chitakunye, R.; MacDonnell, F. M., Electroreduction of the ruthenium complex $[(bpy)_2Ru(tatpp)]Cl_2$ in water: insights on the mechanism of multielectron reduction and protonation of the Tatpp acceptor ligand as a function of pH. *Inorg. Chem.* **2008,** *47* (19), 8847-58.

60. Cynthia Griffith, S. S., Kenneth Abayan, Norma de Tacconi, Abhishek Yadav, Thamara Janaratne, Bradley Pierce, Zachary Breitbach, Daniel W. Armstrong, and Frederick M. MacDonnell, Mechanism of DNA Cleavage By Hypoxia Sensitive Ruthenium Polypyridyl Complexes. *Manuscript to be submitted* **2016**.

61. Yadav, A.; Janaratne, T.; Krishnan, A.; Singhal, S. S.; Yadav, S.; Dayoub, A. S.; Hawkins, D. L.; Awasthi, S.; MacDonnell, F. M., Regression of lung cancer by hypoxia-sensitizing ruthenium polypyridyl complexes. *Mol Cancer Ther* **2013,** *12* (5), 643-53.

62. Wang, W.; Yan, Y. K.; Andy Hor, T. S.; Vittal, J. J.; Wheaton, J. R.; Hall, I. H., Synthesis, X-ray structures, and cytotoxicity of rhenium(I) carbonyl 2-(dimethylamino)ethoxide complexes. *Polyhedron* **2002,** *21* (20), 1991-1999.

63. Zhang, J.; Vittal, J. J.; Henderson, W.; Wheaton, J. R.; Hall, I. H.; Hor, T. S. A.; Yan, Y. K., Tricarbonylrhenium(I) complexes of phosphine-derivatized amines, amino acids and a model peptide: structures, solution behavior and cytotoxicity. *J. Organomet. Chem.* **2002,** *650* (1–2), 123-132.

64. Ma, D.-L.; Che, C.-M.; Siu, F.-M.; Yang, M.; Wong, K.-Y., DNA Binding and Cytotoxicity of Ruthenium(II) and Rhenium(I) Complexes of 2-Amino-4-phenylamino-6-(2-pyridyl)-1,3,5-triazine. *Inorg. Chem.* **2007,** *46* (3), 740-749.

65. Choi, A. W.; Louie, M. W.; Li, S. P.; Liu, H. W.; Chan, B. T.; Lam, T. C.; Lin, A. C.; Cheng, S. H.; Lo, K. K., Emissive behavior, cytotoxic activity, cellular uptake, and PEGylation properties of new luminescent rhenium(I) polypyridine poly(ethylene glycol) complexes. *Inorg. Chem.* **2012,** *51* (24), 13289-302.

66. Thorp-Greenwood, F. L.; Coogan, M. P.; Mishra, L.; Kumari, N.; Rai, G.; Saripella, S., The importance of cellular localisation of probes: synthesis, photophysical properties, DNA interactions and cellular imaging properties of rhenium dppz complexes with known cellular localisation vectors. *New J. Chem.* **2012,** *36* (1), 64-72.

67. Amoroso, A. J.; Arthur, R. J.; Coogan, M. P.; Court, J. B.; Fernandez-Moreira, V.; Hayes, A. J.; Lloyd, D.; Millet, C.; Pope, S. J. A., 3-Chloromethylpyridyl bipyridine fac-tricarbonyl rhenium: a thiol-reactive luminophore for fluorescence microscopy accumulates in mitochondria. *New J. Chem.* **2008,** *32* (7), 1097-1102.

68. Fernandez-Moreira, V.; Thorp-Greenwood, F. L.; Amoroso, A. J.; Cable, J.; Court, J. B.; Gray, V.; Hayes, A. J.; Jenkins, R. L.; Kariuki, B. M.; Lloyd, D.; Millet, C. O.; Williams, C. F.; Coogan, M. P., Uptake and localisation of rhenium fac-tricarbonyl polypyridyls in fluorescent cell imaging experiments. *Org Biomol Chem* **2010,** *8* (17), 3888-901.

69. Parson, C.; Smith, V.; Krauss, C.; Banerjee, H. N.; Reilly, C.; Krause, J. A.; Wachira, J. M.; Giri, D.; Winstead, A.; Mandal, S. K., The effect of novel rhenium compounds on

lymphosarcoma, PC-3 prostate and myeloid leukemia cancer cell lines and an investigation on the DNA binding properties of one of these compounds through electronic spectroscopy. *Journal of bioprocessing & biotechniques* **2013,** *4* (1), 141.

70. Thorp-Greenwood, F. L.; Coogan, M. P.; Mishra, L.; Kumari, N.; Rai, G.; Saripella, S., The importance of cellular localisation of probes: synthesis, photophysical properties, DNA interactions and cellular imaging properties of rhenium dppz complexes with known cellular localization vectors. *New J. Chem.* **2012,** *36* (1), 64-72.

71. Lippert, B., *Cisplatin Chemistry and Biochemistry of a Leading Anticancer Drug*. Wiler-VCH: Weinheim, 1999.

72. Gasser, G.; Metzler-Nolte, N., The potential of organometallic complexes in medicinal chemistry. *Curr. Opin. Chem. Biol.* **2012,** *16* (1-2), 84-91.

73. Levina, A.; Mitra, A.; Lay, P. A., Recent developments in ruthenium anticancer drugs. *Metallomics* **2009,** *1* (6), 458-70.

74. Sava, G.; Zorzet, S.; Turrin, C.; Vita, F.; Soranzo, M.; Zabucchi, G.; Cocchietto, M.; Bergamo, A.; DiGiovine, S.; Pezzoni, G.; Sartor, L.; Garbisa, S., Dual Action of NAMI-A in Inhibition of Solid Tumor Metastasis: Selective Targeting of Metastatic Cells and Binding to Collagen. *Clinical Cancer Research* **2003,** *9* (5), 1898-1905.

75. Hartinger, C. G.; Zorbas-Seifried, S.; Jakupec, M. A.; Kynast, B.; Zorbas, H.; Keppler, B. K., From bench to bedside--preclinical and early clinical development of the anticancer agent indazolium trans-[tetrachlorobis(1H-indazole)ruthenate(III)] (KP1019 or FFC14A). *J. Inorg. Biochem.* **2006,** *100* (5-6), 891-904.

76. Dwyer, F. P. J.; Mellor, D. P., *Chelating agents and metal chelates*. Academic Press: New York, 1964.

77. Shulman, A.; Laycock, G. M.; Bradley, T. R., *Chem-Biol. Interactions* **1977,** *16*, 89-99.

78. Kleineweischede, A.; Mattay, J., Synthesis of Amino- and Bis(bromomethyl)-Substitued Bi- and TetradentateN-Heteroaromatic Ligands: Building Blocks for Pyrazino-Functionalized Fullerene Dyads. *Eur. J. Org. Chem.* **2006,** *2006* (4), 947-957.

79. Bolger, J.; Gourdon, A.; Ishow, E.; Launay, J.-P., Mononuclear and Binuclear Tetrapyrido[3,2-a:2‘,3‘-c:3‘‘,2‘‘-h:2‘‘‘,3‘‘‘-j]phenazine (tpphz) Ruthenium and Osmium Complexes. *Inorg. Chem.* **1996,** *35* (10), 2937-2944.

80. Kim, M.-J.; Konduri, R.; Ye, H.; MacDonnell, F. M.; Puntoriero, F.; Serroni, S.; Campagna, S.; Holder, T.; Kinsel, G.; Rajeshwar, K., Dinuclear Ruthenium(II) Polypyridyl Complexes Containing Large, Redox-Active, Aromatic Bridging Ligands: Synthesis, Characterization, and Intramolecular Quenching of MLCT Excited States. *Inorg. Chem.* **2002,** *41* (9), 2471-2476.

81. Wrighton, M.; Morse, D. L., Nature of the lowest excited state in tricarbonylchloro-1,10-phenanthrolinerhenium(I) and related complexes. *JACS* **1974,** *96* (4), 998-1003.

82. Kleineweischede, A.; Mattay, J., Synthesis, spectroscopic and electrochemical studies of a series of transition metal complexes with amino- or bis(bromomethyl)-substituted dppz-ligands: Building blocks for fullerene-based donor–bridge–acceptor dyads. *J. Organomet. Chem.* **2006,** *691* (9), 1834-1844.

83. Aslan, J. M. Photo-driven one and two-electron processes of tetraazatetrapyridopentacene and substituted dipyridophenazine ligands in the presence or absence of zinc and ruthenium complexation. Ph.D., The University of Texas at Arlington, Ann Arbor, 2012.

84. Luong, J. C.; Faltynek, R. A.; Wrighton, M. S., Competitive radiative decay and metal-metal bond cleavage from the lowest excited state of triphenyltin- and triphenylgermanium tricarbonyl(1,10-phenanthroline)rhenium. *JACS* **1979,** *101* (6), 1597-1598.

85. Caspar, J. V.; Meyer, T. J., Application of the energy gap law to nonradiative, excited-state decay. *The Journal of Physical Chemistry* **1983,** *87* (6), 952-957.

86. Bates, W. D.; Chen, P.; Dattelbaum, D. M.; Jones, W. E.; Meyer, T. J., Excited State Competition in fac-[ReI(dppz)$(CO)_3$(py-PTZ)]$^+$. *The Journal of Physical Chemistry A* **1999,** *103* (27), 5227-5231.

87. R. Waterland, M.; C. Gordon, K.; J. McGarvey, J.; M. Jayaweera, P., Spectroscopic and electrochemical studies of a series of copper(I) and rhenium(I) complexes with substituted dipyrido[3,2-a:2',3'-c]phenazine ligands†. *J. Chem. Soc., Dalton Trans.* **1998,** (4), 609-616.

88. Stoeffler, H. D.; Thornton, N. B.; Temkin, S. L.; Schanze, K. S., Unusual Photophysics of a Rhenium(I) Dipyridophenazine Complex in Homogeneous Solution and Bound to DNA. *JACS* **1995,** *117* (27), 7119-7128.

89. Coogan, M. P.; Fernández-Moreira, V.; Kariuki, B. M.; Pope, S. J. A.; Thorp-Greenwood, F. L., A Rhenium Tricarbonyl 4′-Oxo-terpy Trimer as a Luminescent Molecular Vessel with a Removable Silver Stopper. *Angew. Chem. Int. Ed.* **2009,** *48* (27), 4965-4968.

90. Wrighton, M.; Morse, D. L., Nature of the lowest excited state in tricarbonylchloro-1,10-phenanthrolinerhenium(I) and related complexes. *J. Amer. Chem. Soc.* **1974,** *96* (4), 998-1003.

91. Díaz, R.; Francois, A.; Loeb, B., Synthesis and characterization of rhenium(I) complexes with the polypyridinic quinone functionalized electron acceptor ligand [3,2-a:2′,3′-c]-benzo[3,4]-phenazine-11,16-quinone, Nqphen. *Polyhedron* **2011,** *30* (5), 697-701.

92. Rau, S.; Schwalbe, M.; Losse, S.; Görls, H.; McAlister, C.; MacDonnell, F. M.; Vos, J. G., Photoinduced Ligand Transformation in a Ruthenium Polypyridophenazine Complex. *Eur. J. Inorg. Chem.* **2008,** *2008* (7), 1031-1034.

93. Ragone, F.; Saavedra, H. H. M.; Gara, P. M. D.; Ruiz, G. T.; Wolcan, E., Photosensitized Generation of Singlet Oxygen from Re(I) Complexes: A Photophysical Study Using LIOAS and Luminescence Techniques. *The Journal of Physical Chemistry A* **2013,** *117* (21), 4428-4435.

94. Spada, R. M.; Cepeda-Plaza, M.; Gómez, M. L.; Günther, G.; Jaque, P.; Pizarro, N.; Palacios, R. E.; Vega, A., Clean Singlet Oxygen Production by a ReI Complex Embedded in a Flexible Self-Standing Polymeric Silsesquioxane Film. *The Journal of Physical Chemistry C* **2015,** *119* (18), 10148-10159.

95. Meyer, S.; Tietze, D.; Rau, S.; Schäfer, B.; Kreisel, G., Photosensitized oxidation of citronellol in microreactors. *Journal of Photochemistry and Photobiology A: Chemistry* **2007,** *186* (2–3), 248-253.

96. DeRosa, M. C.; Crutchley, R. J., Photosensitized singlet oxygen and its applications. *Coord. Chem. Rev.* **2002,** *233–234*, 351-371.

97. Singh, S.; de Tacconi, N. R.; Diaz, N. R.; Lezna, R. O.; Munoz Zuniga, J.; Abayan, K.; MacDonnell, F. M., Photochemical two-electron reduction of a dinuclear ruthenium complex containing a bent tetraazatetrapyridopentacene bridging ligand: pushing up the LUMO for storing more energy. *Inorg. Chem.* **2011,** *50* (19), 9318-28.

98. Janaratne, T. K.; Yadav, A.; Ongeri, F.; MacDonnell, F. M., Preferential DNA Cleavage under Anaerobic Conditions by a DNA-Binding Ruthenium Dimer. *Inorg. Chem.* **2007,** *46* (9), 3420-3422.

99. Luong, J. C.; Nadjo, L.; Wrighton, M. S., Ground and excited state electron transfer processes involving fac-tricarbonylchloro(1,10-phenanthroline)rhenium(I). Electrogenerated chemiluminescence and electron transfer quenching of the lowest excited state. *JACS* **1978,** *100* (18), 5790-5795.

100. Kuimova, M. K.; Alsindi, W. Z.; Dyer, J.; Grills, D. C.; Jina, O. S.; Matousek, P.; Parker, A. W.; Portius, P.; Zhong Sun, X.; Towrie, M.; Wilson, C.; Yang, J.; George, M. W., Using picosecond and nanosecond time-resolved infrared spectroscopy for the investigation of excited states and reaction intermediates of inorganic systems. *Dalton Transactions* **2003,** (21), 3996-4006.

101. Lo, K. K.-W., Luminescent Rhenium(I) and Iridium(III) Polypyridine Complexes as Biological Probes, Imaging Reagents, and Photocytotoxic Agents. *Acc. Chem. Res.* **2015,** *48* (12), 2985-2995.

102. Lo, K. K.-W.; Zhang, K. Y.; Li, S. P.-Y., Recent Exploitation of Luminescent Rhenium(I) Tricarbonyl Polypyridine Complexes as Biomolecular and Cellular Probes. *Eur. J. Inorg. Chem.* **2011,** *2011* (24), 3551-3568.

103. Warnmark, K.; Thomas, J. A.; Heyke, O.; Lehn, J.-M., Stereoisomerically controlled inorganic architectures: synthesis of enantio- and diastereo-merically pure ruthenium-palladium molecular rods from enantiopure building blocks. *Chem. Commun.* **1996,** (6), 701-702.

104. Janaratne, T. K.; Yadav, A.; Ongeri, F.; MacDonnell, F. M., Preferential DNA Cleavage under Anaerobic Conditions by a DNA-Binding Ruthenium Dimer. *Inorg. Chem. (Washington, DC, U. S.)* **2007,** *46* (9), 3420-3422.

105. Dayoub, A. S. Cytotoxicty, Cellular Localization And Fluorescent Microscopy Of Malignant Cells Treated With Ruthenium (II) Complexes Of The Tetraazatetrapyridopentacene Ligand. THE UNIVERSITY OF TEXAS AT ARLINGTON, 2015.

106. Li, S. D.; Howell, S. B., CD44-targeted microparticles for delivery of cisplatin to peritoneal metastases. *Mol Pharm* **2010,** *7* (1), 280-90.

107. Olson, E. J. C.; Hu, D.; Hörmann, A.; Jonkman, A. M.; Arkin, M. R.; Stemp, E. D. A.; Barton, J. K.; Barbara, P. F., First Observation of the Key Intermediate in the “Light-Switch” Mechanism of $[Ru(phen)_2dppz]^{2+}$. *JACS* **1997,** *119* (47), 11458-11467.

108. Hotze, A. C. G.; van der Geer, E. P. L.; Kooijman, H.; Spek, A. L.; Haasnoot, J. G.; Reedijk, J., Characterization by NMR Spectroscopy, X-ray Analysis and Cytotoxic Activity of the Ruthenium(II) Compounds $[RuL_3](PF_{6)2}$(L = 2-Phenylazopyridine or o-Tolylazopyridine) and $[RuL'_2L'](PF_6)_2$(L', L'' = 2-Phenylazopyridine, 2,2'-Bipyridine). *Eur. J. Inorg. Chem.* **2005,** *2005* (13), 2648-2657.

109. Puckett, C. A.; Barton, J. K., Targeting a ruthenium complex to the nucleus with short peptides. *Bioorg. Med. Chem.* **2010,** *18* (10), 3564-9.

110. Baggaley, E.; Gill, M. R.; Green, N. H.; Turton, D.; Sazanovich, I. V.; Botchway, S. W.; Smythe, C.; Haycock, J. W.; Weinstein, J. A.; Thomas, J. A., Dinuclear ruthenium(II) complexes as two-photon, time-resolved emission microscopy probes for cellular DNA. *Angew. Chem. Int. Ed. Engl.* **2014,** *53* (13), 3367-71.

111. Chen, T.; Liu, Y.; Zheng, W.-J.; Liu, J.; Wong, Y.-S., Ruthenium Polypyridyl Complexes That Induce Mitochondria-Mediated Apoptosis in Cancer Cells. *Inorg. Chem.* **2010,** *49* (14), 6366-6368.

112. Onfelt, B.; Gostring, L.; Lincoln, P.; Norden, B.; Onfelt, A., Cell studies of the DNA bis-intercalator Delta-Delta [mu-C4(cpdppz)(2)-(phen)(4)Ru(2)](4+): toxic effects and properties as a light emitting DNA probe in V79 Chinese hamster cells. *Mutagenesis* **2002,** *17* (4), 317-20.

113. Chiorboli, C.; Fracasso, S.; Ravaglia, M.; Scandola, F.; Campagna, S.; Wouters, K. L.; Konduri, R.; MacDonnell, F. M., Primary photoinduced processes in bimetallic dyads with extended aromatic bridges. tetraazatetrapyridopentacene complexes of ruthenium(II) and osmium(II). *Inorg. Chem.* **2005,** *44* (23), 8368-78.

114. Chiorboli, C.; Fracasso, S.; Scandola, F.; Campagna, S.; Serroni, S.; Konduri, R.; MacDonnell, F. M., Primary charge separation in photoinduced multielectron storage systems. A dinuclear ruthenium(II) species featuring a charge-separated state with a lifetime of 1.3 µs. *Chem. Commun.* **2003,** (14), 1658-1659.

115. Pooja Ahuja, Adam. S. Dayoub., Frederick M. Macdonnell, Tracking the cellular distribution and determining the cellular targets of heterobimetallic Ru(II)-Re(I)tatpp complex. *Manuscript in preparation* **2016**.

BIOGRAPHICAL INFORMATION

Pooja Ahuja was born and grew up in the holy city of Haridwar located on the banks of river Ganges in Northern India. She received her B.S degree from Ch. Charan Singh University, India (formerly Meerut University) in the year 2002 and M.S degree in Chemistry from Gurukula Kangri University (GKU), India in 2004. She pursued her M.S research project entitled “Toxic Elements Assessment in Fly Ash by Atomic Absorption Spectroscopy” at the Pollution Control Research Institute (PCRI), of Bharat Heavy Electrical Limited (B.H.E.L), Haridwar, India.

After completing her M.S degree, Pooja worked as a Senior Quality Control Chemist in Lotus Beauty Care Products Pvt Ltd (LBCPPL), India, for a period of two years (2004-2006). LBCPPL is a personal care products franchise of Hindustan Unilever Ltd (HUL). In 2006, Pooja came to United States on spouse visa and began her Ph.D. degree in the ‘Soil and Water Science’ Department of the University of Florida (UF) at Gainesville in 2010. She began her graduate studies on prestigious UF Graduate School Alumni Fellowship (2010 – 2014). Her research focus was ‘Biochar as efficient low cost sorbent for environmental pollutants’. Due to family relocation, however, Pooja had to quit the UF program and move to Dallas, Texas in 2011, where she was accepted to the Ph.D. program in the Department of Chemistry and Biochemistry of the University of Texas at Arlington in the Fall of 2011. She was awarded the ‘Outstanding Achievement Award’ for maintaining a GPA of 4.0 after her short term of two semesters in the Ph.D. program at UF.

At UTA, Pooja worked under the supervision of Dr. Frederick M. Macdonnell. Her research focus was development and investigation of novel Re(I) based anticancer drugs. Pooja graduated from UTA with a Ph.D. degree in Chemistry in the Spring of 2016.